INAUGURAL-DISSERTATION

zur Erlangung der Doktorwürde der
Naturwissenschaftlich-Mathematischen
Gesamtfakultät der
Ruprecht-Karls-Universität Heidelberg

vorgelegt von
M. Sc. Nikolay V. Golubev
aus Kolomna

Tag der mündlichen Prüfung:
14.12.2017

Electron-nuclear dynamics and its control by external electromagnetic fields

Gutachter:
Priv.-Doz. Dr. Alexander Kuleff
Prof. Dr. Hans-Dieter Meyer

This thesis is dedicated to my parents and my wife

Abstract:

In recent years, the rapid development of attosecond pulse techniques opened the door for studying and eventually controlling electronic dynamics. Due to strong coupling between the electronic and nuclear motion, control over the pure electronic step offers the extremely interesting possibility to steer the succeeding chemical reactivity by predetermining the reaction outcome at a very early stage. Using the electron dynamics and quantum coherence to induce a particular chemical process is the new paradigm in the emerging field of "attochemistry".

One example of physical phenomena, where an electronic dynamics significantly affect on reactivity is the process of an ultrafast charge migration. The positive charge created upon ionization of a molecule can migrate throughout the system on a few-femtosecond time scale solely driven by the electron correlation and electron relaxation. Charge migration triggered by ionization appeared to be a general phenomenon taking place both after inner- and outer-valence ionization of molecules.

This thesis is devoted to the theoretical investigation of the fascinating interplay between the faster electron and the slower nuclear dynamics appearing upon ionization of a molecular system in the presence of an external electromagnetic field. The possibilities to manipulate quantum molecular dynamics by applying specifically tailored ultrashort laser pulses are inspected and analyzed. In particular, the focus is made on the role which the coherent electronic dynamics plays and how the control of the electronic movement influences the outcomes of induced processes. We present here both analytical and numerical approaches allowing one to design laser pulses which can force the evolution of a quantum system in a predefined way. We demonstrate by fully *ab initio* calculations on experimentally interesting molecules that simple pulses can be used to control the charge-migration oscillations. It is further shown how the correlated treatment of electronic and nuclear dynamics affects the coherence of the electronic wave packet. Our full-dimensional calculations on the propiolic acid molecule show that the electronic decoherence time can be long enough to allow one to observe several oscillations of the charge before nuclear dynamics eventually traps it. Utilizing the strong coupling between the electronic and the nuclear motion, we exemplify the key idea of the attosecond control of molecular reactivity. We demonstrate on a simple model of molecular fragmentation that the nuclear rearrangement can be guided by a manipulation of the electronic dynamics only. We argue that this example clearly illustrates the concept of attochemistry and thus can be used as a starting point to deepen our understanding of the possibilities to control chemical reactions.

Kurzfassung:

Die rapide Entwicklung der Technologie von Attosekundenpulsen hat den Weg geebnet für die Untersuchung und eventuelle Kontrolle der Elektronendynamik in molekularen Systemen. Da die Elektronen- und Kernbewungen stark gekoppelt sind, eröffnet die Kontrolle der Elektronendynamik die Möglichkeit der Steuerung der chemischen Reaktivität, wobei speziel die Anfangsphase die Reaktion wichtig ist. Der Einsatz von Elektronendynamik und Quantenkohärenz um einen chemischen Prozess zu induzieren, ist das Paradigma des sich entwickelnden Forschungsfeldes der Attosekunden-Chemie.

Ein Beispiel der physikalischen Phänomene, bei denen die Elektronendynamik signifikanten Einfluss auf die Reaktivität hat, ist der Prozess der ultraschnellen Ladungsmigration. Dabei kann die durch Ionisation erzeugte positive Ladung eines Moleküls auf einer Zeitskala von einigen wenigen Femtosekunden durch das System wandern, lediglich bedingt durch Elektronenkorrelationen und Elektronenrelaxation. Durch Ionisierung induzierte Ladungsmigration stellte sich als ein generelles Phänomen heraus, sowohl beider Ionisierung von inneren als auch äußeren Valenzelektronen von Molekülen.

Die vorliegende Dissertation beschäftigt sich mit der theoretischen Untersuchung des Zusammenspiels von schneller Elektronen- und langsamer Kernbewegung in ionisierten Molekülen in äußeren elektromagnetischen Feldern. Die Möglichkeit der Manipulation der molekularen Quantendynamik durch speziell geformte ultrakurze Laserpulse wird analysiert. Spezielles Augenmerk wird auf die Rolle der kohärenten Elektronendynamik gelegt, d.h. wie die Kontrolle der Elektronenbewegung das Resultat induzierter Prozesse beeinflusst. Es werden sowohl analytische als auch numerische Herangehensweisen präsentiert, welche es erlauben, Laserpulse so zu formen, dass die Evolution des Quantensystems in einer vorab definierten Art und Weise abläuft. Mithilfe von ab-initio-Rechnungen für experimentell interessante Moleküle wird gezeigt, dass simple Pulse zur Kontrolle der Oszillationen bei Ladungsmigration verwendet werden können. Des weiteren wird gezeigt, wie die korrelierte Betrachtung der Elektronen- und Kerndynamik die Kohärenz des elekrtonischen Wellenpakets beeinflusst. Die Rechnungen für ein Propiolsäuremolekül zeigen, dass die elektronische Dekohärenzzeit lang genug sein kann, um mehrere Perioden der Ladungsoszillation innerhalb des Moleküls zu beobachten, bevor die Kernbewegung dies eventuell verhindert. Die grundlegende Idee der Attosekunden-Kontrolle der molekularen Reaktivität wird mithilfe der starken Kopplung der Elektronen- und Kernbewegung veranschaulicht. Für ein einfaches Modell molekularer Fragmentierung wird demonstriert, dass eine Umordnung der Atomkerne ausschließlich mithilfe der Manipulation der Elektronendynamik gesteuert werden kann. Dieses Beispiel legt deutlich das Konzept der Attosekunden-Chemie dar und kann deswegen benutzt werden, um das Verständnis der Kontrollmöglichkeiten einer chemischen Reaktion zu vertiefen.

List of Papers

Results presented in this work:

- **N. V. Golubev** and A. I. Kuleff, "Control of populations of two-level systems by a single resonant laser pulse", *Physical Review A*, vol. 90, no. 3, Sep. 2014.
- **N. V. Golubev** and A. I. Kuleff, "Control of charge migration in molecules by ultrashort laser pulses", *Physical Review A*, vol. 91, no. 5, May 2015.
- **N. V. Golubev**, V. Despré, and A. I. Kuleff, "Quantum control with smoothly varying pulses: general theory and application to charge migration", *Journal of Modern Optics*, vol. 64, no. 10-11, pp. 1031–1041, Jun. 2017.
- **N. V. Golubev**, L. S. Cederbaum, and A. I. Kuleff, "Direct numerical solution of the exact factorization problem", in preparation.
- V. Despré, **N. V. Golubev**, and A. I. Kuleff, "Charge migration in propiolic acid: A full quantum dynamics calculation", in preparation.

Papers not included in the thesis:

- K. Nagaya, D. Iablonskyi, **N. V. Golubev**, *et al.*, "Interatomic Coulombic decay cascades in multiply excited neon clusters", *Nature Communications*, vol. 7, p. 13 477, Dec. 2016.
- T. Takanashi, **N. V. Golubev**, C. Callegari, *et al.*, "Time-Resolved Measurement of Interatomic Coulombic Decay Induced by Two-Photon Double Excitation of Ne_2", *Physical Review Letters*, vol. 118, no. 3, Jan. 2017.
- M. C. E. Galbraith, S. Scheit, **N. V. Golubev**, *et al.*, "Few-femtosecond passage of conical intersections in the benzene cation", *Nature Communications*, vol. 8, no. 1, Dec. 2017.

Papers published prior PhD:

- **N. V. Golubev**, D. S. Bezrukov, M. Gustafsson, G. Nyman, and S. V. Antipov, "Formation of the SiP Radical through Radiative Association", *Journal of Physical Chemistry A*, vol. 117, no. 34, pp. 8184–8188, Aug. 2013.
- É. Brémond, **N. V. Golubev**, S. N. Steinmann, and C. Corminboeuf, "How important is self-consistency for the dDsC density dependent dispersion correction?", *Journal of Chemical Physics*, vol. 140, no. 18, 18A516, May 2014.

Acknowledgement

First of all, I would like to thank Dr. Alexander Kuleff, my advisor, for suggesting some of the problems investigated in this thesis, for many helpful discussions regarding both my research and other topics, for helping me to improve my writing and presentations skills, for giving me the possibility to work independently and for the financial support. I highly appreciate his positive outlook and confidence in success of my research.

Besides my advisor, I would like to express my sincere gratitude to Prof. Lorenz Cederbaum for many things. Notably, for creating the unique research environment in which I have performed my graduate studies. I will always be very grateful for the opportunity I have had to hear his acutely intuitive and insightful explanations and views.

I also would like to acknowledge Prof. Hans-Dieter Meyer for evaluating my thesis.

I want to thank every member of the Theoretical Chemistry group for creating a friendly and supportive atmosphere. In particular, I would like to thank Dr. Victor Despré with whom I closely collaborated on the subject of this thesis and Dr. Shachar Klaiman for numerous valuable discussions. I want to acknowledge Prof. Hans-Dieter Meyer and Dr. Markus Schröder for helping me to understand how MCTDH package is organized. I am much obliged to other current and former members of the TC group, Prof. Jochen Schirmer, Prof. Horst Köppel, Dr. Markus Pernpointner, Raphael Beinke, Dr. Kirill Gokhberg, Dr. Aryya Ghosh, Dr. Tsveta Miteva, Dr. Ghazal Jabbari, Dr. Nikolai Kryzhevoi, Dr. David Mendive-Tapia, Dr. Evgeniy Gromov, Dr. Simona Scheit, Yi-Fan Yang, for many discussions and their wonderful company both inside and outside of the office. I got much help at my first days in Germany from Dr. Vasili Stumpf. I thank Vasili for being always available when I had questions about how the German bureaucratic machine works. I thank our secretaries, Annette Braun and Julie Pusch, for always being ready to help me in administrative and personal matters.

I have profited scientifically from correspondence and insightful discussions with Denis Artiukhin. I also would like to acknowledge Andrei Bavykin for many entertaining conversations in the past years.

I gratefully acknowledge the funding provided by the International Max Planck Research School for Quantum Dynamics (IMPRS-QD) that made my PhD work possible.

Finally, I am deeply thankful to my family for their encouragement and support, without which this work would not have been possible. This last word of acknowledgment I have saved for my wife Dr. Kseniia Korchagina for her never ending patience and her support in every phase of my PhD project.

Contents

1

Introduction

The first chapter highlights the motivation of the research conducted in the present thesis

One of the key problems of physics, which once led to the emergence of quantum mechanics, is to understand how electrons and nuclei behave in a molecule. The investigation of molecules and chemical reactions in which they can participate is of fundamental interest to comprehend the diversity of the world or even life.

From a chemical point of view, the chemical reaction is a process that leads to the transformation of one chemical substance to another. In terms of the molecular structure it could be interpreted as the dynamical metamorphosis which leads to rearrangement of the nuclei in space. Tracking the motion of the individual atoms inside a molecule is an enormously difficult task since a time scale of this movement is awesomely rapid. As a case in point, the molecular vibrations typically occur on a time scale of tens to hundreds of femtoseconds (1 fs = 10^{-15} s) which corresponds to atomic movement with the speed $\sim$ 1 km/s. It is obvious that to measure this process one needs to have experimental techniques which are precise enough to guarantee the required time and space resolution.

Since the earliest days of lasers, they are proven to be a source of the electromagnetic radiation with extraordinary parameters. Laser beams can be focused to very tiny spots, achieving a very high irradiance, while their temporal and spatial resolution can be enough to observe fundamental processes appearing on a microlevel. Utilizing the exceptional properties of the laser radiation, one was able to "freeze" molecular structures far from equilibrium and to observe in this way vibrational motion of the nuclei on its natural time scale [1].

The aim of the scientific efforts has not only been to investigate molecules, but also to use specific features of a quantum nature of matter in order to control their properties. For example, one may use the quantum interference and the properties of the laser-matter interaction to directly exert control over the chemical reactivity of a molecule. This is the concept behind the research field known nowadays as "femtochemistry" [1, 2], where by specifically tailored femtosecond laser pulses, one tries to steer the motion of the nuclei in the molecule and thus guide the system throughout the desired reaction channel. Born in the second half of the past century, femtochemistry is now a well-established scientific discipline [1–4].

Despite the fact that chemistry is defined by rearrangement of nuclei, the factor which leads to formation or destruction of chemical bonds between atoms is determined by the electrons. Being much lighter than the nuclei, the electrons move much faster and the typical time scale of their motion lies in the range from few femtoseconds down to hundreds of attoseconds [5]. At the same time, the dynamics of the electrons and the nuclei inside a molecule are strongly coupled, leading in such a way to the potential opportunity to affect the nuclei through manipulation of the electronic motion only. Within the Born–Oppenheimer approach, i.e. supposing that the nuclei are moving on the potentials of electronic states, this can be understood as the possibility to guide the nuclear rearrangement by the redistribution of electronic density between different potential-energy landscapes. To use the electron dynamics and the quantum coherence

for inducing a particular chemical process is the new paradigm of the emerging field of "attochemistry" [6].

This novel concept was to a large extent motivated by the impressive progress in the laser pulse technology in the past two decades [7, 8]. With the advent of the twenty-first century, developments of coherent light sources permitted to create attosecond laser pulses with remarkably well controlled parameters [9, 10]. It has revitalized the field of atomic and molecular physics due to the possibility to investigate phenomena which have been long-predicted theoretically but never observed experimentally. Using advanced laser technologies available nowadays, one is able to initiate and probe processes that take place before the nuclear dynamics comes into play, i.e., to study and manipulate electron dynamics on its natural time scale [11–15].

One phenomenon of particular interest for the attosecond science is the process of transfer of electronic charge within a single molecule. The movement of charge along a molecular chain is a key step in many essential biological processes and chemical reactions. It plays an important role in photosynthesis [16], catalysis [17], DNA damage by ionizing radiation [18], and many other fascinating phenomena in nature [19]. The investigation of the mechanisms and physical characteristics of charge transfer in biologically relevant molecules is attracting a great attention both experimentally and theoretically [5].

The term charge transfer stands for many different physical phenomena irrespective of the particular mechanism and generally describes the flow of electronic charge along a molecule. The charge is usually driven from the "donor" to the "acceptor" site by a nuclear rearrangement caused by an energy stabilization along a reaction coordinate. Depending on the particular mechanism, the transfer time may vary strongly, but time scales as short as few tens of femtoseconds have been reported [20, 21].

In contrast to this nuclear dynamics driven mechanisms, it was shown [22] that charge transfer can take place exclusively on an electronic level and, therefore, on a much shorter time scale. In their pioneering work [22], Cederbaum and Zobeley demonstrated that due to the electron correlation, the removal of an electron from a molecular orbital may create an electronic wave packet (a simultaneous population of a multitude of cationic states), which will evolve in time. To distinguish this mechanism from the nuclear driven ones it was termed "charge migration". Theory predicts [23] that such ultrafast migration of a charge is driven solely by electron correlation and thus can happen even with frozen nuclei. Even though the charge migration is governed by the electronic motion, it affects the dynamics of the whole molecule. Although in the first few femtoseconds the process represents an ultrafast charge oscillation from one site of the molecule to another, there were already strong indications [24–31] that the coupling to the slower nuclear motion can lead to a trapping of the charge and, thus, achieving irreversibility of the process [23].

The scientific attempts to investigate the interplay between the ultrafast charge

migration and the slower nuclear motion were pioneered by Schlag, Weinkauf, and co-workers. In a series of experiments they observed a charge-directed reactivity [32] in electronically excited ionic states of various peptide chains [33–35]. It was reported that, after localized ionization of the chromophore site of the peptide, the positive charge is transferred to the remote end of the chain, causing a bond breaking. Time-resolved measurement on a smaller, prototype molecule (2-phenylethyl-N,N-dimethylamine, abbreviated as PENNA) showed that the process takes place on the time scale of few tens of femtoseconds [36, 37]. Extensive *ab initio* many-body calculations on PENNA suggested [27] as an explanation that the charge-directed reactivity is a concerted electron-nuclear dynamics: Immediately after ionization, pure electron dynamics is triggered and the positive charge starts to oscillate between the chromophore and the remote amine end of the molecule on a few-femtosecond time scale, while at later times the coupling to the slower nuclear dynamics causes the trapping of the charge on the amine site and the bond breaking.

The above mentioned experiments on PENNA molecule were performed using pulses with durations of 200 and 120 fs for the pump and the probe, respectively, allowing one to extract information about ultrafast processes on time scale down to few tens of femtoseconds. The pure electronic dynamics were therefore our of reach. Nowadays, however, observing and tracing the faster electronic processes became feasible due to the strongly improved experimental techniques. Several recent experiments have shown that ultrafast quantum coherences in complex molecules can be followed in time and analyzed. Using XUV-pump–IR-probe technique, Calegari et al. were able to observe pure electronic, few-femtosecond charge oscillations triggered by a broadband ionization of phenylalanine [38] (see also Ref. [39]). Also, electronic wave packets were created by field ionization and their evolution reconstructed via time-resolved high-harmonic generation spectroscopy in iodoacethylen [40].

The particular challenge to perform experiments on molecular systems in comparison with those for atoms is the involvement of many degrees of freedom. For example, electronic and nuclear motion is usually coupled due to non-adiabatic effects, and its interplay can crucially affect the possibility to observe the properties of interest. For this reason, the role of theory as a prerequisite to outline new experiments, and to disclose their feasibility and informational content, will be stronger than ever before [5]. The aim of the present thesis is to contribute to the theoretical treatment of the molecular dynamics under influence of the external electromagnetic field. Special attention is paid to the possibilities to manipulate ultrafast electronic dynamics by attosecond laser pulses. The influence of the slower nuclear dynamics on the pure electronic charge migration process has been studied on model systems and by performing a full-dimensional coupled electron-nuclear dynamics calculation on an experimentally interesting molecule. The concept of controlling chemical reactivity by manipulating electron coherences has been demonstrated.

The thesis is organized as follows. In the next chapter, we present an overview of the

theoretical methods used for the mathematical treatment of electrons and nuclei in a molecule. The approaches allowing one to treat electron-nuclear dynamics under influence of the external electromagnetic field will be considered in some detail. In chapter 3, we present our results on the control of quantum dynamics by specifically tailored ultrafast laser pulses. We will show that by applying simple laser field with controlled parameters one may force the evolution of a quantum system in a practically arbitrary way. Chapter 4 contains our theoretical study of the control of charge migration in real molecules. In chapter 5 we demonstrate the theoretical approach allowing one to treat the coherent electron-nuclear dynamics. The key concept of attochemistry will be illustrated. Finally, in chapter 6 we discuss future perspectives of the attosecond quantum control of charge migration, summarize results obtained within the present thesis, and conclude.

2

Theory

This chapter gives a short overview of the theoretical methods for description of dynamics in a molecular system under the influence of external electromagnetic fields

Contents

2.1 Introduction

Quantum dynamics simulations are now established as an essential tool for understanding experiments probing the nature of matter at the microscopic level and on fundamental time-scales. To describe an evolution of a quantum system in time, one needs to solve the quantum mechanical equation of motion, which is known as the time-dependent Schrödinger equation

$$\hat{H}\Psi = i\hbar\frac{\partial\Psi}{\partial t}, \tag{2.1}$$

where $\hat{H}$ denotes the Hamilton operator, which characterizes all possible physical properties of the system, and Ψ is the time-dependent wavefunction, which defines the particular state of the system at any moment of time.

Solving the many-particle Schrödinger Eq. (2.1) is a tedious task. In fact, an analytical solution can be obtained only for systems with no more than two interacting particles. In all other cases of interest, one needs to introduce approximations, mathematical or physical, which will allow to treat more complicated situations. The objective of the present chapter is to provide a general ansatz for solution of the Schrödinger equation for systems with several degrees of freedom. To be specific, in this thesis we will concentrate on the solution of Eq. (2.1) for molecules – the systems consisting of electrons and nuclei interacting with each other. Special emphasis will be put on the treatment of the interaction between a molecular system and an external field. The electromagnetic radiation can strongly influence the motion of both the electrons and nuclei, and consequently the dynamics of the molecule in general. Therefore, an accurate theoretical description of the coupling between the electromagnetic field and the molecule is required.

The chapter is organized as follows. In section 2.2 we will provide an overview of the basic theoretical concepts underlying the *ab initio* description of the non-adiabatic dynamics of a molecule. Starting from formally exact way to represent the molecular wavefunction in a basis of the electronic states, we will introduce the concept of nuclear wavefunctions and the equations which govern their evolution in time. Section 2.3 is devoted to the description of methods for calculation of the electronic wavefunctions of a molecular system for a given nuclear configuration. Finally, in section 2.4 the Hamiltonian which represents interaction of a molecule with an external electromagnetic field is derived and discussed in some detail.

2.2 Electron-nuclear dynamics

The Hamiltonian $\hat{H}$ that governs the motion of the nuclei and the electrons can be written in the following form

$$\hat{H}(\mathbf{r}, \mathbf{R}) = \hat{T}_n + \hat{T}_e + U(\mathbf{r}, \mathbf{R}), \tag{2.2}$$

where $\hat{T}_n$ and $\hat{T}_e$ are the kinetic energy operators of the nuclei and the electrons, respectively, and $U(\mathbf{r}, \mathbf{R})$ is the total potential energy of the nuclei and the electrons. The vectors $\mathbf{r}$ and $\mathbf{R}$ denote the sets of electronic and nuclear coordinates, respectively. At this point, we do not have to be specific about the choice of these coordinates and will discuss it more specifically on cases of interest later.

The solution of the Schrödinger Eq. (2.1) with the given Hamilton operator (2.2) is being represented by a full molecular wavefunction $\Psi(\mathbf{r}, \mathbf{R}, t)$ which holds information about the coupled dynamics of both electrons and nuclei. A key development making this problem tractable for realistic systems is the idea that the molecular wavefunction can be efficiently constructed as a tensor product of the Hilbert subspaces associated with the electronic and nuclear degrees of freedom [41–43]. The fundamental reason allowing this separation is the large mass of the nuclei compared to that of the electrons indicating a clear difference in the fundamental time scales of their motion. As a consequence of this heterogeneity, one can expect that a basis set ensuring the completeness of the electronic subspace will vary slowly during rearrangement of the nuclei.

2.2.1 Born–Oppenheimer expansion

A convenient way to choose a basis for the representation of a molecular wavefunction is to use the eigenstates of the Hamiltonian associated with the movement of the electrons on potential formed by stationary nuclei

$$\hat{H}_e(\mathbf{r}, \mathbf{R}) = \hat{T}_e + U(\mathbf{r}, \mathbf{R}), \tag{2.3}$$

which is defined for each set of positions of the nuclei $\mathbf{R}$. The eigenvalues $V_i(\mathbf{R})$ and eigenfunctions $\Phi_i(\mathbf{r}, \mathbf{R})$ of this Hamiltonian fulfill

$$\hat{H}_e(\mathbf{r}, \mathbf{R})\Phi_i(\mathbf{r}, \mathbf{R}) = V_i(\mathbf{R})\Phi_i(\mathbf{r}, \mathbf{R}), \tag{2.4}$$

and, obviously, also have a parametric dependence on the nuclear coordinates. The set of eigenfunctions $\{\Phi_i(\mathbf{r}, \mathbf{R})\}$ form a complete basis in the electronic space at every value of $\mathbf{R}$

$$\sum_i \Phi_i^*(\mathbf{r}', \mathbf{R})\Phi_i(\mathbf{r}, \mathbf{R}) = \delta(\mathbf{r} - \mathbf{r}'), \tag{2.5}$$

where every eigenfunction satisfies the orthonormality condition

$$\langle \Phi_i(\mathbf{r}, \mathbf{R}) | \Phi_j(\mathbf{r}, \mathbf{R}) \rangle_{\mathbf{r}} = \delta_{ij}. \tag{2.6}$$

We introduced the notation $\langle ... | ... \rangle_{\mathbf{r}}$ meaning that the integration is performed over the electronic coordinates $\mathbf{r}$ only. Hereafter, if no subscript indices are present, the integration is made over all spatial degrees of freedom.

The electronic Hamiltonian commutes with the nuclear position operator, $[\hat{\mathbf{R}}, \hat{H}_e] = 0$, and thus an arbitrary state $\Psi(\mathbf{r}, \mathbf{R}, t)$ of the full system at any moment of time can be expanded in a basis of the electronic eigenfunctions

$$\Psi(\mathbf{r}, \mathbf{R}, t) = \sum_i \chi_i(\mathbf{R}, t)\Phi_i(\mathbf{r}, \mathbf{R}). \tag{2.7}$$

Here,

$$\chi_i(\mathbf{R}, t) = \langle \Phi_i(\mathbf{r}, \mathbf{R}) | \Psi(\mathbf{r}, \mathbf{R}, t) \rangle_{\mathbf{r}} \tag{2.8}$$

are the expansion coefficients which carry information about the nuclear position associated with a given electronic eigenstate. These coefficient are ofter referred to as nuclear wavefunctions. Mathematically they quantify the fraction of the full molecular state, defined on the Hilbert space of the Hamilton operator (2.2), onto a set of electronic states.

The expression (2.7) is known as the Born–Oppenheimer expansion (or Born–Huang, or adiabatic expansion) [42], and is the starting point for most of the approaches to describe the dynamics of molecular systems. Formally, the expansion (2.7) is exact, since the set $\{\Phi_i(\mathbf{r}, \mathbf{R})\}$ is complete. It is only when the expansion is truncated that approximations are introduced [44]. Such a representation of the molecular wavefunction allows the calculation of dynamical processes in molecules to be divided into two stages. In the first stage, the stationary electronic problem (2.4) is solved keeping the atomic nuclei fixed in space. In the second stage, the nuclear dynamics on a set of predetermined electronic states is treated [45].

The full description of the dynamics of a molecular system involves the determination of the time evolution of the functions $\chi_i(\mathbf{R}, t)$. This can be done by projecting the full

Schrödinger Eq. (2.1) on a set of electronic eigenfunctions and integrating over the electronic coordinates $\mathbf{r}$

$$\langle \Phi_i(\mathbf{r},\mathbf{R})|\hat{H}|\Psi(\mathbf{r},\mathbf{R},t)\rangle_{\mathbf{r}} = i\hbar\frac{\partial}{\partial t}\langle \Phi_i(\mathbf{r},\mathbf{R})|\Psi(\mathbf{r},\mathbf{R},t)\rangle_{\mathbf{r}}. \tag{2.9}$$

To proceed, we have to make use of the form of the kinetic energy operator $\hat{T}_n$ of the nuclei. This choice is not unique, and here the option is made for a rectilinear coordinate system that yields a diagonal kinetic energy operator, i.e., for which the different nuclear coordinates are not kinetically coupled [46] (for example Jacobi coordinates). The nuclear kinetic energy can thus be written as

$$\hat{T}_n = \sum_{\alpha}\left(-\frac{\hbar^2}{2M_\alpha}\right)\nabla_\alpha^2, \tag{2.10}$$

where the sum extends over the nuclear coordinates and M_α is an appropriate reduced mass.

Inserting ansatz (2.7) into Eq. (2.9) and utilizing relation (2.10), one obtains the equation [44]

$$\begin{aligned} i\hbar\frac{\partial}{\partial t}\chi_i(\mathbf{R},t) =& \sum_{j,\alpha}\left(-\frac{\hbar^2}{2M_\alpha}\right)\left(2\mathbf{F}_{ji}^{\alpha}(\mathbf{R})\cdot\nabla_\alpha + G_{ji}^{\alpha}(\mathbf{R})\right)\chi_j(\mathbf{R},t) \\ &+ \left(\sum_{\alpha}\left(-\frac{\hbar^2}{2M_\alpha}\right)\nabla_\alpha^2 + V_i(\mathbf{R})\right)\chi_i(\mathbf{R},t), \end{aligned} \tag{2.11}$$

where we have introduced the non-adiabatic derivative couplings

$$\mathbf{F}_{ji}^{\alpha}(\mathbf{R}) = \langle \Phi_j(\mathbf{r},\mathbf{R})|\nabla_\alpha|\Phi_i(\mathbf{r},\mathbf{R})\rangle_{\mathbf{r}}, \tag{2.12}$$

which are obviously vectors in the nuclear coordinate space, and the non-adiabatic scalar couplings

$$G_{ji}^{\alpha}(\mathbf{R}) = \langle \Phi_j(\mathbf{r},\mathbf{R})|\nabla_\alpha^2|\Phi_i(\mathbf{r},\mathbf{R})\rangle_{\mathbf{r}}. \tag{2.13}$$

By expanding the Laplace operator, it is possible to express the kinetic coupling as a function of the derivative coupling terms

$$G_{ji}^{\alpha}(\mathbf{R}) = \nabla_\alpha\cdot\mathbf{F}_{ji}^{\alpha}(\mathbf{R}) + \mathbf{F}_{ji}^{\alpha}(\mathbf{R})\cdot\mathbf{F}_{ji}^{\alpha}(\mathbf{R}), \tag{2.14}$$

where the first term is the divergence of the derivative coupling vector field. The derivative coupling terms $\mathbf{F}_{ji}^{\alpha}(\mathbf{R})$ form an anti-hermitian matrix, which implies that for real-valued electronic wavefunctions its diagonal terms are zero. Diagonal terms of the scalar coupling matrix are not zero due to the second term in Eq. (2.14).

The solution of Eq. (2.11) completely describes the non-adiabatic dynamics of a molecular system at any moment of time. We see from Eq. (2.11) that all terms in

the Born–Oppenheimer expansion of the total wavefunction, Eq. (2.7), are coupled through the nuclear motion, namely by the non-adiabatic coupling terms $\mathbf{F}^{\alpha}_{ji}(\mathbf{R})$ and $G^{\alpha}_{ji}(\mathbf{R})$. Such a formulation of the molecular dynamics demonstrates that the coupled motion of electrons and nuclei can be reduced to the study of nuclear motion on the predefined set of the electronic potentials $V_i(\mathbf{R})$.

In general, in order to describe the dynamics of the molecule all electronic states must be considered. In practice, however, a truncated set of electronic states can be used. Moreover, as one can see from Eq. (2.11), redistribution of the nuclear density between electronic states in time depends on the non-adiabatic coupling terms. In regions of nuclear space where these terms are important, the magnitude of the coefficients $|\chi_i(\mathbf{R}, t)|$ vary in time and the system can be seen as to undertake electronic transitions.

As one can see from the definition of the non-adiabatic couplings (see Eq. (2.12)), $\mathbf{F}^{\alpha}_{ji}(\mathbf{R})$ depends on the form of the electronic eigenstates $\Phi_j(\mathbf{r}, \mathbf{R})$ and $\Phi_i(\mathbf{r}, \mathbf{R})$. By applying the gradient operator to the electronic Schrödinger Eq. (2.4), one readily obtains the following useful expression for the derivative couplings

$$\mathbf{F}^{\alpha}_{ji}(\mathbf{R}) = \frac{\langle \Phi_j(\mathbf{r}, \mathbf{R}) | (\nabla_\alpha \hat{H}_e) | \Phi_i(\mathbf{r}, \mathbf{R}) \rangle_{\mathbf{r}}}{V_i(\mathbf{R}) - V_j(\mathbf{R})}. \tag{2.15}$$

This equation shows that the non-adiabatic coupling terms become important when the differences between the energies of the electronic states become small, and diverge for nuclear geometries for which the electronic states are degenerate. Nuclear configurations where the derivative coupling is singular are known as conical intersections [44, 47, 48].

The singularity appearing due to dependence of the electronic states on the nuclear configuration is problematic in numerical computations when treating the nuclear motion quantum mechanically. However, it can be circumvented by choosing a different representation of the electronic Hamiltonian $\hat{H}_e(\mathbf{r}, \mathbf{R})$ for which the derivative couplings are zero. Such a basis is termed a diabatic basis [49–51]. Contrary to the usual adiabatic electronic states, the diabatic ones are not the eigenstates of the electronic Hamiltonian which thus acquires off-diagonal matrix elements in the diabatic representation.

A diabatic basis can be obtained by an orthogonal transformation $\hat{\Theta}(\mathbf{R})$ of the adiabatic wavefunctions, taken as the solution of Eq. (2.4), and constructed such that the derivative couplings become negligibly small (or, ideally, vanish)

$$\langle \Phi^d_j(\mathbf{r}, \mathbf{R}) | \nabla_\alpha | \Phi^d_i(\mathbf{r}, \mathbf{R}) \rangle_{\mathbf{r}} = \langle \Phi_j(\mathbf{r}, \mathbf{R}) | \hat{\Theta}^\dagger(\mathbf{R}) \nabla_\alpha \hat{\Theta}(\mathbf{R}) | \Phi_i(\mathbf{r}, \mathbf{R}) \rangle_{\mathbf{r}} = 0, \tag{2.16}$$

where we denoted the new diabatic electronic states as $\Phi^d_i(\mathbf{r}, \mathbf{R}) = \hat{\Theta}(\mathbf{R}) \Phi_i(\mathbf{r}, \mathbf{R})$.

Within this transformation, Eq. (2.11) for the dynamics of a molecular system become

$$\begin{aligned} i\hbar\frac{\partial}{\partial t}\chi_i^d(\mathbf{R},t) = &\sum_\alpha \left(-\frac{\hbar^2}{2M_\alpha}\right)\nabla_\alpha^2\chi_i^d(\mathbf{R},t) \\ &+\sum_j \langle\Phi_j^d(\mathbf{r},\mathbf{R})|\hat{H}_e(\mathbf{r},\mathbf{R})|\Phi_i^d(\mathbf{r},\mathbf{R})\rangle_{\mathbf{r}}\chi_j^d(\mathbf{R},t), \end{aligned} \tag{2.17}$$

where the coupling between electronic states now transferred from the nuclear kinetic part to the off-diagonal elements of the electronic Hamiltonian. The obtained equation operates on the new set of nuclear wavefunctions $\{\chi_i^d(\mathbf{R},t)\}$ which are, in turn, a result of the projection of the total state of the system onto a particular diabatic basis set.

The detailed description of the methods for transformation from adiabatic electronic states to diabatic ones, as well as the methods for description and characterization of conical intersections is out of scope of the present thesis. A comprehensive overview of these interesting phenomena can be found elsewhere (see, e.g., Refs. [44, 48] and references therein).

2.2.2 Born–Oppenheimer approximation

In the case when the electronic states are well separated and vary slowly along the nuclear coordinates $\mathbf{R}$, it is possible to neglect all non-adiabatic coupling terms in Eq. (2.11). This corresponds to the physical picture that the electrons are always equilibrated to the much slower motion of the nuclei. In this case, the nuclear terms in Eq. (2.11) are uncoupled and reduce to

$$i\hbar\frac{\partial}{\partial t}\chi_i(\mathbf{R},t) = \left(\sum_\alpha \left(-\frac{\hbar^2}{2M_\alpha}\right)\nabla_\alpha^2 + V_i(\mathbf{R})\right)\chi_i(\mathbf{R},t). \tag{2.18}$$

This simplification and the resulting equation is known as the Born–Oppenheimer approximation [41, 42]. Contrary to the full set of Eqs. (2.11), the resulting simplified Eqs. (2.18) can be solved independently for every electronic state of interest.

In the frame of the Born–Oppenheimer approximation, the system prepared in a given electronic state will remain in the same state. Thus, the nuclear motion being described on the independent potential energy surfaces $V_i(\mathbf{R})$ and the population of the involved electronic states remains constant in time. This approximation and the underlying idea is central to most dynamical treatments in chemistry and even in those cases where it fails, it remains the reference to which one can compare and in terms of which one discusses this failure [44].

2.2.3 Static nuclei approximation

Various dynamical effects in a molecular system can take place before the nuclear dynamics comes into play. In this case, we can consider some particular nuclear geometry $\mathbf{R}_0$ and concentrate only on dynamics of electrons while the nuclear frame is fixed. Using Taylor approximation, the expansion of the nuclear wavefunctions in small region around $\mathbf{R}_0$ can be expressed as

$$\chi_i(\mathbf{R},t) = \chi_i(\mathbf{R}_0,t) + \frac{\chi_i'(\mathbf{R}_0,t)}{1!}(\mathbf{R}-\mathbf{R}_0) + ... \tag{2.19}$$

Truncating this series on the first term, we assume that the changes of the nuclear wavefunctions $\chi_i(\mathbf{R},t)$ around $\mathbf{R}_0$ with respect to $\mathbf{R}$ are negligible. Therefore, the action of the Laplace operator on it becomes zero

$$\nabla_\alpha^2 \chi_i(\mathbf{R}_0,t) = 0. \tag{2.20}$$

Substituting this relation into Eq. (2.18), we obtain

$$i\hbar\frac{\partial}{\partial t}\chi_i(\mathbf{R}_0,t) = V_i(\mathbf{R}_0)\chi_i(\mathbf{R}_0,t). \tag{2.21}$$

Multiplying this equation by the electronic eigenstates $\Phi_i(\mathbf{r},\mathbf{R}_0)$ on both sides, summing up over the electronic subspace, and using Eq. (2.4), we find

$$i\hbar\frac{\partial}{\partial t}\sum_i \chi_i(\mathbf{R}_0,t)\Phi_i(\mathbf{r},\mathbf{R}_0) = \hat{H}_e(\mathbf{r},\mathbf{R}_0)\sum_i \chi_i(\mathbf{R}_0,t)\Phi_i(\mathbf{r},\mathbf{R}_0), \tag{2.22}$$

which, after substitution of Eq. (2.7), becomes

$$i\hbar\frac{\partial}{\partial t}\Psi(\mathbf{r},\mathbf{R}_0) = \hat{H}_e(\mathbf{r},\mathbf{R}_0)\Psi(\mathbf{r},\mathbf{R}_0). \tag{2.23}$$

As one can see, the dynamics of electrons on fixed nuclear geometry $\mathbf{R}_0$ can be computed by solving the time-dependent Schrödinger equation with the electronic Hamiltonian $\hat{H}_e(\mathbf{r},\mathbf{R}_0)$ obtained on the corresponding nuclear point. This approach is known in the literature as the multielectron wave-packet propagation method [52] and allows to calculate *ab initio* fully correlated dynamics of few tens of electrons. The latter can be achieved with the help of the short-iterative Lanczos time-propagation technique [53, 54].

Despite that in the above presented approach the movement of the nuclei is completely neglected, it can serve as the starting point to study the ultrafast dynamics of the electronic cloud before the nuclear movement comes into play. This can be especially

useful in case of the moderate and big sized molecules for which the nuclear vibrations are found to be relatively slow [46].

Concluding this section, we would like to point out that only key milestones of the tremendous set of quantum molecular dynamics methods were considered. Nevertheless, some alternative approaches, such as e.g. the exact factorization of the molecular wavefunction will be discussed more specifically on cases of interest later.

2.3 Electronic structure methods

The main goal of this section is to provide a short insight into the methods for solution of the stationary Schrödinger Eq. (2.4) for the electronic subsystem. As was discussed in the previous section, fixing of the nuclear positions leads to a dependence of the electronic Hamiltonian $\hat{H}_e(\mathbf{r}, \mathbf{R})$ exclusively on the electronic coordinates $\mathbf{r}$, while the nuclear degrees of freedom $\mathbf{R}$ enter the Hamiltonian only as parameters.

To be specific, let us write explicitly the Hamilton operator of N moving electrons placed in the field of M stationary nuclei

$$\begin{aligned}\hat{H}_e(\mathbf{r}, \mathbf{R}) = &- \sum_{i=1}^{N} \frac{\hbar^2}{2m_e} \nabla_i^2 - \sum_{\alpha=1}^{M} \sum_{i=1}^{N} e_0^2 \frac{Z_\alpha}{|\mathbf{r}_i - \mathbf{R}_\alpha|} \\ &+ \sum_{i<j} e_0^2 \frac{1}{|\mathbf{r}_i - \mathbf{r}_j|} + \sum_{\alpha<\beta} e_0^2 \frac{Z_\alpha Z_\beta}{|\mathbf{R}_\alpha - \mathbf{R}_\beta|},\end{aligned} \tag{2.24}$$

where m_e and e_0 are the mass and the charge of the electron, respectively, and Z_α denotes the atomic number of the nucleus α. The presented Hamiltonian includes the kinetic energy operator of the electrons (first term) as well as the potential energy operators describing electron-nuclei, electron-electron and nuclei-nuclei interactions (last three terms), respectively.

Last term of Eq. (2.24), namely, the nuclei-nuclei interaction, enters into the Hamiltonian only as an additive constant and does not affect thus the eigenvectors of the time-independent electronic Schrödinger Eq. (2.4). For the sake of simplicity, it is convenient to exclude this constant term from the solution of Eq. (2.4), thus obtaining the following expression

$$\hat{H}'_e(\mathbf{r}, \mathbf{R}) \Phi_i(\mathbf{r}, \mathbf{R}) = E_i(\mathbf{R}) \Phi_i(\mathbf{r}, \mathbf{R}), \tag{2.25}$$

where the new electronic Hamiltonian is defined by the relation

$$\hat{H}_e(\mathbf{r},\mathbf{R}) = \hat{H}'_e(\mathbf{r},\mathbf{R}) + \sum_{\alpha<\beta} e_0^2 \frac{Z_\alpha Z_\beta}{|\mathbf{R}_\alpha - \mathbf{R}_\beta|}, \tag{2.26}$$

and the electronic potentials seen by nuclei become

$$V_i(\mathbf{R}) = E_i(\mathbf{R}) + \sum_{\alpha<\beta} e_0^2 \frac{Z_\alpha Z_\beta}{|\mathbf{R}_\alpha - \mathbf{R}_\beta|}. \tag{2.27}$$

Further in this section we will omit the dependency of the variables and operators on the spatial degrees of freedom and will use atomic units ($e_0^2 = \hbar = m_e = 1$) for compactness.

Many methods exist to calculate the electronic wavefunction of a molecular system [55]. Giving an overview of the existing approaches is out of scope of the present thesis. Here, we will introduce and examine only briefly one of the most important *ab initio* models of quantum chemistry, namely the Hartree–Fock method, since it serves not only as a useful approximation, but also constitutes a convenient starting point for other, more accurate models of the electronic structure theory. One such a model particularly used in the present work, namely Green's function formalism, will be presented and discussed as well. Special emphasis will be put on the treatment of the ionization process, i.e. the process by which a molecular system acquires a positive charge by losing an electron to form an ion. The effective method for calculation of the ionization potentials by means of the one-particle many-body Green's function, referred to as algebraic diagrammatic construction (ADC) [56, 57] method, will be presented and discussed in some detail.

2.3.1 Hartree–Fock approximation

The most primitive description of a system containing N electrons is given by the model of independent particles. This does not mean that one neglects the inter-electronic interactions, but only that their actual values are replaced by some "averaged" ones [58]. Each electron is moving in an effective field that represents the sum of the field caused by the nuclei and the averaged field created by the other electrons.

Within this model, every state a of a single electron can be described by its own wavefunction $\varphi_a(i) \equiv \varphi_a(\mathbf{r}_i, \sigma_i)$ that depends on both the spatial $\mathbf{r}_i$ and spin σ_i coordinates of i-th electron, and is referred to as the one-particle spin orbital. To ensure all required properties of the many-electron wavefunction (e.g. antisymmetry

with respect to electron permutations) a suitable ansatz representing a determinant of one-particle orbitals (known as a Slater determinant) is used [59]

$$\Phi_0^N = \frac{1}{\sqrt{N!}} \begin{vmatrix} \varphi_1(1) & \varphi_2(1) & \cdots & \varphi_N(1) \\ \varphi_1(2) & \varphi_2(2) & \cdots & \varphi_N(2) \\ \vdots & \vdots & \ddots & \vdots \\ \varphi_1(N) & \varphi_2(N) & \cdots & \varphi_N(N) \end{vmatrix}, \tag{2.28}$$

where $\varphi_a(i)$ is the a-th spin orbital considered as a function of the spatial and spin coordinates of the i-th electron.

We are interested in finding a set of spin orbitals $\{\varphi_a\}$ such that the Slater determinant formed from these orbitals is the best possible approximation to the ground state Φ_0^N of the N-electron system described by an electronic Hamiltonian $\hat{H}'_e$. According to the variational principle [60], the "best" spin orbitals are those which minimize the electronic energy of the ground state

$$E_0 = \langle \Phi_0^N | \hat{H}'_e | \Phi_0^N \rangle_{\mathbf{r}}. \tag{2.29}$$

It can be shown (see, e.g. Ref. [58]) that the optimal one-particle spin orbitals are the solutions of the Hartree–Fock equations

$$\left[\hat{h}(i) + \hat{v}(i)\right] \varphi_a(i) = \varepsilon_a \varphi_a(i), \tag{2.30}$$

where we have introduced two terms, namely the core-Hamiltonian

$$\hat{h}(i) = -\frac{1}{2}\nabla_i^2 + \sum_{\alpha=1}^{M} \frac{Z_\alpha}{|\mathbf{r}_i - \mathbf{R}_\alpha|}, \tag{2.31}$$

and an effective one-electron potential operator called the Hartree–Fock potential

$$\hat{v}(i) = \sum_b \langle \varphi_b(j) | \frac{1}{|\mathbf{r}_i - \mathbf{r}_j|} (1 - \hat{\mathcal{P}}_{ij}) | \varphi_b(j) \rangle_{\mathbf{r}_j}. \tag{2.32}$$

The operator $\hat{\mathcal{P}}_{ij}$ interchanges electrons i and j between orbitals $\varphi_b(j)$ and $\varphi_a(i)$.

In such formulation, the variational search for the ground electronic state Φ_0^N is reduced to the solution of a set of pseudo-eigenvalue problems with the spin orbitals as eigenfunctions and the energies of the spin orbitals as eigenvalues. One uses the term "pseudo" since the operator $\hat{v}(i)$ has a functional dependence on the solutions $\{\varphi_a\}$ of the other coupled equations. Thus, the solution of the Hartree–Fock equations is a nonlinear problem and needs to be solved by iterative procedures.

In practice, the exact mathematical solution of Eq. (2.30) formulated in terms of the search for optimal spin orbitals is possible only for very simple model situations. In other cases of interest, one needs to introduce an ansatz for representation of the

one-particle orbitals. It was shown by Roothaan [61] that the spin orbitals can be approximated by linear combination of some predetermined basis functions (basis orbitals)

$$\varphi_a = \sum_{\mu=1}^{K} c_\mu^a \xi_\mu, \tag{2.33}$$

where the orbitals ξ_μ form the basis set, and c_μ^a is the μ-th orbital coefficient of the a-th molecular orbital φ_a. Substitution of this expansion for every one-particle orbital into the Hartree–Fock Eq. (2.30) leads to the so-called Roothaan equation

$$\mathbf{FC} = \mathbf{SCE}, \tag{2.34}$$

where $\mathbf{F}$ is the representation of the $\hat{h}(i) + \hat{v}(i)$ operator in the basis ξ_μ (the Fock matrix), $\mathbf{C}$ is the matrix of the expansion coefficients, $\mathbf{S}$ is the overlap matrix of the basis orbitals, and $\mathbf{E}$ is the diagonal matrix of orbital energies. At this point, the problem of determining the Hartree–Fock molecular orbitals φ_a and orbital energies ε_a is reduced to solution of the matrix eigenequation (2.34).

Orbital energy ε_a characterizes in some sense the energy of a single electron in a molecule. In order to remove this electron from the molecule one needs to apply an energy sufficient to overcome the sum of kinetic energy of the electron and potential energy of its interaction with the particles in the system (i.e. with the other electrons and nuclei).

If one assumes that after removing/putting an electron from/into a molecule the spin orbitals are identical with those of the neutral molecule then the ionization potentials and electron affinities will be equal to the negative of the orbital energies ε_a. This statement is known as Koopmans' theorem [62], and is widely used as a first approximation for prediction properties of a molecule. By using the powerful formalism of second quantization [63], one can formally define electronic wavefunctions of the cationic and anionic states as

$$\Phi_p^{N-1} = \hat{c}_p \Phi_0^N, \qquad \text{and} \qquad \Phi_q^{N+1} = \hat{c}_q^\dagger \Phi_0^N, \tag{2.35}$$

where $\hat{c}_p$ and $\hat{c}_q^\dagger$ are annihilation and creation operators, respectively, Φ_p^{N-1} is an approximate wavefunction for the $(N-1)$-electron system obtained by removing an electron from spin orbital p, and Φ_q^{N+1} is an approximate wavefunction for the $(N+1)$-particle system obtained by putting an electron into spin orbital q. Utilizing these notations, and also Eq. (2.29), the ionization potential (IP) and electron affinity (EA) energies can be written as

$$-\,\mathrm{IP} = \varepsilon_p = \langle \Phi_0^N | \hat{H}_e' | \Phi_0^N \rangle_{\mathbf{r}} - \langle \Phi_p^{N-1} | \hat{H}_e' | \Phi_p^{N-1} \rangle_{\mathbf{r}}, \tag{2.36}$$

$$-\,\mathrm{EA} = \varepsilon_q = \langle \Phi_q^{N+1} | \hat{H}_e' | \Phi_q^{N+1} \rangle_{\mathbf{r}} - \langle \Phi_0^N | \hat{H}_e' | \Phi_0^N \rangle_{\mathbf{r}}. \tag{2.37}$$

The orbital energies, however, do not give the exact ionization potentials and electron

affinities because of two important effects. First, Φ_p^{N-1} and Φ_q^{N+1} are not the Hartree–Fock wavefunctions of the $(N-1)$- and $(N+1)$-particle systems since they were constructed from spin orbitals of the N-particle system. Second, the correlation effects between electrons must be considered in more accurate manner.

Despite its great success in the qualitative prediction of molecular properties, the neglect of the effects of electronic correlation between one-particle orbitals can lead to large deviations from the real properties of the system. Hence, a number of approaches, collectively called post-Hartree–Fock methods, have been devised to include electron correlation to the multi-electron wavefunction. The main purpose of the Hartree–Fock method is to provide a set of one-electron orbitals and energies, based on which systematic improvement of the electronic wavefunction and the electronic energy can be achieved.

2.3.2 Green's function method

One of these approaches, namely Green's function technique, is one of the most powerful tools of many-body theory. In this subsection we will consider the one-particle Green's function which contains information about the electron affinities and ionization potentials of a N-electron system. The conceptual advantage of Green's function methods lies in the fact that the interesting physical information is calculated directly without the need for separate calculations for the ground and ionic states. This, in turn, eliminates errors related to inconsistent treatment of the initial and final states [64]. The one-particle Green's function theory can provide a systematic framework that improves the ionization potentials and electron affinities obtained within Koopmans' theorem approximation.

The matrix of the one-particle Green's function $\mathbf{G}$ is defined with respect to a suitably chosen basis of one-particle states, which, in our case, is a discrete set of the Hartree–Fock orbitals, by

$$G_{pq}(t,t') = -i\langle\Phi_0^N|\hat{T}\hat{c}_p(t)\hat{c}_q^\dagger(t')|\Phi_0^N\rangle_{\mathbf{r}}, \tag{2.38}$$

where Φ_0^N is the exact non-degenerate ground state of the considered N-particle system, $\hat{c}_p(t)$ and $\hat{c}_q^\dagger(t')$ are the time dependent creation and annihilation operators in the Heisenberg representation and $\hat{T}$ is Wick's time-ordering operator. In the spectral representation, the physical meaning of the one-particle Green's function becomes clear [65]

$$G_{pq}(\omega) = \sum_n \frac{\langle\Phi_0^N|\hat{c}_p|\Phi_n^{N+1}\rangle_{\mathbf{r}}\langle\Phi_n^{N+1}|\hat{c}_q^\dagger|\Phi_0^N\rangle_{\mathbf{r}}}{\omega + E_0^N - E_n^{N+1} + i\eta} + \sum_m \frac{\langle\Phi_0^N|\hat{c}_q^\dagger|\Phi_m^{N-1}\rangle_{\mathbf{r}}\langle\Phi_m^{N-1}|\hat{c}_p|\Phi_0^N\rangle_{\mathbf{r}}}{\omega + E_m^{N-1} - E_0^N - i\eta}, \tag{2.39}$$

where $E_n^{N\pm1}$ and $\Phi_n^{N\pm1}$ denote the energies and states of the $(N \pm 1)$-particle systems, respectively, E_0^N is the ground-state energy, and a positive infinitesimal η is necessary to guarantee the convergence of the Fourier transformation. The first term in Eq. (2.39), let us denote it as $G_{pq}^{+}(\omega)$, contains the physical information on the $(N+1)$-particle system, and the second term (further denoted as $G_{pq}^{-}(\omega)$) on the $(N-1)$-particle one. The spectral representation $G_{pq}^{\pm}(\omega)$ can be written in a compact matrix notation as

$$\mathbf{G}^{\pm}(\omega) = \mathbf{x}^{\dagger}(\omega - \mathbf{\Omega}^{\pm})^{-1}\mathbf{x}, \tag{2.40}$$

where we defined the transition amplitudes matrix $\mathbf{x}$ as

$$x_{np} = \begin{cases} \langle \Phi_0^N | \hat{c}_p | \Phi_n^{N+1} \rangle_{\mathbf{r}}, & n \in \{N+1\} \\ \langle \Phi_n^{N-1} | \hat{c}_p | \Phi_0^N \rangle_{\mathbf{r}}, & n \in \{N-1\}, \end{cases} \tag{2.41}$$

and $\mathbf{\Omega}^{\pm}$ is the diagonal matrix of the ionization energies and electron affinities

$$\Omega_{nn}^{\pm} = \mp(E_0^N - E_n^{N\pm1}). \tag{2.42}$$

Moreover, in general, the spectral representation of any Green's function $\mathbf{\Gamma}(\omega)$ can be written in a form of Eq. (2.40) by choosing the appropriate transition amplitudes matrix $\mathbf{x}$ and the corresponding matrix of eigentransitions $\mathbf{\Omega}$.

As one can see from the definitions (see Eqs. (2.38) and (2.39)), the Green's function formalism operates with the accurate values (the electronic states and their energies), yet, for practical calculations, one has to introduce approximate schemes. The usual approximation procedure to evaluate the Green's function is by using a perturbation expansion. One of the most practical and systematic ways for constructing such type of approximations is the so-called algebraic diagrammatic construction (ADC) scheme introduced by Schirmer et al. [56, 66]. As one can see from the name, the ADC schemes are based on perturbation expansion of the Hamiltonian which can be directly compared to the diagrammatic series for the Green's function of interest.

Most of the methods in the formalism of the one-particle propagators use the so-called Dyson equation [63, 65] since it results to the relatively simple procedure of the comparison of the ADC form and the diagrammatic perturbation series for $\mathbf{\Gamma}(\omega)$. A characteristic (and not always desirable) feature of the Dyson methods is that in these approaches, the $(N \pm 1)$-particle parts of the one-particle Green's function ($\mathbf{G}^{+}(\omega)$ and $\mathbf{G}^{-}(\omega)$, respectively) are interconnected, and the resulting equations are defined with respect to configurational spaces comprising both $(N \pm 1)$-electron configurations. It was shown [57], however, that the ADC approximation can be applied directly to the Green's function of interest ($\mathbf{G}^{+}(\omega)$ or $\mathbf{G}^{-}(\omega)$ in our case), which does not employ the Dyson equation. This non-Dyson (nD) ADC scheme has several important advantages over the usual Dyson ADC scheme. Namely, it leads to a decoupling of the Dyson-type secular equations into two separate sets of equations, one for the ionization energies

and the other for the electron affinities. The price for this splitting of the secular problem into two parts is more complicated perturbation-theoretical expressions for the secular matrix elements.

The ADC approach is based on the following nondiagonal representation for arbitrary Green's function $\mathbf{\Gamma}(\omega)$

$$\mathbf{\Gamma}(\omega) = \mathbf{f}^\dagger(\omega - \mathbf{K} - \mathbf{C})^{-1}\mathbf{f}, \tag{2.43}$$

where $\mathbf{K} + \mathbf{C}$ is the non-diagonal effective interaction matrix and $\mathbf{f}$ is the matrix of effective transition amplitudes. The obtained nondiagonal representation can be transformed to the original Eq. (2.40) by solving the secular equation

$$(\mathbf{K} + \mathbf{C})\mathbf{Y} = \mathbf{Y}\mathbf{\Omega}, \qquad \mathbf{Y}^\dagger\mathbf{Y} = 1, \tag{2.44}$$

where $\mathbf{Y}$ denotes the matrix of eigenvectors, and the relation

$$\mathbf{x} = \mathbf{Y}^\dagger\mathbf{f} \tag{2.45}$$

allows one to determine the corresponding spectroscopic amplitudes. Mathematically, Eq. (2.43) can be treated as a result of transformation of the basis of exact states $\Phi_n^{N\pm1}$ to a complete set of so-called intermediate states $\tilde{\Phi}_J^{N\pm1}$ [67, 68]

$$\Phi_n^{N\pm1} = \sum_J Y_{Jn}\tilde{\Phi}_J^{N\pm1}. \tag{2.46}$$

The intermediate states can be constructed by the orthonormalization of the so-called correlated exited states $\hat{C}_J\Phi_0^N$ where $\hat{C}_J$ denote excitation operators of the manifold

$$\hat{C}_J = \begin{cases} \hat{c}_k, \hat{c}_a^\dagger\hat{c}_k\hat{c}_l, \hat{c}_a^\dagger\hat{c}_b^\dagger\hat{c}_k\hat{c}_l\hat{c}_m, ... & \text{for} \quad \mathbf{G}^-(\omega) \\ \hat{c}_a^\dagger, \hat{c}_a^\dagger\hat{c}_b^\dagger\hat{c}_k, \hat{c}_a^\dagger\hat{c}_b^\dagger\hat{c}_c^\dagger\hat{c}_k\hat{c}_l, ... & \text{for} \quad \mathbf{G}^+(\omega), \end{cases} \tag{2.47}$$

where k, l, m indices denote the occupied and a, b, c the virtual orbitals, respectively. The representation of the Green's function as shown in Eq. (2.43) is thus assigned as the Intermediate State Representation (ISR).

In the ADC method, the approximate schemes are constructed by expanding the matrices $\mathbf{K}$, $\mathbf{C}$, and $\mathbf{f}$ into a perturbation series

$$\begin{aligned} \mathbf{K} + \mathbf{C} = &\quad \mathbf{K} + \mathbf{C}^{(1)} + \mathbf{C}^{(2)} + ... \\ \mathbf{f} = &\quad \mathbf{f}^{(0)} + \mathbf{f}^{(1)} + \mathbf{f}^{(2)} + ... \end{aligned} \tag{2.48}$$

Substitution of these relations into Eq. (2.43) with simultaneous expansion of the denominator in an infinite series and consequent accumulation of the perturbation

terms of the same order leads to

$$\begin{aligned}\mathbf{\Gamma}(\omega) = \quad & \mathbf{f}_1^{(0)\dagger}(\omega - \mathbf{K}_1)^{-1}\mathbf{f}_1^{(0)} \\ + \quad & \mathbf{f}_1^{(0)\dagger}(\omega - \mathbf{K}_1)^{-1}\mathbf{f}_1^{(1)} + \mathbf{f}_1^{(1)\dagger}(\omega - \mathbf{K}_1)^{-1}\mathbf{f}_1^{(0)} \\ + \quad & \mathbf{f}_1^{(0)\dagger}(\omega - \mathbf{K}_1)^{-1}\mathbf{C}_{11}^{(1)}(\omega - \mathbf{K}_1)^{-1}\mathbf{f}_1^{(0)} + \ldots\end{aligned} \tag{2.49}$$

The explicit expressions for the matrix elements $\mathbf{K}_\mu$, $\mathbf{C}_{\mu\nu}^{(n)}$, and $\mathbf{f}_\mu^{(n)}$ can be derived by comparison of the expansion (2.49) with the diagrammatic perturbation expansion for $\mathbf{\Gamma}(\omega)$. Hence, the ADC method opens a highly systematic way for infinite partial summations for the $\mathbf{\Gamma}(\omega)$ complete through a finite order of perturbation theory for formulation of approximations to an arbitrary Green's function. The resulting equations for the ADC matrix elements of the different Green's functions can be found elsewhere [56, 64, 69].

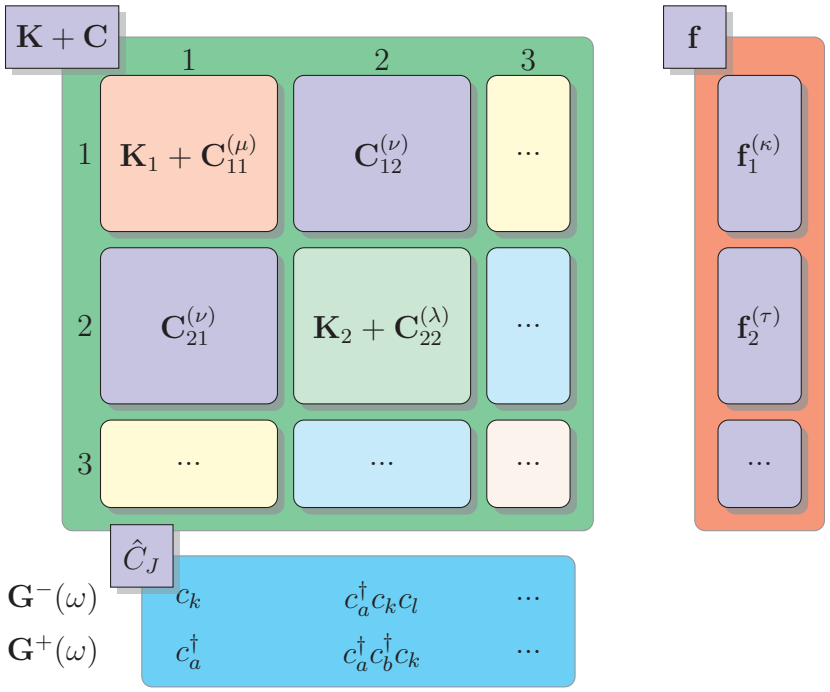

Figure 2.1: Block structure of the secular matrix $\mathbf{K} + \mathbf{C}$ and of the effective transition moment matrix $\mathbf{f}$ of the non-Dyson ADC scheme.

In Fig. 2.1 we show schematically the block structure of the $\mathbf{K} + \mathbf{C}$ and $\mathbf{f}$ matrices, as well as the manifold of the corresponding excitations operators, for representation of the $\mathbf{G}^+(\omega)$ and $\mathbf{G}^-(\omega)$ by nD-ADC scheme. The explicit nD-ADC expressions for matrix elements through third order of perturbations can be found in [57, 70]. The subsequent solution of the eigenvalue problem (2.44) delivers the ionization potentials/electron affinities matrix $\mathbf{\Omega}^\pm$, as well as the explicit form of the transformation matrix $\mathbf{Y}$ in ISR representation.

Among other advantages of the ISR formulation of the Green's function method is the possibility to evaluate the one-electron properties of the final molecular states. Using

Eq. (2.46), transition matrix elements D_{mn} of arbitrary one-particle operator $\hat{D}$ can be written as [70, 71]

$$D_{mn} = \langle \Phi_m^{N\pm1} | \hat{D} | \Phi_n^{N\pm1} \rangle_{\mathbf{r}} = \sum_{I,J} Y_{mI}^* \langle \tilde{\Phi}_I^{N\pm1} | \hat{D} | \tilde{\Phi}_J^{N\pm1} \rangle_{\mathbf{r}} Y_{nJ} = \mathbf{Y}_m^\dagger \tilde{\mathbf{D}} \mathbf{Y}_n, \tag{2.50}$$

where the matrix $\tilde{\mathbf{D}}$ is the representation of the operator $\hat{D}$ in ISR basis. The matrix $\tilde{\mathbf{D}}$ has a similar block and order structure as the $\mathbf{K} + \mathbf{C}$ matrix. The explicit expressions for the matrix elements can be obtained by similar procedure using perturbation theory [70].

The presented Green's function method within the ADC scheme combines matrix diagonalization of a secular matrix and perturbation theory for the matrix elements and the effective transition moments. The advantages of this approach are the regularity of the perturbation expansions, compactness of the configuration spaces, and size-consistency. The most essential drawback of the ADC methods is the restriction to systems with single-determinant character of the neutral electronic ground state. Furthermore, relying on a perturbational expansion scheme, the ADC energies typically do not converge smoothly with the growing perturbational order, but rather exhibit an oscillatory behavior [70, 72]. Nevertheless, the family of the nD-ADC methods in ISR formulation represents a powerful tool for treating the electron correlation and can be efficiently used for the highly-accurate calculation of the electronic states of the system. Another important advantage of the Green's function based methods is that they provide directly the full spectrum of the ionic or excited-state Hamiltonian in a single run. For comparison, with most of the popular wavefunction based methods, these states have to be obtained one by one, which substantially reduces their practical applicability to cases where only the lowest few states are populated and participate in the dynamics [23].

2.4 Interaction of a quantum system with the electromagnetic field

Let us consider two subsystems of particles which interact with each other. The particular form of such interaction depends on a nature of the system, as well as on the individual positions of the participating particles. Our goal here is to describe how one part of the system "feels" the behavior of the other one. Let us assume first that in some particular moment of time the state of the second subsystem is known. In this case, one can describe the influence of second subsystem on the first one by

some function which depends only on the state of the first subsystem. Namely, one can consider how the second subsystem affects a particular particle in the first one. It is clear that such interaction can be described by some function of coordinates which can be referred as a field. If, in addition, the second subsystem is evolving in time then the field will be also time-dependent. In this case, the field can be completely defined by a four-component vector which describes the evolution of the field at every spatial position in time.

As one can see, if we neglect the influence of the first subsystem on the second one then the behavior of the particles in the first subsystem can be completely described by knowing the nature of considered species and how they interact with each other, and by the time-dependent external field. It means that we can move beyond the consideration of the particular physics which leads to the creation of the field and concentrate only on the description of the interaction of this field with the system. In particular, in this section we will concentrate on the consideration of the interaction of the electromagnetic field with charged particles. An ultimate goal is to derive the Hamilton operator which describes a quantum system in the presence of external electromagnetic field. A few useful approximations, such as the dipole approximation, that simplifies dramatically the resulting Hamiltonian, will be discussed.

The text is organized as follows. In subsection 2.4.1 the Hamilton operator which describes the behavior of a particle in a field is derived from classical principles. Subsection 2.4.2 is devoted to the explanation of the connection between the mathematical formulation of electrodynamics and the real physical properties of the electromagnetic field. In subsection 2.4.3 one can find the derivation of the Maxwell equations in terms of the four-component field vector. In subsection 2.4.4 the mathematical gauge invariance of the four-component representation is shown. Finally, subsection 2.4.5 is devoted to the application of the introduced formalism for the derivation of the resulting Hamiltonian describing the quantum system in the presence of an electromagnetic field.

2.4.1 Mathematical description of a particle in a field

We start with the description of the interaction between a particle and a field represented by a four-component vector [73]

$$(\underbrace{A_x, A_y, A_z}_{\mathbf{A}}, \phi) \tag{2.51}$$

with a vector component $\mathbf{A}(\mathbf{r},t)$ and a scalar component $\phi(\mathbf{r},t)$. One needs to keep in mind that although the four-potential is Lorentz covariant, both the vector and scalar potentials by themselves depend upon the frame of reference, and upon a given gauge, and thus in general depend on the spatial position and time. For a particle moving in a given field, the classical action is made up of two parts: the action for the free particle, and a term describing the interaction of the particle with the field. The properties of a particle with respect to interaction with the electromagnetic field are determined by its charge q.

In order to connect the four-component vector describing the field with the three-dimensional physical Euclidean space describing the particle, one needs to project it on the same space. In the following we will concentrate on the description of the system instead of the field. Thus, it is more convenient to project a field vector on the space of a particle. In order to do that, one needs to keep in mind the metric signature of a four-space $(+,+,+,-)$ [74], where first three components represent spatial positions and the forth one represents a time. Thus, the projected field vector will have the spatial coordinates with a plus sign and the time component with a minus sign, respectively.

The action function for a charged particle in an electromagnetic field has the following form [75]

$$\mathcal{S} = \int \left(\frac{m}{2}\dot{\mathbf{r}}^2 dt + q\mathbf{A}\cdot d\mathbf{r} - q\phi dt \right), \tag{2.52}$$

where m is the mass of particle, $\mathbf{r}$ is the spatial position, and $\dot{\mathbf{r}}$ is the velocity. Introducing $d\mathbf{r} = \dot{\mathbf{r}}dt$, and changing to an integration over t,

$$\mathcal{S} = \int \left(\frac{m}{2}\dot{\mathbf{r}}^2 + q\mathbf{A}\cdot\dot{\mathbf{r}} - q\phi \right) dt, \tag{2.53}$$

one can easily extract the Lagrangian $\mathcal{L}$ for a charged particle in an electromagnetic field which is just the integrand in the above equation

$$\mathcal{L} = \frac{m}{2}\dot{\mathbf{r}}^2 + q\mathbf{A}\cdot\dot{\mathbf{r}} - q\phi. \tag{2.54}$$

The derivative $\partial\mathcal{L}/\partial\dot{\mathbf{r}}$ is the generalized momentum of the particle; we denote it by $\mathbf{p}$. Carrying out the differentiation, we find

$$\mathbf{p} = \frac{\partial}{\partial\dot{\mathbf{r}}}\mathcal{L} = m\dot{\mathbf{r}} + q\mathbf{A}. \tag{2.55}$$

From the Lagrangian we can find the Hamiltonian $\mathcal{H}$ for a particle in a field from the Legendre transformation [75]

$$\mathcal{H} = \dot{\mathbf{r}}\cdot\mathbf{p} - \mathcal{L} = \frac{m}{2}\dot{\mathbf{r}}^2 + q\phi. \tag{2.56}$$

However, the Hamiltonian must be expressed not in terms of the velocity, but rather in terms of the generalized momentum of the particle. To do that, one can use relation (2.55). Finally, we find the following expression for the Hamiltonian

$$\mathcal{H} = \frac{1}{2m}\left(\mathbf{p} - q\mathbf{A}\right)^2 + q\phi. \tag{2.57}$$

Using canonical quantization rules [76] we can promote conjugate variables to operators, $\mathbf{p} \to \hat{\mathbf{p}} = -i\hbar\nabla$, $\mathbf{r} \to \hat{\mathbf{r}}$ with commutation relations $[\hat{p}_i, \hat{x}_j] = -i\hbar\delta_{ij}$. Thus, resulting Hamilton operator can be written as

$$\hat{H} = \frac{1}{2m}\left(-i\hbar\nabla - q\mathbf{A}\right)^2 + q\phi. \tag{2.58}$$

In this representation, the coordinate operators work by multiplication and the momentum operators by taking the gradient. Other terms in the Hamiltonian are represented by Hermitian operators $\mathbf{A}(\mathbf{r}, t)$ and $\phi(\mathbf{r}, t)$ obtained from the corresponding classical quantities by replacing $\mathbf{r}$ by its quantum-mechanical counterpart.

One needs to keep in mind also that in the construction of the Hamiltonian, the fundamental property of a quantum particle – namely, its spin – was not considered. Indeed, since spin has no classical counterpart for a point-charge particle, it cannot be incorporated in the Hamiltonian by following the standard procedure for quantization of a classical Hamiltonian. However, in this thesis we will work in the frame of the electric dipole approximation which will be further described in details. Namely, it will be shown that the magnetic field component of the electromagnetic field can be neglected in all considerations of interest for the present work. Thus, here we will neglect the interaction of the magnetic field with the spin of the particle and will not consider ways to include it in the Hamilton operator.

2.4.2 Physical description of the electromagnetic field

A charge placed in an electromagnetic field is a subject of a force exerted by the field. In classical electrodynamics this force is usually referred to as Lorentz force. Following [77] we will give a derivation of the Lorentz force from classical Lagrangian $\mathcal{L}$ in terms of the vector and scalar potentials introduced in the previous subsection. Such a procedure will allow us to connect mathematical quantities introduced previously with physically measurable properties of the field, such as the electric and magnetic intensities of the field.

We must thus find the equations of motion for a charge in a given electromagnetic field. These equations are obtained by varying the action, i.e. they are given by the Lagrange equations [78]

$$\frac{d}{dt}\left(\frac{\partial}{\partial \dot{\mathbf{r}}}\mathcal{L}\right) = \frac{\partial}{\partial \mathbf{r}}\mathcal{L}, \tag{2.59}$$

where $\mathcal{L}$ is given by Eq. (2.54).

Calculating the partial derivatives on a right-hand side of Eq. (2.59), we obtain

$$\frac{\partial}{\partial \mathbf{r}}\mathcal{L} \equiv \nabla\mathcal{L} = q\nabla(\mathbf{A}\cdot\dot{\mathbf{r}}) - q\nabla\phi. \tag{2.60}$$

Using the vector analysis formula

$$\nabla(\mathbf{X}\cdot\mathbf{Y}) = (\mathbf{X}\cdot\nabla)\mathbf{Y} + (\mathbf{Y}\cdot\nabla)\mathbf{X} + \mathbf{X}\times(\nabla\times\mathbf{Y}) + \mathbf{Y}\times(\nabla\times\mathbf{X}), \tag{2.61}$$

where $\mathbf{X}$ and $\mathbf{Y}$ are two arbitrary vectors, and remembering that differentiation with respect to $\mathbf{r}$ is carried out for constant $\dot{\mathbf{r}}$, we find

$$\frac{\partial}{\partial \mathbf{r}}\mathcal{L} = q(\dot{\mathbf{r}}\cdot\nabla)\mathbf{A} + q\dot{\mathbf{r}}\times(\nabla\times\mathbf{A}) - q\nabla\phi. \tag{2.62}$$

The derivative $\partial\mathcal{L}/\partial\dot{\mathbf{r}}$ is the generalized momentum of the particle (2.55). Further, we write

$$\frac{d}{dt}\left(\frac{\partial}{\partial \dot{\mathbf{r}}}\mathcal{L}\right) = m\ddot{\mathbf{r}} + q\frac{d\mathbf{A}}{dt}. \tag{2.63}$$

The total differential $d\mathbf{A}$ consists of two parts: the change $(\partial\mathbf{A}/\partial t)dt$ of the vector potential with time at a fixed point in space, and the change due to the motion from one point in space to another at distance $d\mathbf{r}$. This second part is equal to $(d\mathbf{r}\cdot\nabla)\mathbf{A}$. Thus, we can rewrite the second term in Eq. (2.63)

$$\frac{d\mathbf{A}}{dt} = \frac{\partial\mathbf{A}}{\partial t} + (\dot{\mathbf{r}}\cdot\nabla)\mathbf{A}. \tag{2.64}$$

Therefore, the Lagrange equation, after substitution of both parts and some simplification, takes the form

$$m\ddot{\mathbf{r}} = q\left[-\frac{\partial\mathbf{A}}{\partial t} - \nabla\phi + \dot{\mathbf{r}}\times(\nabla\times\mathbf{A})\right]. \tag{2.65}$$

This is the equation of motion for a particle in an electromagnetic field. On the left-hand side stands the derivative of the particle's momentum with respect to time. Therefore, the expression on the right-hand side in Eq. (2.65) is the force exerted on the charge in an electromagnetic field and is referred to as Lorentz force. One can see that this force consists of two parts. The first part (first and second terms) does not depend on the velocity of the particle. The force of the first type, per unit charge, is

called the electric field; we denote it by **E**. So by definition,

$$\mathbf{E} \equiv -\frac{\partial \mathbf{A}}{\partial t} - \nabla\phi. \tag{2.66}$$

The second part (third term in Eq. (2.65)) depends on the velocity, being proportional to the velocity and perpendicular to it. The force of the second type, per unit charge, is called the magnetic field; we denote it by **B**

$$\mathbf{B} \equiv \nabla \times \mathbf{A}. \tag{2.67}$$

The equation for the Lorentz force, which defines the motion of a charge in an electromagnetic field, can now be written as

$$\mathbf{F} = q(\mathbf{E} + \dot{\mathbf{r}} \times \mathbf{B}). \tag{2.68}$$

Thus, we can connect the vector and scalar potentials **A** and ϕ, which mathematically describe the field, with the real physically measurable quantities **E** and **B**, which are the electric and magnetic field intensities respectively. We note that the potentials **A** and ϕ contain four rather than six components as **E** and **B**. The scalar and vector potentials thus provide a more compact representation of the electromagnetic field than do the observable electric field strength **E** and magnetic induction **B**.

2.4.3 Maxwell's equations in vacuum

The behavior of the electric and magnetic fields is governed by Maxwell's equations. In this subsection, we present only the main definitions and results which are needed for the scope of this thesis; for a detailed description of the electromagnetic theory see, e.g. Refs. [77, 79, 80].

In absence of charges and sources, Maxwell's equations can be expressed as follows

$$\nabla \cdot \mathbf{E} = 0, \qquad \text{Gauss' law (electric)}, \tag{2.69}$$

$$\nabla \times \mathbf{E} = -\frac{\partial \mathbf{B}}{\partial t}, \qquad \text{Faraday's law}, \tag{2.70}$$

$$\nabla \cdot \mathbf{B} = 0, \qquad \text{Gauss' law (magnetic)}, \tag{2.71}$$

$$\nabla \times \mathbf{B} = \varepsilon_0 \mu_0 \frac{\partial \mathbf{E}}{\partial t}, \qquad \text{Ampère-Maxwell law}, \tag{2.72}$$

where ε_0 is the electric constant (the permittivity of vacuum), μ_0 is the magnetic constant (the permeability of vacuum). Such a form of Maxwell's equations is possible

within the assumption that the particles in the system are far enough from a source of the electromagnetic radiation in order to neglect the interaction between them. Consequently, we can restrict ourselves from simultaneous coupled solution of the Schrödinger equation for the system in the field and Maxwell's equations for the electromagnetic field by itself. Thus, here we will consider the solution of Maxwell's equation in a vacuum and further we will use this solution for constructing a particular form of the Hamilton operator (2.58).

Let us now rewrite Maxwell's equations in terms of scalar and vector potentials by using relations (2.66) and (2.67). Defining the electric and magnetic fields through the potentials we automatically fulfill two of Maxwell's equations: Gauss' law for magnetism

$$\nabla \cdot \mathbf{B} = \nabla \cdot (\nabla \times \mathbf{A}) = 0, \tag{2.73}$$

since the divergence of the curl of any vector field $\mathbf{A}$ is always zero, and Faraday's law

$$\nabla \times \mathbf{E} = \nabla \times \left(-\nabla\phi - \frac{\partial \mathbf{A}}{\partial t} \right) = -\frac{\partial}{\partial t}(\nabla \times \mathbf{A}) = -\frac{\partial \mathbf{B}}{\partial t}, \tag{2.74}$$

since the curl of the gradient of any twice-differentiable scalar field ϕ is also always zero. As a consequence, Eqs. (2.71) and (2.70) are satisfied whenever the electric and the magnetic fields are expressed in terms of the vector and scalar potentials according to Eqs. (2.66) and (2.67).

Substituting the scalar and vector potentials into the second pair of Maxwell's equations (Eqs. (2.69) and (2.72)), we obtain the following second-order partial differential equations for the scalar and vector potentials

$$\nabla^2\phi + \frac{\partial}{\partial t}(\nabla \cdot \mathbf{A}) = 0, \tag{2.75}$$

$$\left(\nabla^2 \mathbf{A} - \varepsilon_0\mu_0 \frac{\partial^2 \mathbf{A}}{\partial t^2} \right) - \nabla \left(\nabla \cdot \mathbf{A} + \varepsilon_0\mu_0 \frac{\partial \phi}{\partial t} \right) = 0, \tag{2.76}$$

where we have utilized the curl of a curl relation $\nabla \times (\nabla \times \mathbf{A}) = \nabla(\nabla \cdot \mathbf{A}) - \nabla^2\mathbf{A}$. These equations taken together are as powerful and complete as the original Maxwell's equations. Once we obtain the solution of these equations, we can get $\mathbf{E}$ and $\mathbf{B}$ from the relations (2.66) and (2.67). Thus, we have another form of the electromagnetic laws which are exactly equivalent to Maxwell's equations, and in many situations much simpler to handle.

2.4.4 Gauge invariance of the electromagnetic field

An important consequence of the "conditional independence" of mathematical and physical description of a field is the possibility to introduce a mathematical gauge which retains the physical properties of the field unchanged under some transformation [81]. Namely, if the transformation

$$\mathbf{A} \to \mathbf{A}' = \mathbf{A} + \nabla\Lambda \tag{2.77}$$

is made, then $\mathbf{B}$ remains unchanged, since

$$\mathbf{B} = \nabla \times (\mathbf{A} + \nabla\Lambda) = \nabla \times \mathbf{A}. \tag{2.78}$$

However, this transformation changes $\mathbf{E}$ according to

$$\mathbf{E} = -\nabla\phi - \frac{\partial \mathbf{A}}{\partial t} - \nabla\frac{\partial \Lambda}{\partial t} = -\nabla\left(\phi + \frac{\partial \Lambda}{\partial t}\right) - \frac{\partial \mathbf{A}}{\partial t}. \tag{2.79}$$

If another change

$$\phi \to \phi' = \phi - \frac{\partial \Lambda}{\partial t} \tag{2.80}$$

is made then $\mathbf{E}$ also remains the same. Hence, the electric $\mathbf{E}$ and magnetic $\mathbf{B}$ fields are unchanged if one takes any function $\Lambda(\mathbf{r}, t)$ and simultaneously transforms the vector $\mathbf{A}$ and scalar ϕ potentials via the transformations (2.77) and (2.80). The potentials are therefore not uniquely defined; the vector potential is determined to within the gradient of an arbitrary function, and the scalar potential to within the time derivative of the same function.

Let us now investigate how a gauge transformation changes the Hamilton operator and wavefunction in the Schrödinger Eq. (2.1) [82]. As one can see from Eq. (2.58), the Hamiltonian depends on the scalar ϕ and vector $\mathbf{A}$ potentials. Clearly, a gauge transformation of potentials leads to a different Hamiltonian and as a result to a different solution of the Schödinger equation

$$i\hbar\frac{\partial \psi}{\partial t} = \hat{H}(\mathbf{A}, \phi)\psi \qquad \to \qquad i\hbar\frac{\partial \psi'}{\partial t} = \hat{H}(\mathbf{A}', \phi')\psi'. \tag{2.81}$$

To establish the relationship between ψ and ψ', let us consider the relation for the gauge transformed first term of the Hamiltonian

$$-i\hbar\nabla - q\mathbf{A} - q\nabla\Lambda = \exp\left(iq\frac{\Lambda}{\hbar}\right)(-i\hbar\nabla - q\mathbf{A})\exp\left(-iq\frac{\Lambda}{\hbar}\right), \tag{2.82}$$

where application of $-i\hbar\nabla$ to the exponential introduces the term $-q\nabla\Lambda$. It is easy to see that the square of this operator can be written as

$$(-i\hbar\nabla - q\mathbf{A} - q\nabla\Lambda)^2 = \exp\left(iq\frac{\Lambda}{\hbar}\right)(-i\hbar\nabla - q\mathbf{A})^2 \exp\left(-iq\frac{\Lambda}{\hbar}\right). \tag{2.83}$$

Furthermore, the remaining part of the gauge transformed Schrödinger equation can be written as

$$\left(q\phi - q\frac{\partial\Lambda}{\partial t} - i\hbar\frac{\partial}{\partial t}\right) = \exp\left(iq\frac{\Lambda}{\hbar}\right)\left(q\phi - i\hbar\frac{\partial}{\partial t}\right)\exp\left(-iq\frac{\Lambda}{\hbar}\right). \tag{2.84}$$

Combining these two parts, we can write

$$\left(\hat{H}(\mathbf{A}', \phi') - i\hbar\frac{\partial}{\partial t}\right) = \exp\left(iq\frac{\Lambda}{\hbar}\right)\left(\hat{H}(\mathbf{A}, \phi) - i\hbar\frac{\partial}{\partial t}\right)\exp\left(-iq\frac{\Lambda}{\hbar}\right). \tag{2.85}$$

We find that, if ψ is a solution to the untransformed Schrödinger equation, then $\psi' = \exp(i/\hbar q\Lambda)\psi$ represents a solution of the gauge-transformed Schrödinger equation.

As one can see, the transformations (2.77) and (2.80) lead to the addition of a phase factor to the gauge-transformed wavefunction. However, the real observable properties of the system depend on the absolute square of the wavefunction $|\psi'|^2 = |\psi|^2$ and thus remain unchanged. We, therefore, can conclude that a gauge transformation of the scalar ϕ and vector $\mathbf{A}$ potentials does neither change the electric and magnetic field intensities $\mathbf{E}$ and $\mathbf{B}$, nor the observable properties, resulting from the solution of the Schrödinger equation, and can thus be used for making the problem mathematically more tractable.

In particular, let us investigate the so-called Coulomb, radiation, or transverse gauge [80, 81]. This is the gauge in which the resulting $\mathbf{A}'$ and ϕ' become

$$\nabla \cdot \mathbf{A}' = 0, \qquad \text{and} \qquad \phi' = 0. \tag{2.86}$$

To ensure that the Coulomb gauge conditions are satisfied, we require that the transformation function Λ must satisfy the system of coupled equations, derived from Eqs. (2.77) and (2.80)

$$\nabla^2\Lambda = -\nabla \cdot \mathbf{A}, \tag{2.87}$$

$$\frac{\partial\Lambda}{\partial t} = \phi. \tag{2.88}$$

If we take the transformation in the form $\Lambda = \int \phi(\mathbf{r}, t)dt$, Eq. (2.88) is automatically satisfied, and the solution of Eq. (2.87) also exists, due to the fact that after taking the time derivative $\partial/\partial t$ and using Schwarz's theorem (the symmetry of second derivatives), it is equivalent to the Maxwell Eq. (2.75). To simplify further the notations, we will omit prime indices in $\mathbf{A}'$ and ϕ' and use them in the original form $\mathbf{A}$ and ϕ.

Let us now investigate how the remaining Maxwell's Eqs. (2.75) and (2.76) look like after making a Coulomb gauge transformation. It is clear that by taking the vector and scalar potentials in the form (2.86), Eq. (2.75) is satisfied automatically and the last equation becomes

$$\nabla^2 \mathbf{A} = \varepsilon_0 \mu_0 \frac{\partial^2 \mathbf{A}}{\partial t^2}. \tag{2.89}$$

As one can see, the gauge transformation of the set of Maxwell's equations has led us to the well-known wave equation describing the electromagnetic field in vacuum. The solution of this dramatically simplified equation is still general in the vacuum and in the absence of sources of charge. Thus, by solving this equation one can obtain an electromagnetic wave, which moves in space and affects the particles in a system through the coupling terms in the Hamilton operator (2.58). Moreover, we have showed that a gauge transformation allows us to modify not only Maxwell's equations but also the Hamiltonian without changing the physical properties of the system. But it is even more attractive that we can use one gauge for the solution of the Maxwell equations, in order to obtain a particular view of the electromagnetic potential, and then use another gauge to simultaneously transform the obtained solution and to simplify the resulting Hamiltonian.

2.4.5 Electric dipole Hamiltonian

The most general solution of Eq. (2.89) can be written as a sum of two arbitrary functions [79]

$$\mathbf{A}(\mathbf{r}, t) = f(\mathbf{r} - ct) + g(\mathbf{r} + ct), \tag{2.90}$$

representing a wave propagating through vacuum with the speed of light $c = 1/\sqrt{\varepsilon_0 \mu_0}$. In principle, since the equation is linear, the three-dimensional wave equation can have solutions which are plane waves moving in any direction. Thus, the most convenient way to represent a general solution of the wave equation is to expand it in a basis of plane waves moving in all directions and satisfying Eq. (2.90). Namely, let us use the basis of complex exponents

$$\mathbf{A}(\mathbf{r}, t) = \sum_{\omega, \mathbf{k}} A_0^{\omega, \mathbf{k}}(t) \mathbf{e}^{\omega, \mathbf{k}} \exp\left[i(\mathbf{k} \cdot \mathbf{r} - \omega t + \varphi^{\omega, \mathbf{k}}) \right], \tag{2.91}$$

where each set of indices in the summation represents a particular wave with frequency ω propagating in space in the direction along the wavevector $\mathbf{k}$, with a spatial period $\lambda = 2\pi/|\mathbf{k}|$. The wave has an amplitude $A_0^{\omega, \mathbf{k}}(t)$ which is directed along the polarization unit vector $\mathbf{e}^{\omega, \mathbf{k}}$ and the phase shift $\varphi^{\omega, \mathbf{k}}$.

Now, knowing the explicit expression for the electromagnetic field propagating in

space, we can investigate how such a wave interacts with the system. In principle, by substituting the obtained plane wave expansion into the Hamilton operator (2.58) and remembering that within the introduced Coulomb gauge $\nabla \cdot \mathbf{A} = 0$ and $\phi = 0$, one can obtain the terms which correspond to the interaction of a charged particle with the electromagnetic field. However, the real numerical solution of the Schrödinger equation with this Hamiltonian is still a challenging task, in particular, due to the necessity to calculate the action of the $\exp[i\mathbf{k}\cdot\mathbf{r}]$ operator. One can, however, use the Taylor series and expand this operator around some particular point $\mathbf{r}_0$ in space

$$\exp[i\mathbf{k}\cdot\mathbf{r}] = \exp[i\mathbf{k}\cdot\mathbf{r}_0]\exp[i\mathbf{k}\cdot(\mathbf{r}-\mathbf{r}_0)] = \exp[i\mathbf{k}\cdot\mathbf{r}_0](1 + i\mathbf{k}\cdot\mathbf{r} + ...). \tag{2.92}$$

We are interested in the consideration of the field in a small region around $\mathbf{r}_0$, namely in range of molecular size. In this case, we can assume that the molecule in some fixed moment of time does not feel the changes of the field along different directions and thus we can write $\exp[i\mathbf{k}\cdot\mathbf{r}] \approx \exp[i\mathbf{k}\cdot\mathbf{r}_0]$. This approximation is known as the electric dipole approximation (see, e.g. Refs. [83, 84]). By substituting this relation into Eq. (2.91) we eliminate the dependence of the vector potential on the spatial coordinates

$$\mathbf{A}^{\mathrm{DA}}(t) = \sum_{\omega,\mathbf{k}} A_0^{\omega,\mathbf{k}}(t)\mathbf{e}^{\omega,\mathbf{k}} \exp\Big[i(\mathbf{k}\cdot\mathbf{r}_0 - \omega t + \varphi^{\omega,\mathbf{k}})\Big], \tag{2.93}$$

where we have denoted the vector potential in the electric dipole approximation as $\mathbf{A}^{\mathrm{DA}}(t) = \mathbf{A}(\mathbf{r},t)|_{\mathbf{r}=\mathbf{r}_0}$. The independence of the vector potential on $\mathbf{r}$ leads to the disappearance of the magnetic field, as it follows from Eq. (2.67). Consequently, as we already mentioned before, we can completely neglect the interaction of the spin of the particle with the magnetic field.

Let us now further simplify the resulting Hamilton operator by choosing another gauge transformation. Namely, let us choose the transformation function in the so-called length form [82]

$$\Lambda = -\mathbf{r}\cdot\mathbf{A}^{\mathrm{DA}}(t). \tag{2.94}$$

It is clear, that the gradient of this function can be written as

$$\nabla\Lambda = -\mathbf{A}^{\mathrm{DA}}(t), \tag{2.95}$$

and as a result the gauge-transformed vector potential $\mathbf{A}' = 0$ (see Eq. (2.77)). The time derivative can thus be written as

$$\frac{\partial\Lambda}{\partial t} = -\mathbf{r}\cdot\frac{\partial\mathbf{A}^{\mathrm{DA}}(t)}{\partial t}, \tag{2.96}$$

which leads to the following gauge-transformed scalar potential (see Eq. (2.80) and remember that $\phi = 0$ in the Coulomb gauge)

$$\phi' = \mathbf{r}\cdot\frac{\partial\mathbf{A}^{\mathrm{DA}}(t)}{\partial t}. \tag{2.97}$$

Since in the new gauge, and within dipole approximation, the vector potential is equal to zero, it follows from Eq. (2.67) that the magnetic field component $\mathbf{B}$ of the field is also zero. Therefore, using Eq. (2.66) the electric field can be expressed as

$$\mathbf{E}(t) = -\nabla\phi' = -\frac{\partial \mathbf{A}^{\mathrm{DA}}(t)}{\partial t}. \tag{2.98}$$

Combining these two equations, one can finally derive

$$\phi' = -\mathbf{r}\cdot\mathbf{E}(t). \tag{2.99}$$

The resulting Hamilton operator can thus be written as

$$\hat{H} = -\frac{\hbar^2}{2m}\nabla^2 - q\mathbf{r}\cdot\mathbf{E}(t), \tag{2.100}$$

where the later term represents the interaction of the particle with the field.

In the more general case of many interacting particles, the derivation of the resulting interaction Hamiltonian is straightforward. In particular, if in the absence of a field the N-particle system can be described by the time-independent Hamiltonian $\hat{H}_0$, then the interaction of this system with the electromagnetic field in the electric dipole approximation can be described by the time-dependent operator

$$\hat{H}_I(t) = -\hat{\mathbf{D}}\cdot\mathbf{E}(t), \tag{2.101}$$

where we have introduced the electric dipole moment operator $\hat{\mathbf{D}} = \sum_{\alpha=1}^{N} q^\alpha \mathbf{r}^\alpha$.

In conclusion, we derived in this section an interaction Hamiltonian, which represents the influence of the electromagnetic field on the system of interacting charged particles. We considered the particles quantum mechanically, and treated the field classically. For the field we assumed that it only represents a time-dependent interaction potential that acts on the system, but the system does not influence the field. By considering the field in the frame of the electric dipole approximation, we neglected the spatial dependence of the field around a small region and in such a way simplified the resulting Hamiltonian.

3

Control of quantum dynamics by external laser field

This chapter contains our theoretical study of the possibilities to manipulate the quantum dynamics in simple model systems by using appropriately prepared ultrashort laser pulses

Contents

3.1 Introduction

The impressive progress in laser technology during last few decades [7, 85] has stimulated theoretical efforts directed on utilizing the exceptional properties of the laser radiation for deepening our understanding of fundamental properties of matter. As was already discussed in the introduction to this thesis, the development of coherent light sources permitted the creation of ultrashort light pulses with a duration from few femtoseconds in the infrared region and up to a few tens of attoseconds in the extreme ultraviolet region. Clearly, such ultrashort laser pulses has opened the door for scientists to deal with phenomena which were not accessible before.

Among the many possible applications of the ultrashort laser pulses, a very exciting one is the possibility to study and eventually control the electronic motion in molecular systems. The time scale of the electronic dynamics in a quantum system is defined by the particular energy states which are participating in the process. That is, in polyatomics the spacing between the electronic levels in the atoms and molecules ranges from sub-eV to tens of keV determining the time scale of the electronic motion from tens of femtoseconds to even below an attosecond [23]. Therefore, it is obvious that in order to manipulate such an ultrafast processes specific experimental techniques, allowing certain precision in the controlling of the laser pulse parameters are needed. A promising way to prepare required laser pulses which allows for a certain flexibility in designing wave forms with few-femtosecond durations based on the coherent spatial and temporal superposition of optical wave packets, has been developed by Goulielmakis and co-workers [86–88]. Being inspired by the possibility to synthesize laser pulses with arbitrary envelopes, we developed a methodology allowing one to obtain analytical expressions for laser pulses that can drive a two-level system in an arbitrarily chosen way [89].

The technique based on the control of the laser pulse envelope, however, has clear limitations and disadvantages. In particular, for very short laser pulses shaping of the field is still very challenging experimentally. Thus, alternative theoretical approaches taking into account the current experimental limitations are required. One of the possible ways to tackle this problem is the application of a numerical optimization procedure. The idea to use a numerical optimization to find pulse parameters for controlling the nuclear dynamics of a molecule undergoing an elementary chemical reaction was successfully applied in femtochemistry [2]. There, such schemes profited substantially from the large flexibility provided by the liquid crystals pulse-shaping techniques [90, 91], allowing the generation of practically arbitrarily complicated electrical fields with varying in time envelope and frequency. These techniques are,

unfortunately, not applicable for performing a direct control over the electron dynamics, as the resulting pulses are with a duration of tens or even hundreds of femtoseconds. One can, however, use the same idea but restrict substantially the set of parameters of the external electromagnetic field to be manipulated.

The aim of the present chapter is to demonstrate that by manipulating a very limited number of laser pulse parameters, one can still achieve a good enough control over the dynamics in complicated quantum systems. We illustrate here on model examples that by appropriately tailored simple laser pulses one can still manipulate the evolution of a quantum system, redistributing populations between involved states in a desired way.

The chapter is organized as follows. In section 3.2, the general principles of the quantum control theory are considered. In section 3.3 we present theoretical approaches allowing one to control quantum dynamics by an external electromagnetic field. In section 3.4, the developed methodologies for obtaining control pulses are applied on simple model systems. Finally, in section 3.5 we summarize obtained results, discuss some perspectives and conclude.

3.2 Quantum control theory

In this section, we present briefly the main idea behind the quantum control theory. We start with the description of a quantum system under the influence of external, time-dependent fields and proceed with the discussion of the methods for finding fields that control the evolution of the system. As will be seen, the problem of fully controllable dynamics is unsolvable analytically in most practically relevant cases. Nevertheless, it will be shown that in many situations the appropriate approximations can be used in order to derive analytical expressions for the field that "force" the system to follow the desired quantum path. In other cases of interest, it will be demonstrated that the quantum control problem can be reduced to the search for extreme points on a multidimensional surface formed by varying laser pulse parameters. The methods and algorithms for solving this problem will be discussed in some detail and analyzed.

The control problem discussed in this chapter is defined on a closed N-level quantum system with the Hamiltonian

$$\hat{H}(t) = \hat{H}_0 + \sum_{k=1}^{K} E_k(t)\hat{H}_k, \tag{3.1}$$

which includes a field-free term $\hat{H}_0$ and K Hermitian operators $\{\hat{H}_k\}$ that represent the coupling between K control fields $\{E_k(t)\}$ and the system. Here we will concentrate on the coupling of the system with electromagnetic fields within the dipole approximation and, thus, the coupling operators are, in general, the different directions of the electric dipole moment (detailed description of the dipole approximation can be found in subsection 2.4.5 of the present thesis).

The evolution of the system is governed by the time-dependent Schrödinger Eq. (2.1) with the formal solution

$$\psi(t) = \hat{T} \exp\left(-\frac{i}{\hbar}\int_0^t \hat{H}(t')dt'\right)\psi(0), \tag{3.2}$$

where $\hat{T}$ is the so-called time-ordering operator, ensuring that in a Taylor expansion of the exponent the operators are ordered chronologically, $\psi(t)$ is a time-dependent state vector and $\psi(0)$ is the initial state.

It is clear that by changing the parameters in the Hamilton operator (3.1), one can obtain different evolutions of the system although starting from the same initial condition $\psi(0)$. Since the operators $\{\hat{H}_k\}$ describe characteristic properties of the system and thus cannot be changed, one can alter the evolution of the system by manipulating the external control fields $\{E_k(t)\}$. The state vector, therefore, depends functionally on the external fields, $\psi(t;\{E_k(t)\})$, which play the role of control parameters.

The goal of quantum control theory [92, 93] is to find a set of real functions $\{E_k(t)\}$ which drive the quantum evolution of the system from its initial state $\psi(0)$ along a time-dependent state $\tilde{\psi}(t)$ in such a way that the value of the functional

$$J(t;\{E_k(t)\}) = \left|\langle\tilde{\psi}(t)|\psi(t;\{E_k(t)\})\rangle\right|^2 \tag{3.3}$$

is maximal at any moment of time. In principle, the time-dependent target state $\tilde{\psi}(t)$ can be a result of the action of some operator $\hat{\mathcal{O}}$ on the wave function $\psi(t)$, which, if Hermitian, can represent the control of some observable of the system, for example the electron density.

3.3 Methods to design the laser field

Designing laser fields for reaching a selected state of a quantum system has attracted a lot of efforts in the last few decades. Different schemes for control of the quantum dynamics were proposed, like π- and chirped pulses [94], stimulated Raman adiabatic

passage (STIRAP) [95–97], coherent [98, 99] and optimal control [100, 101], to name a few. It is usually supposed that before the interaction with the laser field the system is in a particular state and the scheme is designed such that after the interaction it is found in another (the desired) state. There are many interesting situations, however, when at the beginning the system is in a superposition of quantum states and we want to drive it to a new superposed state but controlling the weights with which each quantum state participates in the mixing. Thus, the main effort in this section will be put on developing methods of quantum control which are independent on choosing of initial and final states.

3.3.1 Analytical methods for control

In general, the maximization of a functional (3.3) is not a trivial mathematical problem and can be solved analytically only for very simple model systems, like for example a two-level quantum system [102–104]. Although rarely existing in nature in their pure form, two-level quantum systems often serve as models in many areas of physics and are used successfully for describing a large variety of physical phenomena. Situations when an external field is applied with the aim to control the quantum evolution of the two-level system can be encountered in nuclear magnetic resonance techniques [105], Josephson-junction circuits [106], spin rotations in quantum dots [107] and qubit control in general, as well as in laser-induced population transfer in atoms and molecules [95, 98].

Although most of the known schemes or protocols for controlling the dynamics of two-level systems are applicable also to systems being in a superposition of quantum states, they do not allow for control of the final state mixture. Being designed for achieving a population inversion, applied to two-level systems in a superposed state these schemes will bring the system to a new superposed state in which the weights with which each eigenstate participates are just swapped. In this subsection we show how one can obtain an analytic expression for a resonant pulse which is able to control not only the final state superposition, but also the exact path of the transition.

Let us briefly review the general formalism for describing the electric dipole interaction between a two-level system and a classical monochromatic field. The Hamiltonian in this case has the following form

$$\hat{H} = \varepsilon_1 |1\rangle\langle 1| + \varepsilon_2 |2\rangle\langle 2| - \hat{\mathbf{D}} \cdot \mathbf{E}(t), \tag{3.4}$$

where $|1\rangle$, $|2\rangle$ and ε_1, ε_2 are the two eigenstates and eigenenergies, respectively, of the

field-free Hamiltonian, $\hat{\mathbf{D}}$ is the electric dipole operator given by

$$\hat{\mathbf{D}} = \mathbf{e}_d \left(d|1\rangle\langle 2| + d^*|2\rangle\langle 1| \right), \tag{3.5}$$

with $\mathbf{e}_d$ being a unit vector in the direction of the dipole and d denoting the matrix element of the dipole operator between $|1\rangle$ and $|2\rangle$. In the case of a laser pulse with carrier frequency ω, the electric field $\mathbf{E}(t)$ can be written as

$$\mathbf{E}(t) = \boldsymbol{\mathcal{E}}(t)e^{-i\omega t} + \boldsymbol{\mathcal{E}}^*(t)e^{i\omega t}, \tag{3.6}$$

where $\boldsymbol{\mathcal{E}}(t)$ contains the polarization, amplitude, and envelope of the pulse. For simplicity, in the following we will take the dipole transition matrix element as real ($d = d^*$) and will get rid of the vector notations by taking the scalar product between $\hat{\mathbf{D}}$ and $\mathbf{E}(t)$, denoting by μ the projection of the dipole operator on the polarization axis of the electric field.

The general form of the wave function describing the evolution of the system is given by

$$|\psi(t)\rangle = c_1(t)e^{-i\varepsilon_1 t}|1\rangle + c_2(t)e^{-i\varepsilon_2 t}|2\rangle, \tag{3.7}$$

where $c_1(t)$ and $c_2(t)$ are the time-dependent (in general complex) amplitudes of the eigenstates $|1\rangle$ and $|2\rangle$, which, due to the orthonormality of the field-free states satisfy the condition $|c_1(t)|^2 + |c_2(t)|^2 = 1$ at all times.

Plugging this wave function in the time-dependent Schrödinger Eq. (2.1), one obtains the following set of coupled equations

$$\dot{c}_1(t) = ic_2(t)\mu \left(\mathcal{E}(t)e^{-i(\omega+\omega_0)t} + \mathcal{E}^*(t)e^{i(\omega-\omega_0)t} \right), \tag{3.8a}$$

$$\dot{c}_2(t) = ic_1(t)\mu \left(\mathcal{E}(t)e^{-i(\omega-\omega_0)t} + \mathcal{E}^*(t)e^{i(\omega+\omega_0)t} \right), \tag{3.8b}$$

where $\omega_0 = \varepsilon_2 - \varepsilon_1$ denotes the resonance frequency.

Since these equations are generally not solvable in analytical closed form, one usually introduces at this point the so-called rotating-wave approximation (RWA), meaning that the "rapidly oscillating terms", i.e. the exponentials $e^{\pm i(\omega+\omega_0)t}$ in Eqs. (3.8), are neglected. This approximation usually works well if $\omega \approx \omega_0$ (near resonance) and the coupling to the field is not very strong. We note that we need the RWA only for obtaining an analytical expression for the control field. As we will see, this field will give the desired results also when the exact equations [Eq. (3.8)] for the system evolution are used. Within the RWA, Eqs. (3.8) turn into the following set of equations

$$\dot{c}_1(t) = ic_2(t)\mu\mathcal{E}^*(t)e^{i\delta t}, \tag{3.9a}$$

$$\dot{c}_2(t) = ic_1(t)\mu\mathcal{E}(t)e^{-i\delta t}, \tag{3.9b}$$

where $\delta = \omega - \omega_0$ denotes the detuning. Equations (3.9) can be integrated exactly for arbitrary initial conditions to obtain a closed analytical solution.

Our purpose is, however, to find pulses which will bring the system into a state with a desired proportion of the final populations, given by the modulus square of the amplitudes c_1 and c_2. In order to find such solutions we can view Eqs. (3.9) as equations for $\mathcal{E}(t)$ and $\mathcal{E}^*(t)$, i.e.

$$\mathcal{E}^*(t) = -\frac{i}{\mu}\frac{\dot{c}_1(t)}{c_2(t)}e^{-i\delta t}, \tag{3.10a}$$

$$\mathcal{E}(t) = -\frac{i}{\mu}\frac{\dot{c}_2(t)}{c_1(t)}e^{i\delta t}. \tag{3.10b}$$

Substituting these expressions into Eq. (3.6) one obtains

$$E(t) = -\frac{i}{\mu}\left(\frac{\dot{c}_2(t)}{c_1(t)}e^{-i\omega_0 t} + \frac{\dot{c}_1(t)}{c_2(t)}e^{i\omega_0 t}\right). \tag{3.11}$$

Interestingly, the dependence on ω cancels out. Now we have an expression that connects the evolution of the amplitudes with the driving field. Therefore, if we want that the system evolves in a particular way, we can obtain through Eq. (3.11) the field which can drive this evolution.

As we mentioned, the amplitudes $c_1(t)$ and $c_2(t)$ are in principle complex functions, so we can write them in the form

$$c_k(t) = \tilde{c}_k(t)e^{i\varphi_k}, \quad k = 1, 2, \tag{3.12}$$

where $\tilde{c}_k(t)$ are real positive functions. Therefore, Eq. (3.11) takes the form

$$E(t) = -\frac{i}{\mu}\left(\frac{\dot{\tilde{c}}_2(t)}{\tilde{c}_1(t)}e^{-i(\omega_0 t+\varphi)} + \frac{\dot{\tilde{c}}_1(t)}{\tilde{c}_2(t)}e^{i(\omega_0 t+\varphi)}\right), \tag{3.13}$$

where $\varphi = \varphi_1 - \varphi_2$ is the relative phase between the amplitudes $c_1(t)$ and $c_2(t)$.

Let the evolution of the system proceeds according to the function $f(t)$, i.e. let $|c_1(t)|^2 = f(t)$. From the total population conservation condition we automatically have $|c_2(t)|^2 = 1 - f(t)$. Because $\tilde{c}_k(t)$ are both real and positive, we can write that $\tilde{c}_1(t) = \sqrt{f(t)}$ and $\tilde{c}_2(t) = \sqrt{1 - f(t)}$. From Eq. (3.13) we get the following field

$$E(t) = \frac{1}{\mu}\frac{\dot{f}(t)}{\sqrt{f(t)(1 - f(t))}}\sin(\omega_0 t + \varphi), \tag{3.14}$$

which has a carrier frequency exactly on resonance with the transition between the two states ω_0.

We see that if we want to drive the system in a particular way, we just need to describe this evolution via an appropriate control function $f(t)$. The control field obtained via Eq. (3.14) will then "force" the system to follow the quantum path given by $f(t)$. We note that the control field derived in Eq. (3.14) will keep the relative phase between the amplitudes. In principle, one can use a similar procedure assuming a time-dependent relative phase, i.e. taking $c_k(t) = \tilde{c}_k(t)e^{i\varphi_k(t)}$. This will lead to a chirped pulse (φ in Eq. (3.14) will be time-dependent) and we will introduce an additional term in the field containing the time derivatives of the individual phases. Since the field has to be real, one can, in principle, obtain conditions for an additional control function which can fix the way the relative phase evolves in time. However, in the present work we would like to concentrate only on the problem of population control.

Let us now illustrate the above reverse-engineering approach with a concrete analytical example. Suppose that initially our system is in a (superposed) state in which the population of $|1\rangle$ is equal to a_i and we want to drive the system to a state in which the population of $|1\rangle$ will be a_f. A convenient choice for the function controlling this transition is

$$f(t) = a_i(1 - g(t)) + a_f g(t), \tag{3.15}$$

where $g(t)$ is a function which goes smoothly from 0 to 1 and never exceeds 1, i.e. $0 \leq g(t) \leq 1$, $g(t) \xrightarrow{t\to-\infty} 0$, and $g(t) \xrightarrow{t\to\infty} 1$. A possible choice for such a function is the following

$$g(t) = \frac{1}{1 + e^{-\alpha t}}, \tag{3.16}$$

where the parameter α controls the duration of the transition from a_i to a_f.

Plugging this particular choice of control function $f(t)$ in Eq. (3.14), we obtain the following control field

$$E(t) = \frac{1}{\mu} \frac{\alpha(a_f - a_i)e^{\alpha t}}{(1 + e^{\alpha t})\sqrt{(1 - a_i + (1 - a_f)e^{\alpha t})(a_i + a_f e^{\alpha t})}} \sin(\omega_0 t + \varphi). \tag{3.17}$$

The parameter α connects the speed of transition with the field intensity. For a faster transition we will naturally need to apply a stronger field.

We would like to note that although focused on laser-driven population control, the scheme presented in the present subsection is general and could be applied for designing other types of control fields. For example, systems often studied for the purposes of quantum computing are spin systems interacting with a magnetic field. In this case, the Hamiltonian has the same form as in Eq. (3.4), just the interaction term has to be replaced by $-\boldsymbol{\mu} \cdot \mathbf{B}$, where $\boldsymbol{\mu}$ stands here for the magnetic moment and $\mathbf{B}$ for the magnetic field. As far as the resulting dynamical problem is the same, one may use the reverse-engineering approach presented here for obtaining magnetic fields that can drive a spin system in a desired way.

3.3.2 Methods based on numerical optimization

Despite of the great interest from a fundamental point of view, the analytical methods for obtaining optimum control laser fields are usually restricted to very simple systems. In most realistic cases, the analytical derivation of the laser field which drives the evolution of a system in predefined way is hardly feasible. Therefore, more general methods which can be used irrespective of the type of the considered system are required.

From a mathematical point of view, the control problem can be formulated as the search for

$$J_{\mathrm{opt}}(t;\{E_k^{\mathrm{opt}}(t)\}) = \max_{\{E_k(t)\}} J(t;\{E_k(t)\}) \tag{3.18}$$

on the time-dependent infinitely dimensional landscape formed by the projection of all possible solutions of the Schrödinger equation (2.1) on the target state $\tilde{\psi}(t)$. The set of real functions $\{E_k^{\mathrm{opt}}(t)\}$, which maximize the value of the considered functional (3.3), represent the optimal external fields.

In this form, the quantum control problem represents a very well studied optimization task. A large number of algorithms for solving optimization problems have been proposed. They can be divided into two classes: semi-analytical methods (for example the method of Lagrange multipliers [108]) and purely numerical methods (such as different gradient-based methods [109], stochastic methods [110] etc.).

3.3.2.1 Semi-analytical methods

The difficulty to solve a concrete optimization problem depends strongly on the non-linearity of the resulting control landscape, which reflects the nature of the investigated system, as well as on the complexity of the desired evolution path $\tilde{\psi}(t)$. In the case when the evolution of the quantum system is complicated and the initial and the target states are superpositions of several eigenstates of the unperturbed system, it is usually necessary to have enough flexibility in varying the external fields. For this reason, the class of considered functions describing the external fields should be as broad as possible. In this situation, the method of Lagrange multipliers [111] has proven to be especially useful. The solution of the equation (3.18) can be obtained by varying the

following functional

$$J' = J + \int_0^T \langle\chi(t)| \left(i\hbar\frac{\partial}{\partial t} - \hat{H}(t) \right) |\psi(t)\rangle dt, \tag{3.19}$$

where we have introduced the time-dependent Lagrange multiplier $\chi(t)$. In addition, the above functional can also be extended by some constraints, for example by restriction on the duration of the external field or by requirement that the influence of the field on the system is as small as possible etc.

To find the optimal external field from the functional (3.19), one can perform a total variation of it with respect to $\psi(t)$, $\chi(t)$ and $\{E_k(t)\}$. Since we are looking for a maximum of J', the necessary conditions are

$$\delta J' = 0 \quad \Rightarrow \quad \delta J'_{\psi(t)} = 0, \quad \delta J'_{\chi(t)} = 0, \quad \delta J'_{\{E_k(t)\}} = 0. \tag{3.20}$$

Explicit derivation of the corresponding variations leads to a set of coupled Schrödinger equations which can be solved, for example, by different iterative algorithms [112–114]. As a result, one usually obtains a set of complicated functions which represent the dependence of the envelope and frequency of the external field in time. This approach is usually referred to as quantum optimal control (QOC) theory [93] and was very much used in last few decades as a tool to find external fields that control the chemical reactivity of a molecule. The detailed description of the algorithms and implementation of the QOC theory is out of scope of the present thesis and can be found elsewhere (see e.g. [93] and references therein).

3.3.2.2 Purely numerical methods

Despite its great advantages, the application QOC in its classical form for designing pulses to control electron dynamics is somewhat limited. As we discussed above, due to experimental limitations, it is a very challenging to synthesize arbitrarily complicated ultrashort laser pulses. Imposing additional constraints on the pulse parameters, makes the QOC not very efficient. Instead, due to the dependency of the target functional on only a very limited set of parameters, the application of purely numerical methods for optimization becomes more suitable. Thus, the main idea that we follow is to represent the external fields as some simple model functions depending only on a few parameters, which we then optimize in order to achieve the required evolution of the system.

Due to the experimental limitations, the envelope of the ultrashort laser pulses is usually supposed to have a near-Gaussian form. Therefore, one can define the external

fields as

$$E(t) = E_0 \exp\left(-\frac{1}{\sigma^2}(t-t_0)^2\right)\cos\left(\omega(t)t+\varphi\right), \tag{3.21}$$

where E_0 is the electric field strength, t_0 is the time position of the field maximum, $\sigma = \tau/\sqrt{4\ln 2}$ with τ being the pulse duration (at FWHM), $\omega(t)$ is the laser frequency and φ is the carrier envelope phase (CEP).

By solving the time-dependent Schrödinger equation (2.1) with a laser field in the form of Eq. (3.21), one obtains the evolution of the system, which can be fully represented by the time-dependent amplitudes $c_k(t)$ of the eigenstates $|k\rangle$ of the field-free Hamiltonian $\hat{H}_0$ (see Eq. (3.1)), i.e.

$$|\psi(t)\rangle = \sum_k c_k(t)|k\rangle. \tag{3.22}$$

In the present work, however, we are interested only on the problem of population control, i.e. on the evolution of $|c_k(t)|^2$. Moreover, we will focus on controlling only the final population mixture, without paying attention to the particular evolution path. The only requirement is the smoothness of the population transfer, i.e. the absence of Rabi oscillations.

It might seem that the gradient-based methods can be an effective solution to the optimization problem. However, the functional defined in Eq. (3.3) usually forms a hyper-surface with a large number of local extrema. Therefore, purely local methods are not very practical in this case, as they can easily converge to an undesired local solution. Moreover, the curvature of the hyper-surface is usually strongly non-linear along the variations of different parameters. It requires, therefore, the use of adaptive algorithms for changing the variation step. Another important drawback of these methods is the relative difficulty to calculate the Hessians and the gradients.

An interesting alternative, we suggest to use for the problem at hand, are the so-called direct search algorithms. This class of methods for solving optimization problems does not require any information about gradients or higher derivatives of the objective function. Instead, these algorithms search a set of points around the current point, and then look whether the value of the objective function is lower than the value at the current point.

In this work, we have used the so-called mesh adaptive search (MADS) algorithm [115] implemented within NOMAD software package [116]. MADS is an iterative method for blackbox optimization of a functional under general nonlinear constraints. At each step, the algorithm searches a set of points in random directions, called a mesh, around the current point – the point computed at the previous step of the algorithm. The size of the mesh is defined adaptively at every time iteration, taking the computed values of the objective functional as a criterion. The mesh is formed by adding the current point to the scalar multiple of a set of vectors called pattern. If the pattern search algorithm finds a point in the mesh that improves the objective function at the current point, the new point becomes the current point at the next step of the algorithm. Despite

the fact that this algorithm is not fully global optimizer, by choosing an appropriate initial guess and mesh search criteria, it can produce a suitable solution.

3.4 Model examples

In this section, we present a few concrete examples of the implementation of the above described techniques for quantum control. The main idea is to demonstrate that by applying relatively simple tailored laser pulses one can achieve good enough control over quantum dynamics in complicated quantum systems.

3.4.1 Single resonant laser pulse

As a first test example, we will discuss the population control of a two-level system. We start with illustration of the validity of the reverse-engineering approach [89] described in subsection 3.3.1. We will use control function $f(t)$ in the form of Eq. (3.15) with $g(t)$ described by Eq. (3.16). Let us take the following numerical values for the two-level system parameters: $\mu = 6$ a.u., $\omega_0 = 0.02$ a.u., $a_i = 0.4$, $a_f = 1$, $\alpha = 0.01$, and $\varphi = 0$. That is, we have a two-level system which is initially in a non-stationary state, in which 40% of the total population is in level $|1\rangle$ and the remaining 60% are in $|2\rangle$, and we want to drive it such that we transfer the entire population into level $|1\rangle$, i.e., we want that after the pulse the system is in its lower eigenstate.

Substituting these parameters into Eq. (3.17) we obtain a laser pulse which is shown in the upper panel of Fig. 3.1. We see that it is slightly asymmetric with respect to the maximum intensity but otherwise very regular. The asymmetry actually reflects the "asymmetric" way we want to drive the system. The chosen parameters describe the situation in which the system is initially in a non-stationary state (a superposition of $|1\rangle$ and $|2\rangle$, with $|1\rangle$ containing 40% of the total population) and we drive it to a stationary state, i.e. after the pulse the system is in state $|1\rangle$ (see the blue solid curve in lower panel of Fig. 3.1). The special case of population inversion, i.e. when the populations of the states $|1\rangle$ and $|2\rangle$ before and after the pulse are swapped, will require a symmetric pulse. If we take a_f to be 0.6, Eq. (3.17) will give us a symmetric pulse.

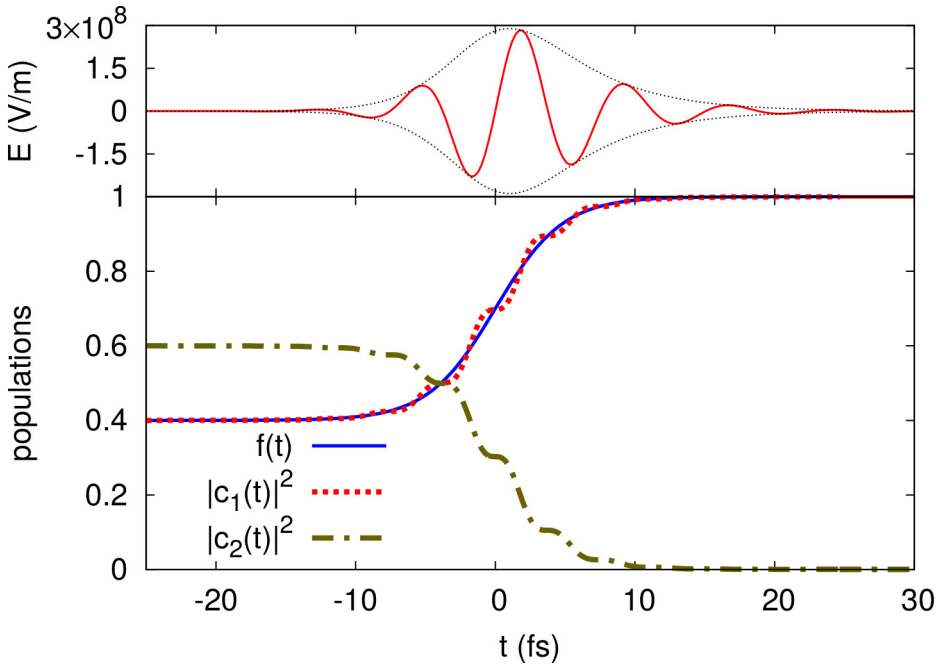

Figure 3.1: Upper panel: Laser pulse obtained through Eq. (3.17) using the following parameters: $\mu = 6$ a.u., $\omega_0 = 0.02$ a.u., $a_i = 0.4$, $a_f = 1$, $\alpha = 0.01$, and $\varphi = 0$. Lower panel: Evolution of the populations of the states $|1\rangle$ (red dotted) and $|2\rangle$ (green dash-dotted) of a two-level system driven by the such a laser pulse. The control function $f(t)$ used to obtain the driving field is depicted in blue solid. We see that the system is driven from a coherent superposition of states $|1\rangle$ (40%) and $|2\rangle$ (60%) to a system being only in state $|1\rangle$.

To check the validity of the above procedure, we can use the field obtained via Eq. (3.17) and solve numerically Eqs. (3.8), i.e. the equations before introducing the rotating-wave approximation. We remind that within the dipole approximation for the interaction with the field, these are the exact equations describing the evolution of the system. The result is depicted in the lower panel of Fig. 3.1, together with the control function $f(t)$ giving the evolution of the system within the RWA. We see that the system indeed follows the desired evolution and that the RWA is a quite good approximation in this case. The neglected rapidly oscillating terms introduce only small variations in the transition path.

It is important to know what is the regime in which the above approach for obtaining the driving field works well, i.e. when the RWA is a good approximation. The condition for the validity of the RWA is that the envelop of the pulse varies slowly with time in comparison to the field oscillations, determined by the carrier frequency ω_0. To exemplify this, let us take the same parameters as above but reduce the time for which we want to drive the system to the chosen final state. The transition time is governed by the parameter α which also determines the width of the pulse envelope. The result for the pulse obtained with $\alpha = 0.05$ (all other parameters were kept the same) is shown in Fig. 3.2 together with the evolution of the system. With these parameters we obtain a single-cycle pulse with which, as we see in the lower panel of Fig. 3.2, the

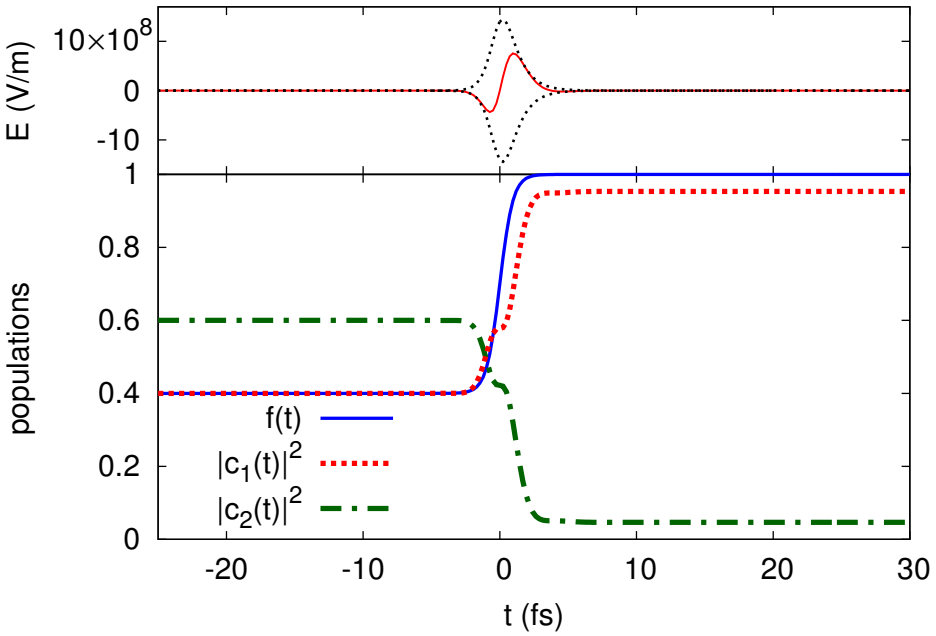

Figure 3.2: Upper panel: Laser pulse obtained through Eq. (3.17) using the same parameters as in Fig. 3.1 except $\alpha = 0.05$. Lower panel: Evolution of the populations of the states $|1\rangle$ (red dotted) and $|2\rangle$ (green dash-dotted) of a two-level system driven by the such a laser pulse. The control function $f(t)$ used to obtain the driving field is depicted in blue solid. We see that the full solution start to deviate from the RWA and the pulse is not able to bring the system 100% to state $|1\rangle$.

full solution starts to deviate more substantially from the one obtained within the RWA and we are no longer able to bring the system 100% to state $|1\rangle$. However, even for such a limiting pulse the RWA still gives reasonable results.

3.4.2 Linearly chirped laser pulses

As we discussed above, finding analytical solutions for the desired control field is possible only in very limited cases. There are many situations when approximations such as above mentioned RWA are not applicable. We will instead look for a numerically-exact solution of the full problem. Moreover, due to experimental limitations the variation of the envelop of an ultrashort laser pulse envelope is not an easy task. That is why, here we present the implementation of the optimization procedure to the two-level quantum control problem by varying of laser pulse frequency, instead of its envelope.

In this example we will look for an optimum laser pulse in the form of Eq. (3.21)

having a linear frequency chirp, i.e.

$$\omega(t) = at + b, \tag{3.23}$$

where a and b are some coefficients which ensure that the frequency has values $\omega(t_1) = \omega_{\min}$ and $\omega(t_2) = \omega_{\max}$ in the time moments t_1 and t_2, respectively. We will use the same parameters of the system as in previous subsection, namely, the energy difference between the levels $\omega_0 = 0.02$ a.u. $= 0.544$ eV, and the levels are coupled by transition dipole moment $\mu = 6$ a.u.

Let us first look at the case when the system is initially in its ground state $|1\rangle$ (i.e., $|c_1(0)|^2 = 1.0$) and we want to perform a population inversion, i.e. to drive the system to its excited state $|2\rangle$, using a Gaussian laser pulse with duration $\tau = 5$ fs, and carrier envelope phase $\varphi = 0$. The optimization of the population inversion has been done, therefore, by adjusting the maximum field strength E_0, and the frequency-chirping constants a and b. The results are presented in Fig. 3.3. We see that the pulse drives a full population transfer and that the transition is relatively smooth. The obtained optimal chirp is rather small, with a frequency sweep between 0.58 and 0.62 eV, i.e the pulse is slightly detuned from the resonant frequency of 0.544 eV. The maximum field strength of the pulse is a bit higher then in previous example, since the duration of a laser pulse is chosen to be shorter.

An especially interesting situation in the context of the electronic dynamics is when the system is initially in a superposition of states. Due to fact that the relative phase between two states starts to play a role in this case, for controlling the system we will need an additional flexibility in choosing the pulse parameters. Since we want to keep the Gaussian form of the pulse, such an additional parameter can be the CEP. To demonstrate this, let us take the initial state to be a superposition of the states $|1\rangle$ (60 %) and $|2\rangle$ (40 %) and try to find a pulse that can drive the system such that it finally lands on state $|2\rangle$. The parameters of the system are taken as before, but in addition to the laser pulse strength and frequency, we allow also the CEP φ to vary in the optimization procedure. The results are presented in Fig. 3.4. We see that for performing the desired transition, the pulse should have a frequency sweep which is about ten times larger (about 0.5 eV) compared to the previous case. The pulse intensity is lower than in previous case, indicating the fact that we start dynamics from mixture of states $|1\rangle$ and $|2\rangle$ instead of the 100% populated state $|1\rangle$ as was done in the first example.

Importantly, in both cases it is possible to find laser pulse parameters that can control the outcome of the evolution of a two-level system. Indeed, even by fixing some parameters (e.g., the laser pulse envelope and the duration), one has still enough flexibility to control a two-level system in a basically arbitrary way.

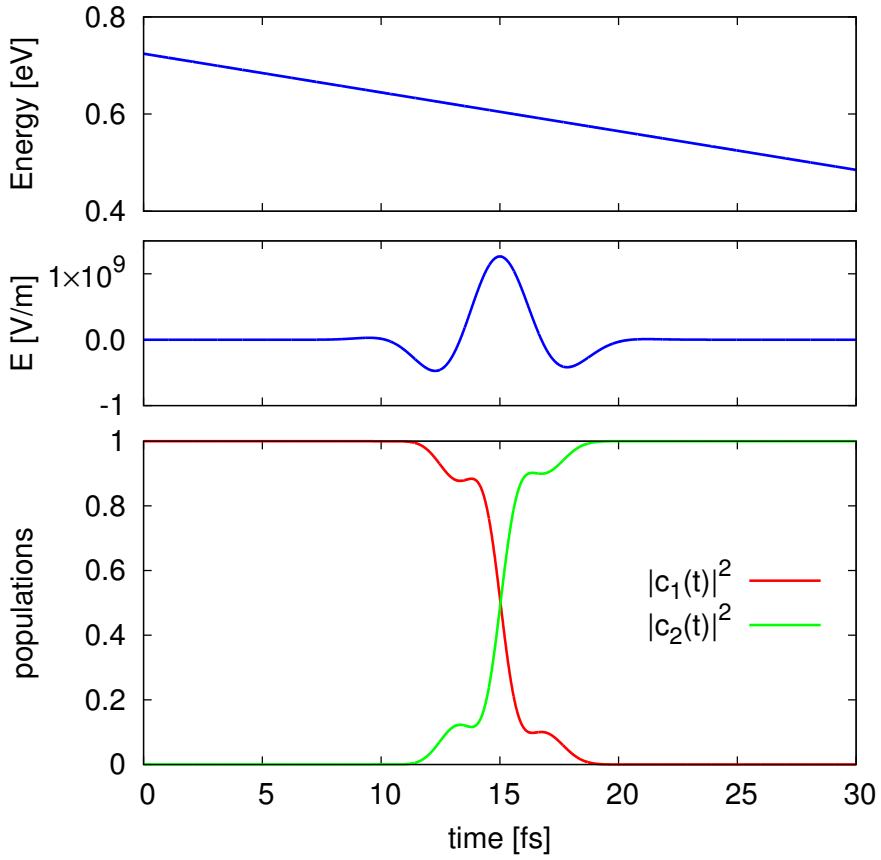

Figure 3.3: Population inversion in a two-level system driven by a single 5 fs Gaussian pulse with linear chirp. The optimized frequency variation of the pulse is shown in the upper panel and the pulse itself in the middle panel. The two-level system has the following parameters: the energy difference is taken to be 0.02 a.u. and the transition dipole moment $\mu = 6$ a.u.

3.4.3 Laser pulses with an arbitrary chirping

In case of more complex systems, e.g. when more than two states are participating in the population transfer or when there is no coupling between the initial and final states, one usually needs to have more freedom in manipulating the external fields. An interesting possibility is to make a nonlinear modulation of the pulse frequency. To demonstrate this, we will show in this example how one can achieve a population transfer in the so-called Λ-type three-level quantum system by using an ultrashort Gaussian pulse with a nonlinear chirp.

Consider the three-level Λ system schematically represented in Fig. 3.5. Suppose that in the beginning the system is in its ground state $|1\rangle$ and we want to transfer all the

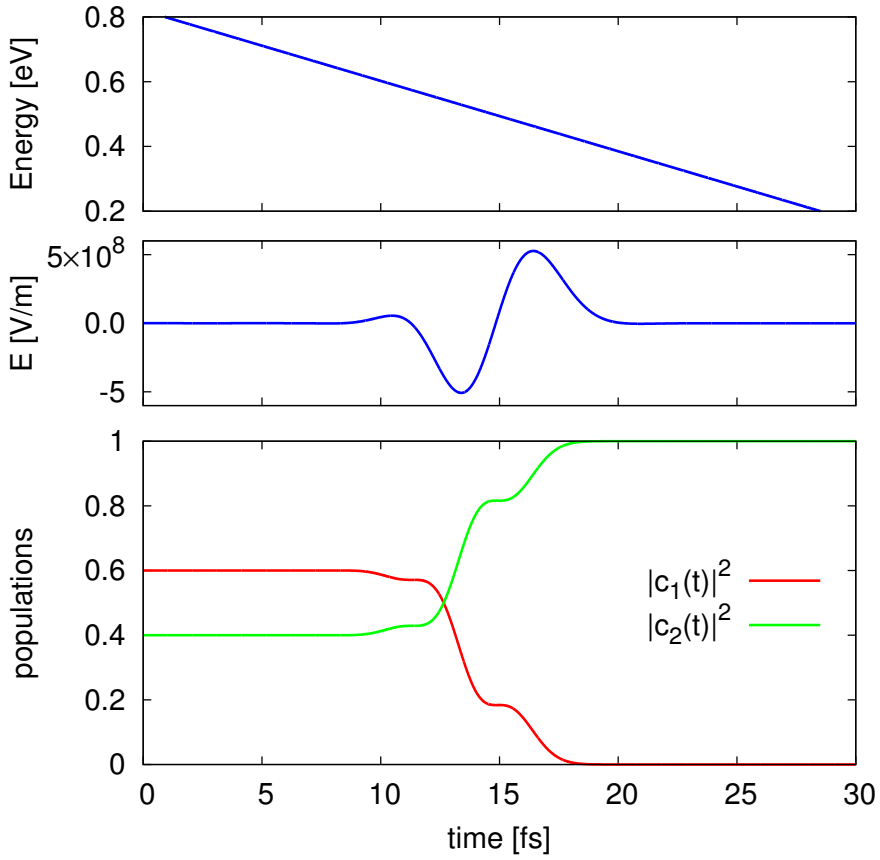

Figure 3.4: Population control of a two-level system in a superposition state $|\psi(t)\rangle = \sqrt{0.6}|1\rangle + \sqrt{0.4}|2\rangle$ by a single 5 fs Gaussian pulse with a linear chirp. The optimized frequency variation of the pulse is shown in the upper panel and the pulse itself in the middle panel. The two-level system has the same parameters as before (see Fig. 3.3). The pulse is optimized to drive the system to the excited state $|2\rangle$.

population into the middle excited state $|2\rangle$, but the states $|1\rangle$ and $|2\rangle$ are not coupled directly. In this case, one can use the state $|3\rangle$, coupled both to $|1\rangle$ and $|2\rangle$, as an intermediate step, and through it transfer the population into the target state $|2\rangle$.

In the classical stimulated Raman adiabatic passage (STIRAP) technique [96, 97], one uses two delayed laser pulses with different frequencies, tuned on the resonances between the levels $|1\rangle$ and $|3\rangle$, and $|3\rangle$ and $|2\rangle$, respectively. Here, we would like to drive the same transition, but with only one ultrashort laser pulse with a Gaussian form. To be able to perform a complete transfer, however, we have to allow for more freedom in the functional form of the frequency chirp.

A way to describe an arbitrary function with only a few parameters is to use a polynomial expansion and take the expansion coefficients as varying parameters. We,

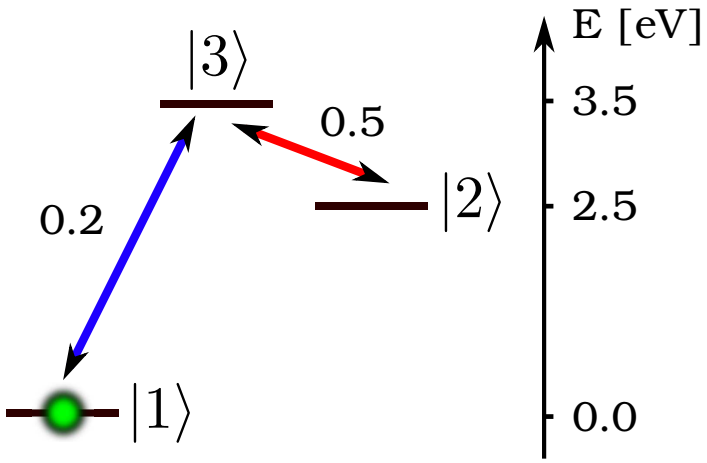

Figure 3.5: Schematic representation of the used three-level Λ system. The states $|1\rangle$ and $|2\rangle$ are coupled through the intermediate state $|3\rangle$.

therefore, can represent the laser pulse frequency by an expansion

$$\omega(t) = \sum_{l=1}^{N} c_l P_l(t), \tag{3.24}$$

where $P_l(t)$ is an orthogonal polynomial of order l and c_l is an expansion coefficient. In the present example we use Legendre polynomials, but in principle one can use any square-integrable function defined on the interval of action of the laser field. For example, a set of quasimonochromatic wave packets, like those used in the ultrahort puse-shaping technique of Goulielmakis *et al.* [86], can play the role of the $P_l(t)$'s in Eq. (3.24).

In this particular example, we restricted the number of basis functions N to six and optimized the laser pulse duration and the field strength, together with the six c_l coefficients for expanding the frequency chirping function. The results are presented in Fig. 3.6. The upper panel of the figure shows the interpolated function, representing the frequency dependence of the obtained laser pulse on time, while the laser pulse itself is depicted in the middle panel. The evolution of the populations of all three levels is presented in the bottom panel. One can see that the population is transferred completely from state $|1\rangle$ to state $|2\rangle$ through the intermediate state $|3\rangle$.

Note that the laser pulse frequency is changing smoothly in the range from 0.5 eV to around 2 eV, which is far from the resonance between levels $|1\rangle$ and $|3\rangle$. Interestingly, the population of the intermediate level follows the modulations of the applied laser pulse. Namely, the increase of the electromagnetic field induces a stimulated absorption and transfers a population to the intermediate level. The decrease of the field, on the contrary, induces a stimulated emission and transfers the population from the intermediate level to the final one.

Such a technique appears to be very useful also when preparing pulses exactly on

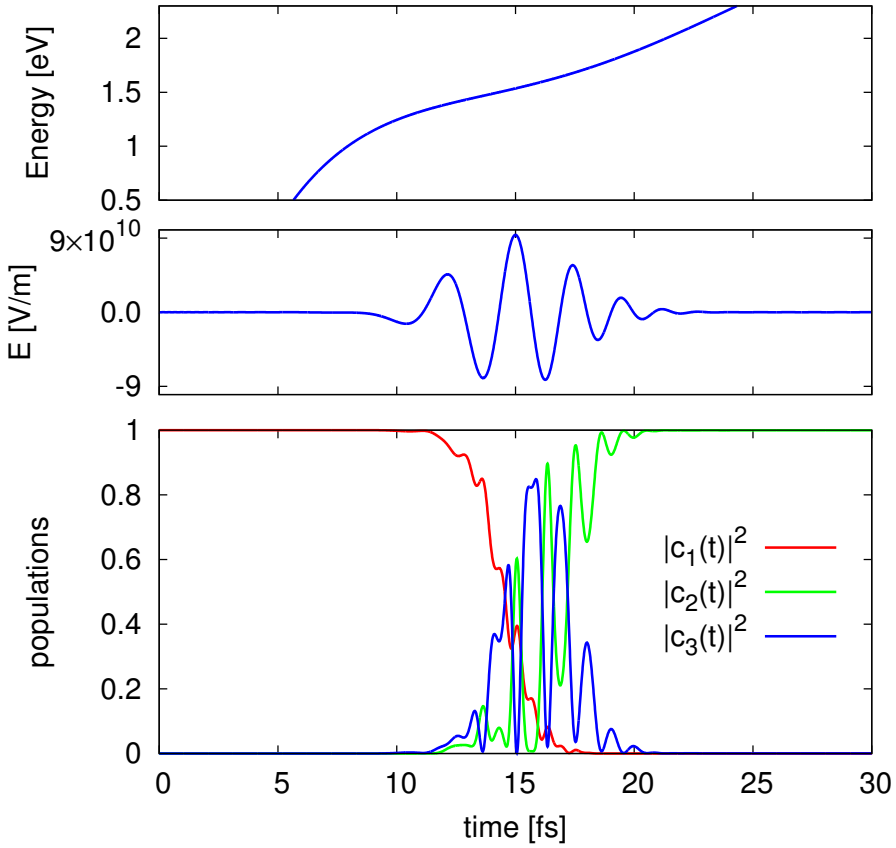

Figure 3.6: Population transfer in the Λ-type three-level system shown in Fig. 3.5 by a single Gaussian pulse having a non-linear chirp. The optimized frequency variation of the pulse is shown in the upper panel and the pulse itself in the middle panel.

resonance is not possible. In this case, smoothly varying Gaussian pulses with an appropriately tailored frequency chirp might provide a very practical alternative to drive the desired population transfer between the states of the system.

3.4.4 Two delayed laser pulses

Although quite versatile, the above technique still has a limited application due to the experimental limitations in preparation of laser pulses with arbitrary chirping. The present-day experimental capabilities, however, allow for an extremely good control over the time delay between two (nearly) identical pulses. Indeed, beam split and delay techniques are routinely used nowadays in every femto/atto laser laboratory, permitting to control the time-delay with an attosecond resolution. It is, therefore,

insightful to see what kind of possibilities for quantum dynamics control a sequence of two identical Gaussian pulses might offer.

The idea of the suggested method is to split the initially prepared ultrashort laser pulse in two identical copies and by varying the time delay between them to control the evolution of a quantum system. Using a sequence of pulses automatically adds an additional parameter that affects the system evolution, which, in addition, can be very precisely controlled. In this way, the relatively poor accuracy in controlling of other laser pulse parameters will be compensated by adjusting of the time delay.

To demonstrate the large possibilities this method offers, we will consider a rather involved four-level quantum system with couplings between all levels, schematically shown in Fig. 3.7. The difficulty to control the population transfer in such a system is associated with several factors. First of all, the levels of this system are nearly equally coupled between each other. Second, the middle levels are energetically quite close to each other. And finally, level $|4\rangle$ is located in the range of the two-photon resonance relative to the energy difference between ground state and levels $|2\rangle$ and $|3\rangle$. All these factors, together with the intrinsic wide energy bandwidth of the ultrashort laser pulses, make the population transfer in such system a complicated task, and therefore will be a stringent test for the optimization procedure.

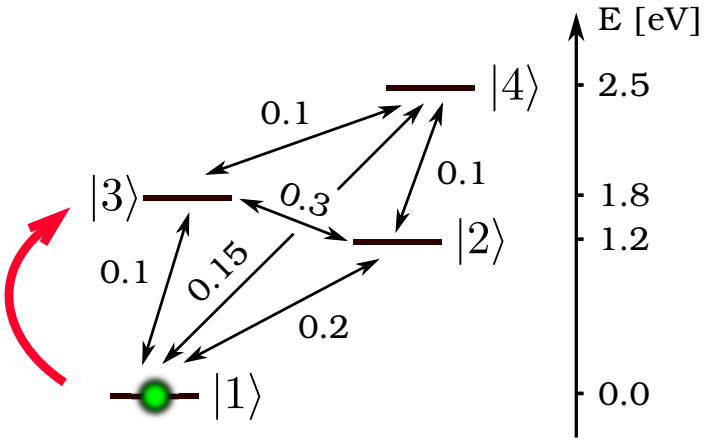

Figure 3.7: Schematic representation of the used four-level quantum system. All states are similarly strongly coupled between each other.

Let us suppose that the system is initially in its ground state $|1\rangle$ and we want to transfer the population exclusively to state $|3\rangle$. The laser field in this case is represented by two delayed laser pulses in the form of Eq. (3.21) with identical parameters. We optimize the field strength, the duration, the frequency, and the CEP, as well as the time delay Δt between the two pulses.

The results are depicted in Fig. 3.8. The two delayed laser pulses are shown in the upper panel. In this particular example, the obtained duration of each of the pulses is around 4 fs, and the delay between them is about 0.6 fs. The strength of the laser field

is not very high, which as we noted above, depends on the transition dipole moments between the participating states. The optimized frequency is around 1 eV, which is again far from the resonance between any pair of states. One can see that despite the similar coupling between the states, it is possible to completely transfer the population from the initial state to the intermediate one just by varying the time delay between two completely identical laser pulses.

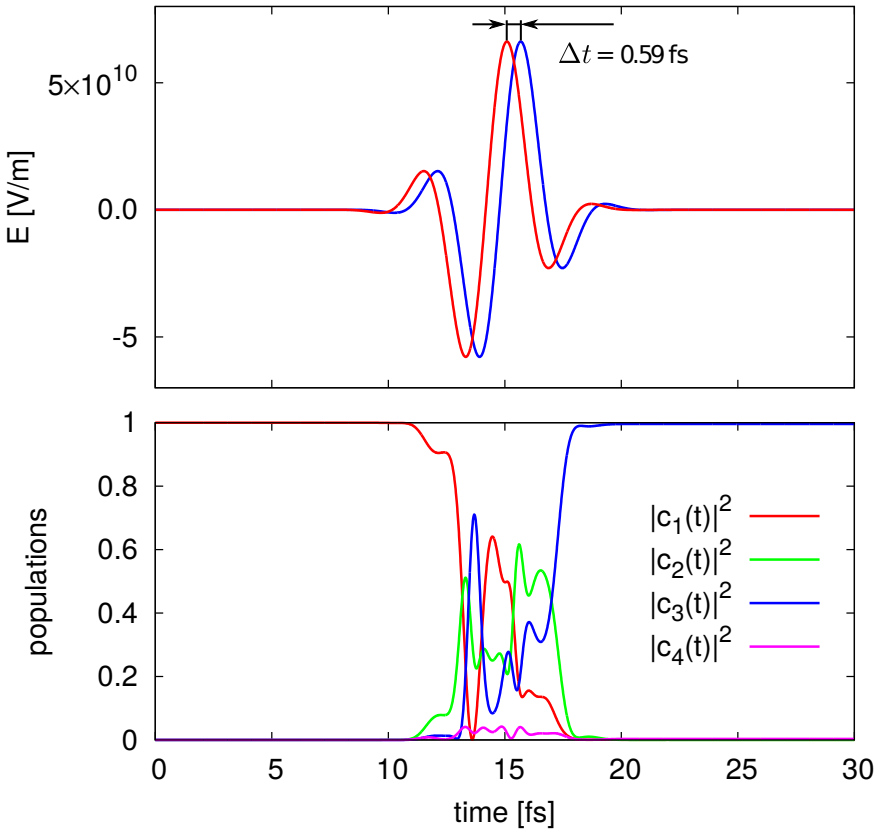

Figure 3.8: Population transfer in the four-level system shown in Fig. 3.7 by a sequence of two identical Gaussian pulse. The field is obtained by optimization of strength, duration, frequency, and CEP of the pulses, as well as the time delay between them. We see that despite the rather complicated system with close lying states and nearly equally strong coupling one is able to drive the desired transition, transferring all the population from state $|1\rangle$ to state $|3\rangle$.

3.5 Conclusions

The main motivation of the current chapter was to demonstrate that, although still limited, the possibilities to manipulate ultrashort pulses offer enough flexibility to

exert control over the quantum evolution of complex systems. We presented several examples demonstrating that relatively simple laser pulses can be used in order to achieve controllable population transfer between desired energy levels.

In subsection 3.3.1, we proposed a simple method allowing to obtain laser pulses that can drive a two-level system in a desired way. Importantly, not only the final populations can be controlled. By choosing the function $f(t)$, we can exactly predetermine the evolution of the system and control the population of each state at any moment of time during the interaction with the field. We exemplified this on a system being in a superposition of the two states and showed that the analytically obtained resonant laser pulse can smoothly drive the system such that it lends on only one of the states.

Proposing to use direct search algorithms for solving the control problem, we were able to find Gaussian-shaped laser pulses that can drive the population of the system in a predefined way. One of the main advantages of the presented methodologies, in comparison to the other schemes for population control, is the relative simplicity in its experimental realization.

By several concrete examples, parameterized mostly to reflect the outer-valence electronic structure of molecules, we showed a few different techniques for population control from simple and more involved frequency chirping of single pulses to the application of a sequence of identical monochromatic pulses with appropriately chosen time delay and CEP. All those schemes are based on optimizing ultrashort laser-pulse parameters, for which a certain degree of control have already been demonstrated by the state-of-the-art laser technology.

4

Controlling charge migration in molecules

Several examples of charge migration control in complex molecules are presented in this chapter

Contents

4.1 Introduction

Molecules exposed to short light pulses may undergo many fascinating processes caused by the "shaking" of the electronic cloud. One of such processes of particular interest which was already discussed in the introduction to the present thesis is the purely electronic transfer of the positive charge created upon ionization of a molecular system. This ultrafast charge migration is caused by the coherent superposition of electronic states [22] generated by the ionization pulse. The particular physics which leads to the creation of the electronic wave packet can vary from case to case, and is influenced by the specific properties of a system under investigation. It depends also strongly on the applied laser pulse. The coherent population of electronic states can be produced, for example, by the broad energy spectrum of the pulse, which thus can cover several ionization thresholds of the electronic states of a molecule. Another possibility, which is especially important in the case of inner shell ionization, is the electronic correlation effects. The electron leaving into the continuum creates a hole in a certain place in the electronic cloud, while the remaining electrons respond on this action.

Irrespective of the particular mechanism which has led to the initiation of the charge migration, it is expected that the created charge will oscillate between the molecular orbitals, taking part in the construction of the electronic states involved in the dynamics. It was shown theoretically [25, 27] that the molecular orbitals participating in the process can be localized on the opposite sides of a system, leading thus to an oscillation of the charge from one site of a molecule to the other one. Since molecular bonds are more likely to break in places where the hole has migrated, this ultrafast redistribution of the charge could be ultimately exploited to obtain a charge-directed reactivity [19]. It is, therefore, very appealing to use attosecond laser pulses to modulate the electronic motion and redistribute the charge on different sites of the molecule, influencing in that way the follow-up nuclear rearrangement.

Since its first theoretical prediction [22], charge migration has been intensively studied theoretically [24–31, 52, 117–141], provoking a rapidly growing experimental interest on the subject [38–40, 142, 143]. The charge migration has turned out to be a rich phenomenon, with many facets that are rather characteristic of the molecule studied (for a recent review, see, e.g. Refs. [5, 19, 23]). Despite the great interest, however, until now there were only a very limited number of theoretical studies [144–147] devoted to the investigation of the possibilities to control the charge migration in complex systems. The goal of this chapter is to demonstrate on real molecules that the charge can be efficiently controlled by laser pulses prepared using methodologies presented earlier in this thesis.

The key aspect in the theoretical treatment of the initiated charge motion is the proper description of the many-body dynamics appearing on a molecular level. Since the typical time scale of the charge migration process belongs to few-femtosecond interval, we can consider the nuclear frame as fixed, and solve the time-dependent Schrödinger Eq. (2.1) for the electronic part only, i.e. to study the multielectron wave-packet dynamics (see subsection 2.2.3 of the present thesis). Of course, the ultimate goal will be to treat on a fully quantum level both the electronic and the nuclear motion, which will be considered in chapter 5 of this work. The description of the charge migration process exclusively on the electronic level, however, can give us a useful information about the physical phenomena appearing on a very first femtoseconds of the evolution of the ionized molecule.

The chapter is organized as follows. In section 4.2, we review briefly the theoretical foundations lying behind the charge migration dynamics. We present theoretical approaches, that one can use in order to analyze the evolution of the charge created upon ionization of a molecular system. Section 4.3 is aimed at demonstrating the possibilities to control the charge dynamics by applying specifically tailored ultrashort laser pulses. Finally, in section 4.4 we summarize results obtained and conclude.

4.2 Theory

In this section, we will review briefly the most relevant theoretical approaches to describe charge migration in real molecules. We concentrate here only on a fully *ab initio* methods to trace the charge dynamics in time and space. Thus, other approaches based for example on the popular density functional theory will not be considered.

All results presented in this chapter are obtained in the frame of the so-called "sudden approximation" (see, e.g. Ref. [64]). In this approximation, it is assumed that a hole is created in a specific molecular orbital of the initial wavefunction and that this hole has no time to relax, thus leading to an electronic wave packet in terms of the eigenfunctions of the final molecular ion. In this context, the study of charge migration processes does not require a very challenging dynamical description of the ionization process, which is currently out of reach for large molecules. We would like to note, however, that very recently a ground-breaking contribution in this direction was made by developing a many-body Green's function-based technique called B-spline ADC [148] that gives access to first-principles simulation of the many-electron ionization process in a polyatomic molecule. At the current stage, however, due to its computational complexity this method can be applied only to very small molecules.

4.2.1 Charge migration analysis

Irrespective of the method chosen for evaluation of the many-electron wave packet, one also needs to find ways to analyze its evolution. A convenient quantity for visualization, or for tracing in time and space the charge dynamics is the so-called hole density [22, 117]. The hole density is defined as the difference between the electronic density of the neutral and that of the cation

$$Q(\mathbf{r},t) = \langle \Phi_0^N | \hat{\rho}(\mathbf{r}) | \Phi_0^N \rangle_{\mathbf{r}} - \langle \Phi^{N-1}(t) | \hat{\rho}(\mathbf{r}) | \Phi^{N-1}(t) \rangle_{\mathbf{r}} = \rho_0(\mathbf{r}) - \rho_{\text{ion}}(\mathbf{r},t), \tag{4.1}$$

where $\hat{\rho}(\mathbf{r})$ is the one-body electronic density operator, Φ_0^N is the ground state of the neutral, and $\Phi^{N-1}(t)$ is the propagated cationic wave packet. The quantity $Q(\mathbf{r},t)$ describes the density of the hole at position $\mathbf{r}$ and time t and by construction is normalized at all times t. The first term in Eq. (4.1) is the time-independent ground-state density of the neutral system, $\rho_0(\mathbf{r})$, and the second one, $\rho_{\text{ion}}(\mathbf{r},t)$, is the time-dependent electronic density of the cation, since created ionic state is not an eigenstate of the cation.

The time-dependent part of Eq. (4.1) can be written using resolution of identity within the complete basis set $\{\Phi_I\}$ in the following form

$$\begin{aligned} \rho_{\text{ion}}(\mathbf{r},t) &= \sum_{I,J} \langle \Phi^{N-1}(t) | \Phi_I \rangle_{\mathbf{r}} \langle \Phi_I | \hat{\rho}(\mathbf{r}) | \Phi_J \rangle_{\mathbf{r}} \langle \Phi_J | \Phi^{N-1}(t) \rangle_{\mathbf{r}} \\ &= \sum_{I,J} \langle \Phi^{N-1}(t) | \Phi_I \rangle_{\mathbf{r}} \rho_{IJ} \langle \Phi_J | \Phi^{N-1}(t) \rangle_{\mathbf{r}}, \end{aligned} \tag{4.2}$$

where ρ_{IJ} is the matrix representation of the density operator within the full set $\{\Phi_I\}$ of states associated with the cation.

To evaluate the hole density we can use the second-quantization representation of the density operator $\hat{\rho}(\mathbf{r})$ within a one-particle basis, e.g. using the full set of molecular orbitals $\{\varphi_p(\mathbf{r})\}$

$$\hat{\rho}(\mathbf{r}) = \sum_{p,q} \varphi_p^*(\mathbf{r}) \varphi_q(\mathbf{r}) \hat{c}_p^\dagger \hat{c}_q, \tag{4.3}$$

where $\hat{c}_p^\dagger$ and $\hat{c}_q$ are the corresponding creation and annihilation operators, respectively. Within this representation the hole density, Eq. (4.1), can be rewritten in the following form

$$Q(\mathbf{r},t) = \sum_{p,q} \varphi_p^*(\mathbf{r}) \varphi_q(\mathbf{r}) N_{pq}(t), \tag{4.4}$$

where the matrix $\mathbf{N}(t)$ with elements

$$N_{pq}(t) = \langle \Phi_0^N | \hat{c}_p^\dagger \hat{c}_q | \Phi_0^N \rangle_{\mathbf{r}} - \sum_{I,J} \langle \Phi^{N-1}(t) | \Phi_I \rangle \rho_{IJ} \langle \Phi_J | \Phi^{N-1}(t) \rangle_{\mathbf{r}}, \tag{4.5}$$

is referred to as the hole density matrix. Diagonalizing the hole-density matrix $\mathbf{N}(t)$ at each time point t leads to the following expression for the hole density

$$Q(\mathbf{r}, t) = \sum_p |\tilde{\varphi}_p(\mathbf{r}, t)|^2 \tilde{n}_p(t), \tag{4.6}$$

where $\tilde{\varphi}_p(\mathbf{r}, t)$ are called natural charge orbitals, and $\tilde{n}_p(t)$ are their hole-occupation numbers. The hole-occupation number, $\tilde{n}_p(t)$, contains the information what part of the initially created hole charge is in the natural charge orbital $\tilde{\varphi}_p(\mathbf{r}, t)$ at time t. The hole occupation numbers, together with the hole density, are central quantities in the observation and interpretation of the multielectron dynamics taking place after the removal of an electron [52].

As one can see, by representing one-particle density operator $\hat{\rho}(\mathbf{r})$, as well as the electronic wavefunction $\Phi^{N-1}(t)$ within some predefined basis set $\{\Phi_I\}$, it is possible to analyze the evolution of the ionized system in time and space. Convenient choice for such a basis is the ADC-ISR representation discussed in subsection 2.3.2 of the present thesis. Details on how one can construct the hole density employing the ADC approach for obtaining the cationic eigenstates can be found in [117, 120]. Additionally, we would to point out that any complete basis set $\{\Phi_I\}$ can be used for the presented analysis. It will be shown later in chapter 5 that the use of basis of electronic eigenstates can be helpful for tracing the charge dynamics coupled to the corresponding non-adiabatic nuclear motion.

4.2.2 Choice of the initial state

As was discussed above, due to electronic correlation the ionization of a molecule by an ultrashort laser pulse can trigger electron dynamics. However, currently there are neither theoretical, nor experimental methods that can tell us what exactly will be the state of the system after its interaction with a particular laser pulse. At the same time, the particular form of the initial wave packet directly affects the follow-up dynamics.

In case of the ionization caused by a high-energy photon (well above the corresponding ionization threshold), the removed electron has a high kinetic energy and, thus, leaves rapidly the interaction volume. The remaining electrons have no time to respond on such effect implying that the ionized electron is removed from the system on a very short time scale. This is the essence of the "sudden approximation" [64].

The time needed for the remaining electrons to respond to a sudden ionization was found to be about 50 asec [149]. It was shown [149] that this time is universal, i.e., it does not depend on the particular system, and as such appears as the time scale of the electron correlation. Thus, in practice, sudden ionization is equivalent to ionization performed faster than the electron correlation.

Mathematically the ionization from a particular molecular orbital can be written by using annihilation operator $\hat{c}_i$ in the following form

$$\Phi_i^{N-1}(0) = \hat{c}_i \Phi_0^N, \tag{4.7}$$

where index i indicates that we destroys an electron in the molecular orbital φ_i of the neutral molecule. As will be shown in the next subsection, due to the final-state correlation, this ansatz for the initial ionic state is equivalent to the creation of a wave packet.

4.2.3 Mechanisms of charge migration

Depending on the type of populated cationic states, different mechanisms of charge migration have been identified and studied [23, 117, 120, 122]. It appeared that there is a close relation between the ionization spectrum of the considered molecule and a particular charge migration mechanism initiated after removing an electron from the system. Therefore, in what follows we will take a closer look on a typical structure of the cationic state of a molecule.

The wavefunction corresponding to cationic eigenstate Φ_I^{N-1} can be expended in terms of the configuration interaction (CI) series

$$\Phi_I^{N-1} = \sum_k c_k^{(I)} \hat{c}_k \Phi_0^N + \sum_{a,k<l} c_{akl}^{(I)} \hat{c}_a^\dagger \hat{c}_k \hat{c}_l \Phi_0^N + ..., \tag{4.8}$$

where the indices k, l refer to occupied and a to virtual orbitals of the ground state Φ_0^N. Accordingly, the electronic configurations $\hat{c}_k \Phi_0^N$ are the so-called one-hole (1h) configurations, where one electron has been removed from the neutral ground state Φ_0^N, and $\hat{c}_a^\dagger \hat{c}_k \hat{c}_l \Phi_0^N$ are two-hole one-particle (2h1p) configurations, where one electron has been removed and another one excited into an unoccupied orbital of Φ_0^N. The quantities $c_k^{(I)}$ and $c_{akl}^{(I)}$ are the corresponding CI coefficients [117].

Let us now examine different classes of cationic states appearing in the ionization spectrum by considering particular terms in Eq. (4.8). Without correlation effects between molecular orbitals, i.e. within an independent particle model, the resulting

cationic state is constructed from a single configuration $\hat{c}_k\Phi_0^N$ corresponding to removing an electron from molecular orbital φ_k and can be described by Koopmans' theorem (see subsection 2.3.1 for details).

If correlation effects are weak – and this is typically the case for ionization from outer valence orbitals of a molecule – the resulting cationic states will consist of the so-called main lines which are the combination of 1h configurations. In this case, the molecular orbital picture is still valid, or, in other words, the quasi-particle approximation applies.

In case of ionization from the inner valence orbitals, the correlation effects are stronger, and the cationic states formed by such process are predominantly a sum of 2h1p configurations with moderate contributions of 1h ones. These so-called satellite states [150] can be classified in two different groups: relaxation satellites where at least one of the two holes in the 2h1p configuration is identical to the 1h contribution, and correlation satellites where both holes differ from the 1h configuration.

At higher ionization energies, when one removes an electron from deep inner valence and core orbitals, the appeared cationic configurations makes the distinction between the main lines and the satellites ceases to exist. In this case the spectrum becomes a quasi-continuum of lines with small to moderate intensities. This phenomenon is known as the breakdown of the molecular orbital picture of ionization [150].

In general, when a molecule is ionized, different kinds of cationic states can be populated simultaneously thus creating an electronic wave packet. Depending on the type of states involved into dynamics, one can classify the follow-up charge migration in three basic mechanisms: the hole-mixing case, the dominant-satellite case and the breakdown-of-the-molecular-orbital-picture case. In this thesis, we only deal with the hole-mixing case which will be described briefly below. Detailed description of other charge migration mechanisms can be found elsewhere [117, 120].

We start with description of the situation when two populated ionic states represent a linear combinations of two 1h configurations. These two states can be written as

$$\begin{aligned} \Phi_I^{N-1} =& c_1\hat{c}_i\Phi_0^N + c_2\hat{c}_j\Phi_0^N, \\ \Phi_J^{N-1} =& c_2\hat{c}_i\Phi_0^N - c_1\hat{c}_j\Phi_0^N, \end{aligned} \tag{4.9}$$

where, due to the orthonormality of the states, the two coefficients c_1 and c_2 satisfy the equation $c_1^2 + c_2^2 = 1$. The time-dependent electronic wave packet formed from these two states in the Schrödinger representation reads

$$\Phi^{N-1}(t) = x_I(t)\Phi_I^{N-1} + x_J(t)\Phi_J^{N-1}. \tag{4.10}$$

In the above expression, $x_I(t)$ and $x_J(t)$ are the time-dependent (in general, complex) amplitudes of the cationic eigenstates, satisfying $|x_I(t)|^2 + |x_J(t)|^2 = 1$ at all times.

Combining these two expressions leads to the following representation of the wave packet in terms of the involved molecular orbitals

$$\Phi^{N-1}(t) = (x_I(t)c_1 + x_J(t)c_2)\hat{c}_i\Phi_0^N + (x_I(t)c_2 - x_J(t)c_1)\hat{c}_j\Phi_0^N. \tag{4.11}$$

In case of sudden ionization, when an electron is removed from a particular molecular orbital, say φ_i, it is easy to examine the conditions for amplitudes x_I and x_J at the initial moment of time which leads to the situation described by Eq. (4.7) and in such a way to extract the populations of the involved cationic states. Namely, by requiring $x_I(0)c_1 + x_J(0)c_2 = 1$ and $x_I(0)c_1 + x_J(0)c_2 = 0$, one finds $x_I(0) = c_1$ and $x_J(0) = c_2$. As one can see, creating the initial hole in one of the orbitals, will create a coherent superposition of the ionic states launching in that way electronic wave-packet dynamics representing quantum beatings. The hole will oscillate between the two orbitals φ_i and φ_j with a frequency determined by the energy difference between the two ionic states. If the two orbitals are localized on two different sites of the system, the hole-mixing mechanism will lead to an oscillation of the initially created positive charge between these two sites [23, 117]. This mechanism has been extensively studied and was identified as the driving force of the ultrafast charge migration following outer- and inner-valence ionization in many different molecular systems [23].

4.3 Control of charge migration

In the course of our study we have analyzed the possibilities to control ultrafast charge migration in several experimentally interesting systems. As was already pointed out in the introduction to this chapter, the charge migration depend significantly on a molecule under study. Namely, the possibility to localize created charge on a particular place in a molecule depends on the electronic structure of the considered system. In this section we will demonstrate on two different molecules how one can stop the pure electronic, few-femtosecond oscillation of the electronic density, either localizing or redistributing it along a molecular chain.

4.3.1 3-methylen-4-penten-N,N-dimethylamine molecule

A showcase example of strong hole mixing appearing already in the outer valence orbitals of the molecule is 3-methylen-4-penten-N,N-dimethylamine (MePeNNA) cation.

Many-body *ab initio* calculations showed that, due to the electron correlation, the ground and the first excited ionic states of the molecule are a strong mixture of two 1h configurations: an electron missing in the highest occupied molecular orbital (HOMO) and an electron missing in the HOMO−1 (see Fig. 4.1 and Refs. [25, 151]). Therefore, if we suddenly remove an electron either from HOMO or from HOMO−1, we will create an electronic wave packet in the form of Eq. (4.10).

Due to the hole-mixing structure of the ionic states, the evolution of the system described by the wave packet (4.10) will represent an oscillation of the hole charge between the two involved 1h configurations, or between HOMO and HOMO−1. Since HOMO is localized on the chromophore and HOMO−1 on the amine group of the molecule (see Fig. 4.1), the charge migration will represent an oscillation of the charge between the two ends of the molecule with frequency determined by the energy difference of the two states $\omega_0 = E_J - E_I$, which is 0.55 eV, meaning that the time needed for the charge to reach the remote end of the molecule is only 3.8 fs [25, 151].

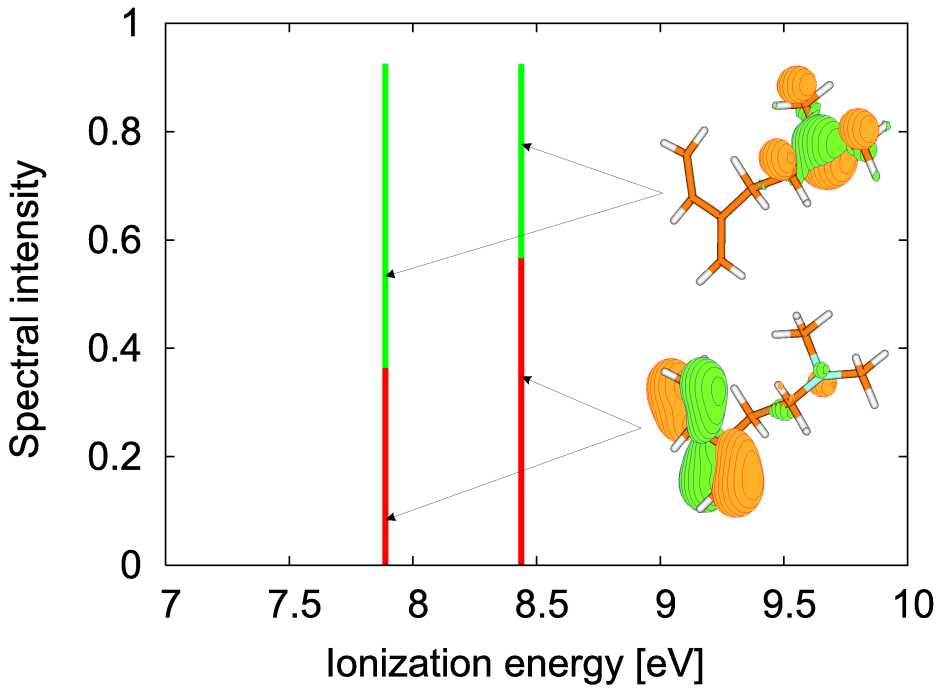

Figure 4.1: Ground and first excited cationic states of the molecule MePeNNA computed using the *ab initio* many-body Green's function ADC(3) method [57]. The next ionic state is located at 10.5 eV. The spectral intensity is defined as the combined weight of the one-hole configurations in the expansion of the ionic state and is a quantity directly related to the ionization cross section [150]. The contributions of the 1h configuration $(\mathrm{HOMO})^{-1}$ are given in red (lower part of the states), while those of $(\mathrm{HOMO}-1)^{-1}$ are shown in green (upper part of the states). The two molecular orbitals localized on the chromophore and the amine moieties of the molecule, respectively, are also depicted. The figure is adapted from Ref. [25].

Interestingly, the ionization spectrum of MePeNNA suggests that an initial state of the form of Eq. (4.10) can be achieved experimentally without approaching the

sudden-approximation limit of removing an electron from a single orbital. As we see from Fig. 4.1, to prepare such a wave packet, we need a coherent population of the first two ionic states only, which can be done via a laser pulse with the photon energy centered between the two states and a bandwidth sufficient to embrace both of them. Since the states are about 0.5 eV apart, one needs a pulse with a duration of about 1 fs. The next ionic state is located at 10.5 eV, and therefore its population by such a pulse will be negligible. The initial localization site of the charge (chromophore or N-terminal) is determined by the relative phase between the two ionization channels. The latter can be controlled through the ionization pulse parameters, e.g., by chirping the pulse [152], or by using a π-pulse [94].

We now pose the question whether, after the electron dynamics is triggered and the charge has started to bounce back and forth between the two ends of the system, we can control its motion by applying a short laser pulse. The interaction of the system with an external electric field $\mathbf{E}(t)$ can be described (in the dipole approximation) by the Hamiltonian

$$\hat{H}(t) = \hat{H}_{\text{ion}} - \hat{\mathbf{D}} \cdot \mathbf{E}(t), \tag{4.12}$$

where $\hat{H}_{\text{ion}}$ is the full electronic Hamiltonian of the ionized system and $\hat{\mathbf{D}} = (\hat{D}_x, \hat{D}_y, \hat{D}_z)$ is the vector operator of the dipole moment.

To describe the correlated motion of 69 electrons (the number of electrons in MePeNNA cation) in the presence of a laser field is an extremely difficult problem, but we solved it using *ab initio* methods only. The cationic Hamiltonian $\hat{H}_{\text{ion}}$ is constructed using nD-ADC(3) scheme [57]. Standard double-zeta (DZ) basis sets [153] were used to construct the uncorrelated reference states.

One can include the interaction of the field by diagonalizing the cationic Hamiltonian matrix and using the field-free eigenstates as a basis to expand the dipole operator, computing the transition dipole matrix elements. Alternatively, when the diagonalization is very expensive, one can represent the dipole operator $\hat{\mathbf{D}}$ in the many-electron basis of the molecular Hamiltonian (in the present case in the intermediate-state-representation basis [70]) and then directly propagate with the full Hamiltonian [52]. For this purpose, or to perform the wave packet propagation, Eq. (2.23), we used the short-iterative Lanczos technique [54]. Details of this technique, which allow one to study the correlated-electron dynamics in systems containing a few tens of electrons, are given in Ref. [52].

Our aim is to find laser fields $\mathbf{E}(t)$ which can steer the evolution of the wave function of a system. As mentioned above, under certain ionization conditions, the initial state of the MePeNNA molecule will be a linear combination of the two lowest eigenstates of the ionic Hamiltonian and, therefore, can be regarded as a two-level system. In subsection 3.3.1 of the present thesis, we proposed a general approach to obtain resonant laser pulses that can drive the populations of a two-level system in a predefined way [89].

Using this method, we are able to force the evolution of a two-level quantum system in a practically arbitrary way.

It should be noted that the two-level model is used here only to obtain the field parameters. To compute the evolution of the hole charge in MePeNNA molecule in the presence of the control pulse, the propagation was performed with the full Hamiltonian, Eq. (4.12), as described above.

Let us now examine two situations of particular interest for achieving control over the charge-migration dynamics, namely, stopping the charge oscillations and localizing the charge on one of the two molecular sites. To be specific, we will assume that the initial ionization of our test molecule, MePeNNA, is performed such that the electron is removed from the HOMO, i.e., the initial hole charge is localized on the chromophore. As discussed above, this will trigger pure electron dynamics in which the charge will oscillate between the chromophore and the amine site, and we would like to apply a control pulse which will stop this oscillation and localize the charge on the amine group or on the chromophore.

Such control can be achieved by a laser pulse obtained via Eq. (3.17) by choosing the desired initial and final populations of the two states in the wave packet. In the case of MePeNNA, if we want to drive the system to a stationary state in which the charge is entirely localized in the HOMO, we need to choose $a_f = 1$, while if we want to localize the charge on the amine site, we need to take $a_f = 0$. The initial population is $a_i = 0.4$, reflecting the fact that an initial state with a hole localized in the HOMO has the form $\Phi^{N-1}(0) = \sqrt{0.4}\Phi_I^{N-1} + \sqrt{0.6}\Phi_J^{N-1}$ (see also Fig. 4.1).

As was mentioned in subsection 3.3.1, the parameter α in Eq. (3.17) controls the interplay between the duration and the intensity of the pulse needed to perform the transition – a slow transition can be achieved with a weak pulse, while a shorter pulse will naturally need higher intensity. Since we want to modulate the charge migration before the nuclear motion will start to influence the dynamics, we would like that the pulse is as short as possible. On the other hand, the high intensity of the control pulse may lead to undesired multiphoton processes, which can, for example, further ionize the system. Therefore, we need to balance between these two factors. In the case of MePeNNA, the minimum pulse duration (corresponding to a single-cycle pulse) needed to perform the transition is about 10 fs, giving an electric field strength which never exceeds 10^9 V/m. This corresponds to a pulse with a peak intensity of about 10^{11} W/cm^2, which is rather weak.

The results of our full propagation, accounting for the influence of the control field with the above parameters, are shown in Fig. 4.2. The figure depicts the hole density, defined in Eq. (4.1), of the molecule MePeNNA after creating the initial hole on the chromophore at time $t = 0$ and applying a control laser pulse (also shown in the figure) with the maximum of the field centered at $t = 15$ fs. As $Q(\mathbf{r}, t)$ is difficult to visualize, it is convenient to keep only the axis along the molecular chain (z in

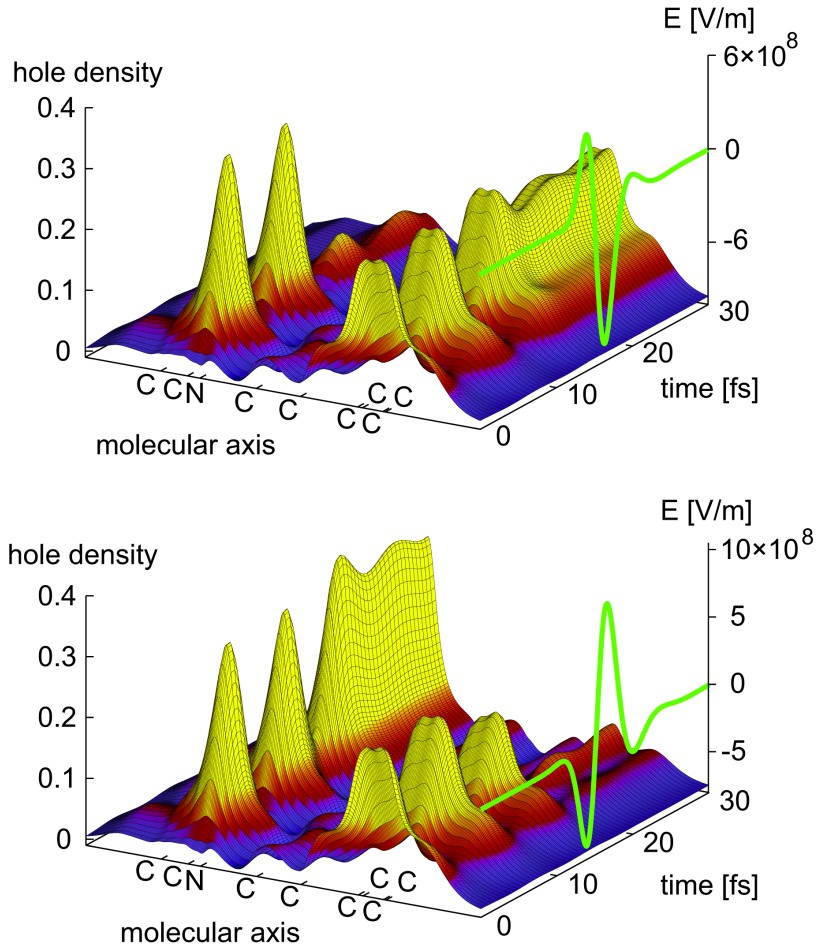

Figure 4.2: Time evolution of the hole density, Eq. (4.1), along the molecular axis of the molecule MePeNNA, after an initial localized ionization of the chromophore, controlled with a laser pulse (shown on the right) centered at 15 fs. The molecular axis is chosen to pass through the longest spatial extension of the molecule. Upper panel: The laser pulse is designed to achieve localization of the charge on the chromophore. Lower panel: The laser pulse is designed to achieve localization of the charge on the amine site.

our case) and integrate over the remaining two coordinates. The molecular axis is chosen to pass through the longest spatial extension of the molecule. It is seen that immediately after ionization, the charge-migration dynamics takes place with the hole jumping from one end of the system to the other. We clearly see that between $t \sim 10$ and 20 fs, the time during which the system is exposed to the control pulse, the charge oscillations are nearly completely stopped and the hole becomes localized on the desired site – on the chromophore (upper panel of Fig. 4.2) or on the amine group (lower panel of Fig. 4.2). We would also like to emphasize that the charge stays put at the desired site of the molecule after the pulse is over, that is, the pulse is tailored such that it brings the system to a superposition of electronic states in which the density is essentially stationary. The small oscillations taking place after the pulse is over reflect the fact that the molecule is, of course, not a perfect two-

level system. Because of the electron correlation, in addition to the two mixed 1h configurations, the two involved ionic eigenstates also contain small contributions from the two-hole–one-particle (2h1p) configurations [150]. The latter represent an excitation of an additional electron accompanying the ionized one. The combined weight of the 2h1p configurations forms the missing to one part in the states depicted in Fig. 4.1. Through the 2h1p configurations, other molecular orbitals also contribute to the dynamics and get populated, while the pulse is optimized to account only for the HOMO and the HOMO−1. Nevertheless, the suggested simple scheme to obtain the needed control-pulse parameters works remarkably well in such a complicated system as the MePeNNA molecule. We note also that the control pulse has a rather simple form and can be synthesized using spatial-light-modulator (e.g., liquid-crystal mask) techniques [154, 155].

4.3.2 Propiolic acid molecule

In this subsection we would like to demonstrate implementation of the numerical optimization procedure described previously in subsection 3.3.2 of the present thesis. For this purpose we chose the molecule of propiolic acid (HC_2COOH), the simplest acetylenic carboxylic acid, and the ultrafast charge migration which can be triggered in this molecule by removing an electron from an outer-valence molecular orbital.

The main motivation to investigate the propiolic acid is that it appears to be suitable [156] for performing an experimental study on the charge migration phenomenon. The molecule can be easily brought to the gas phase, and, due to its linear structure, can be aligned and oriented, making it amenable to the time-resolved high-harmonic generation technique, employed recently by Wörner and co-workers for reconstructing the pure electron dynamics initiated by the ionization of iodoacetylene [40].

Our calculation consists of the following steps. First, the ground-state geometry of the neutral molecule is optimized using the standard density functional theory method [157], with the B3LYP functional [158]. The optimization was done with Gaussian 09 Package [159]. The molecule is planar and thus belongs to the C_s symmetry group with irreducible representations a' and a'', and has the following electronic configuration:

$$\begin{aligned}(\text{core})^{10}(6a')^2(7a')^2(8a')^2(9a')^2(10a')^2(11a')^2(12a')^2\\ (1a'')^2(13a')^2(2a'')^2(14a')^2(15a')^2(3a'')^2\end{aligned}$$

The next step is the construction of the cationic Hamiltonian $\hat{H}_{\text{ion}}$. This is done

using the nD-ADC(3) scheme [57] for representing the one-particle Green's function. Standard double-zeta plus polarization (DZP) basis sets [160] were used in all calculations.

For including the interaction of the system with the external laser field (see Eq. (4.12)), we represented the dipole operator in the many-electron basis of the cationic Hamiltonian (in the present case this is the intermediate-state-representation basis [70]). The chosen initial states is then directly propagated with the resulting Hamiltonian, using the short-iterative Lanczos technique [52].

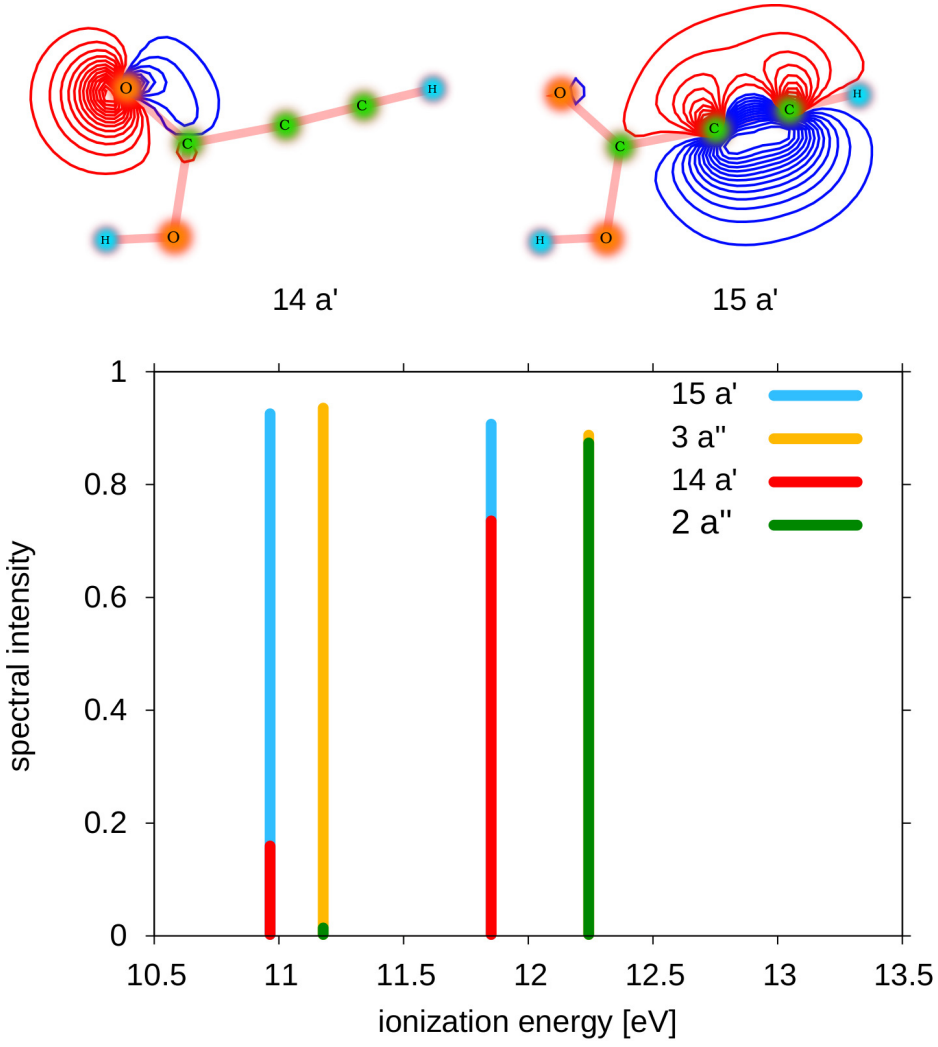

Figure 4.3: First four cationic states of the propiolic acid computed using the *ab initio* many-body Green's function ADC(3) method. The next ionic state is located at 15.1 eV. The spectral intensity is defined as the combined weight of all 1h configurations in the configuration-interaction expansion of the ionic state. The orbitals involved in the hole-mixing in the first and third state are also depicted.

Let us first look at the ionization spectrum of the propiolic acid. The first four ionic states are shown in Fig. 4.3. The next excited cationic state is located at 15.1 eV.

The contribution of the different one-hole (1h) configurations (electrons removed from a particular molecular orbital) are depicted in different colors. We see that two 1h configurations, $(15a')^{-1}$ and $(14a')^{-1}$, are strongly mixed in the first and the third ionic state. The two orbitals involved in this hole-mixing are also depicted in Fig. 4.3. We note in passing that the ionization spectrum of propiolic acid has been calculated previously using lower level of theory, giving, however, very similar results [161].

If we now remove an electron from orbital $15a'$, due to the hole mixing we will populate the ground and the second excited state of the cation and thus create an electronic wave packet. Importantly, although close in energy, the other two cationic states belong to a different symmetry irrep (a'') and their population can be effectively suppressed in an experiment by using the orientation of the molecule with respect to the laser polarization. Within only the electronic space, the evolution of the wave packet, created by the ionization out of molecular orbital $15a'$, will represent quantum beatings, in which the charge will oscillate between orbitals $15a'$ and $14a'$, i.e. between the carbon triple bond and the carbonyl oxygen. The period of these oscillations is about 6.2 fs, given by the energy splitting between the two cationic states forming the wave packet. The time scale of this pure electron dynamics is such that the charge will probably perform a few oscillations before the slower nuclear motion traps it (the detailed investigation of the time scale of this process will be presented in section 5.3 of the present thesis). Clearly, the final position of the charge will affect the reactivity of the molecule. Puling even partially the charge from the carboxylic group may hinder the proton loss and thus decrease the acidity of the molecule.

Let us now examine the possibility to achieve control over the charge migration dynamics by the two-pulse technique discussed in subsection 3.4.4 of the present thesis and, for example, stop the charge oscillations and redistribute the charge along the molecule. For this, it will suffice to bring the system in its ground ionic state. The optimal sequence of pulses that can carry out such a transition were found by fixing the pulse frequency to the resonance between the first and third ionization states of the system and the CEP to zero, while optimizing the laser pulse intensity, the duration, and the delay between the two identical laser pulses. We also introduced constraints on the optimization parameters, in order to assure that the transition is performed as fast as possible and at the same time the pulse intensities are not very high, in order to avoid unwanted processes, like further ionization of the molecule by multiphoton absorption. The optimization procedure was thus run with setting the upper limit for the total duration of the pulse sequence to 10 fs, and the maximum field strength to 2×10^9 V/m.

With all this constraints we obtained that the optimal pulse sequence that can drive the desired transition is composed of two pulses with a duration of 4.2 fs, arriving with a time difference of 1.38 fs. The maximum field strength of the pulses is 1.5×10^9 V/m. This corresponds to a pulse with a peak intensity of about 5×10^{11} W/cm^2, which is relatively weak. The obtained control pulse sequence is, therefore, fully within the

current experimental capabilities and at the same time is "soft" enough to not induce other unwanted processes.

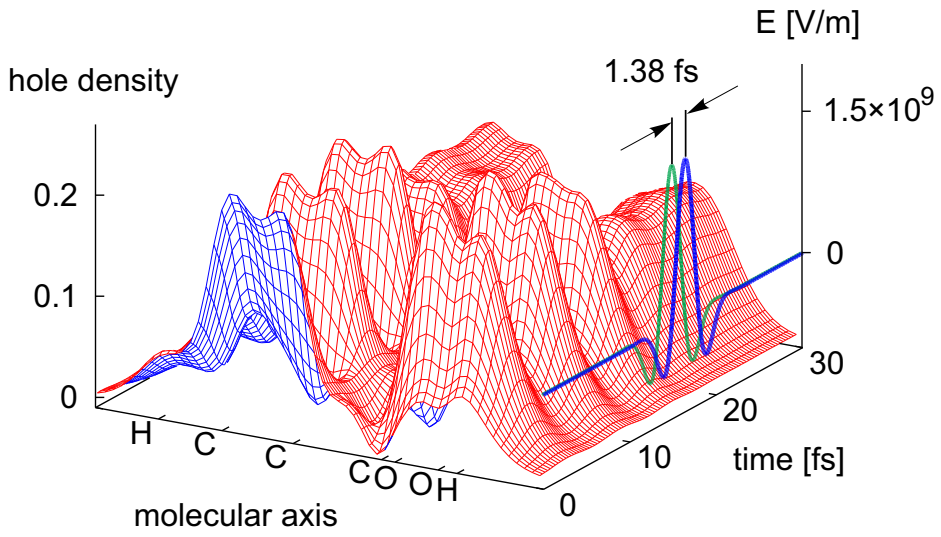

Figure 4.4: Time evolution of the hole density, Eq. (4.1), along the molecular axis of propiolic acid, after an ionization out of molecular orbital $15a'$. The triggered charge migration is controlled by a sequence of two identical monochromatic laser pulses (shown on the right), the first one of which is centered at 15 fs. We see that the pure electronic charge oscillation can be stopped nearly completely within about 10 fs.

Let us now see how this pulse sequence controls the charge migration triggered by the ionization out of orbital $15a'$. For this purpose, we computed the evolution of the hole density, defined in Eq. (4.1), during the first 30 fs after the removal of the electron. The evolution of the resulting $Q(z,t)$ is plotted in Fig. 4.4. For better exhibit the field-free charge migration dynamics initiated by the ionization, we set the arrival time of the first pulse to 15 fs. We see that immediately after the ionization the charge is localized on the carbon triple bond and, as discussed above, starts to oscillate to the carboxyl group and back with a period of 6.2 fs. Between $t \sim 10$ and 20 fs, the time during which the system is exposed to the control field, the charge oscillations are nearly completely stopped and the hole becomes spread between two sides of the system.

Importantly, such a control over the electron dynamics can be achieved also with a sequence of two laser pulses with 800 nm wavelength, the standard operational wavelength of Ti:Sapphire lasers. In Fig. 4.5, the obtained laser pulses together with the evolutions of the populations of the first four cationic states of the propiolic acid are shown. As one can see, the pulses have nearly the same characteristics as in the example above, except that the optimal CEP is π. Due to the large detuning, though, the peak intensity of the pulses is not so small anymore ($\sim 6 \times 10^{12}$ W/cm^2) and might induce some "parasitic" processes.

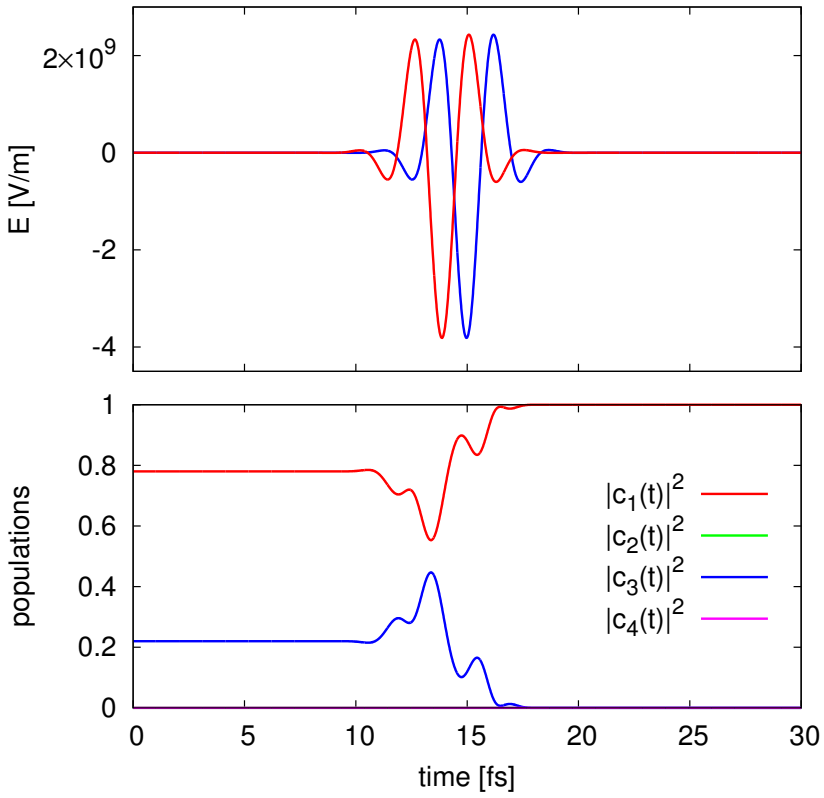

Figure 4.5: Upper panel: Two identical Gaussian laser pulses with wavelength of 800 nm obtained by the numerical optimization of the laser pulse intensity, the duration, the CEP, and the delay between them. Lower panel: Evolution of the populations of the four lowest in energy cationic states of the propiolic acid molecule driven by the such a laser field. The field is optimized to drive the system to the ground cationic state.

4.4 Conclusions

With the above examples we demonstrated that the charge migration in complicated molecular systems can be efficiently controlled by external laser fields. We demonstrated by fully *ab initio* calculations on two experimentally interesting molecules that simple pulses can be used to stop the pure electronic, few-femtosecond oscillation of the charge. We would like to emphasize that the examples of charge migration control presented in this chapter are only a few notable cases of possibilities to manipulate a charge in a molecule. The schemes of quantum control developed in the chapter 3 of the present thesis are general and not restricted to only stopping the charge-migration oscillations. Through an appropriate choice of a control parameters, one is able to

obtain pulses that can drive the system to any combination of electronic states, and thus bring the molecule to the optimum initial condition for the desired follow-up nuclear motion.

Let us now comment on the possible further evolution of the studied systems. Due to the similarity of the MePeNNA molecule with the PENNA molecule mentioned in the introduction to the present thesis [36, 37], one may expect a similar charge-directed reactivity after localized ionization of the chromophore. The charge starts to oscillate between the two ends of the molecule until the nuclear motion eventually traps it at the amine site and the molecule dissociates by breaking the bridging carbon-carbon bond. However, as we have noted above, the nuclear motion is strongly influenced by the electron dynamics and, therefore, by controlling the charge migration we may be able to predetermine the nuclear rearrangement. Localizing the charge on the chromophore may substantially slow down or even prevent the dissociation, while its localization on the amine site will most probably speed up the breakup of the molecule.

The same kind of the follow-up evolution is valid also for the molecule of propiolic acid. Our calculations showed that with two monochromatic laser pulses with about 4 fs duration and separated by about 1.4 fs one can stop the charge, oscillating between the two sites of the system, and distribute it along the molecular backbone. It is intuitively clear that a particular distribution of the charge in the molecule will induce a particular chemical reaction path, in the form of dissociation or isomerization of the molecule. It is, therefore, extremely interesting to see whether and how we can predetermine the chemical reaction path by controlling the initial charge migration step.

To check these plausible hypotheses, one needs a full quantum treatment of the coupled electron-nuclear dynamics. The correlated description of electronic and nuclear motion in such complex systems is extremely challenging for theory. The next chapter of the present thesis is aimed to tackle this complicated problem.

5

Correlated electron-nuclear dynamics

In this chapter results on the treatment of coupled electron-nuclear dynamics are presented

Contents

5.1 Introduction

Molecular quantum dynamics, aiming to solve the time-dependent Schrödinger Eq. (2.1), is extremely difficult and numerically demanding. In section 4.3, it was shown that one can treat *ab initio* the correlated motion of systems with more than fifty electrons with potential possibility to deal with up to few hundreds. Whereas accurate quantum mechanical simulation of the molecule with more then ten nuclei in general is not feasible now [162]. At this point a question naturally arises: what is the fundamental difference in the description of these two kinds of particles, the electrons and nuclei?

To answer this question let us analyze how the dynamics of a molecule is treated within the Born–Oppenheimer approach. As was shown in section 2.2, the solution of this problem usually starts with obtaining eigenstates and eigenenergies of the electronic Hamiltonian $\hat{H}_e(\mathbf{r}, \mathbf{R})$. Since at this stage the nuclei are assumed to be stationary, they enter into the Hamiltonian only as parameters (see Eq. (2.24)). Mathematically, it means that only the electronic degrees of freedom are acting as operators in the Hamiltonian. The terms which are responsible for the interactions between the different kinds of particles in Eq. (2.24) are the Coulomb potentials, rather structureless two-body interactions. It allows, in turn, to utilize the specific properties of the Coulomb potential and to develop systematic approaches able to treat many interacting electrons.

The follow-up nuclear dynamics problem, on the other hand, has to cope with complicated many-body potentials appearing as solutions of the stationary electronic problem, which are not general but specific for the system under investigation. The strong interaction between the electronic clouds of atoms that come close to each other may lead to a very strongly correlated motion [162] which, in turn, makes every system rather unique for studying. An additional complexity arises when the electronic and the nuclear motion is strongly coupled. Although the electrons usually equilibrate to the much slower motion of the nuclei, very often in the polyatomic molecules there are regions in the configuration space, the so-called conical intersections of potential energy surfaces, where the Born–Oppenheimer picture completely breaks down and one needs specific techniques to tackle the problem. It becomes especially challenging when the non-adiabatic dynamics takes place on several coherently populated electronic states [5].

In this chapter, we study several interesting effects appearing due to the coupling between the electron and nuclear dynamics. In section 5.2, a simple model illustrating the charge migration between two molecular orbitals of a system with a fully quantum treatment of the nuclei is presented. It will be shown how the electronic decoherence

caused by nuclear motion leads to the damping of the charge oscillations. In section 5.3, we will extend these studies by examining the effect of the nuclear dynamics on the charge migration in propiolic acid, investigated earlier in subsection 4.3.2 of the present thesis within the fixed nuclei approximation. We will present full-dimensional *ab initio* calculations of the electron-nuclear dynamics triggered by an ultrafast ionization of the molecule. In section 5.4, we demonstrate the possibilities to control a chemical reaction by using ultrashort laser pulses designed to manipulate the electronic coherence. A simple model illustrating the charge-directed reactivity will be presented and analyzed. Finally, in section 5.5 we summarize the results obtained, discuss some perspectives and conclude.

5.2 Coherent electron-nuclear dynamics

In the static nuclei approximation (see subsection 2.2.3 of the present thesis), the evolution of the electronic subsystem is not perturbed by the nuclear motion, and therefore the electronic coherence is conserved for an infinitely long time. In case of ionization, this results in an ultrafast charge migration with frequencies defined by the energy differences between involved cationic states at the particular nuclear geometry.

The fixed-nuclei and single-geometry approximations have, however, a limited validity, as the nuclear motion will alter the potential seen by the electrons and thus the initially created electronic coherence. In a series of theoretical works [28, 29, 127, 132, 135, 163, 164], Robb and co-workers made a step further by treating the nuclear motion in a semi-classical way using the Ehrenfest method. It was shown that such classical treatment of the nuclei only slightly modifies the electron dynamics. The nuclear motion alters the charge oscillations and their period, but does not affect strongly the amplitude of the oscillations. However, due to the intrinsic distribution of geometries in a nuclear wave packet, a fast dephasing of the oscillations in the electronic density was shown to appear on a femtosecond time scale [130, 132, 133, 135]. Despite the fact that this approach takes into account the spatial delocalization of the nuclear wave packet, a fundamental question remains, namely, what is the role played by nuclear motion in the dephasing process?

Very recently, a more sophisticated approach with a quantum mechanical treatment of both electron and nuclear dynamics, was presented in a two complementary studies [30, 31]. The results obtained suggest that in molecular systems, the purely electronic

dynamics that can be described in terms of a coherent electronic wave packet exists only for a few femtoseconds, and the nuclear motion cannot be neglected.

Coherence appearing between different electronic states does not give by itself an explicit information about the dynamics of a particular observable property of the system. Indeed, in order to calculate the desired dynamical quantity one needs to find the expectation value of the corresponding quantum-mechanical operator. Continuing the approach presented in Refs. [30, 31], one can reconstruct the full molecular wavefunction taking into account the electronic structure explicitly. It allows, in turn, to calculate the time-dependent expectation value of any electronic observable, for example the hole density.

In this work, we used the multi-configuration time-dependent Hartree method (MCTDH) to simulate the quantum nuclear dynamics on potential energy surfaces defined by the electronic Hamiltonian at the respective nuclear geometries. MCTDH is a powerful grid-based method for numerical integration of the time-dependent Schrödinger Eq. (2.1), particularly suitable for threating multi-dimensional problems [162]. The Heidelberg MCTDH package [165] has been used for all calculations. Having the time-dependent nuclear wavefunctions at hands, we will demonstrate the influence of electronic decoherence on the dynamics of the electronic density.

5.2.1 Theory of electronic decoherence

In order to describe the electron-nuclear dynamics we use Born–Huang anzatz (2.7) for representation of the molecular wavefunction in terms of stationary electronic eigenstates (for details see subsection 2.2.1 of the present thesis). The decomposition of the total wavefunction thus reads

$$\Psi(\mathbf{r},\mathbf{R},t) = \sum_i \chi_i(\mathbf{R},t)\Phi_i(\mathbf{r},\mathbf{R}), \tag{5.1}$$

where the summation is taken over all involved electronic states i. The expectation value of an electronic operator $\hat{O}(\mathbf{r},\mathbf{R})$ can be calculated via

$$\begin{aligned}\langle O(\mathbf{r},\mathbf{R})\rangle &= \langle\Psi(\mathbf{r},\mathbf{R},t)|\hat{O}(\mathbf{r},\mathbf{R})|\Psi(\mathbf{r},\mathbf{R},t)\rangle \\ &= \sum_{i,j}\langle\chi_i(\mathbf{R},t)\Phi_i(\mathbf{r},\mathbf{R})|\hat{O}(\mathbf{r},\mathbf{R})|\chi_j(\mathbf{R},t)\Phi_j(\mathbf{r},\mathbf{R})\rangle.\end{aligned} \tag{5.2}$$

Since the operator $\hat{O}(\mathbf{r}, \mathbf{R})$ acts only on the electronic degrees of freedom $\mathbf{r}$ and depends on the nuclear ones $\mathbf{R}$ only parametrically, we can eliminate the following terms

$$O_{ij}(\mathbf{R}) = \langle \Phi_i(\mathbf{r}, \mathbf{R}) | \hat{O}(\mathbf{r}, \mathbf{R}) | \Phi_j(\mathbf{r}, \mathbf{R}) \rangle_{\mathbf{r}}, \tag{5.3}$$

where the integration is performed only over the electronic coordinates. These quantities represent the expectation values of the electronic observable $\hat{O}(\mathbf{r}, \mathbf{R})$ calculated between a pair of stationary electronic states $\Phi_i(\mathbf{r}, \mathbf{R})$ and $\Phi_j(\mathbf{r}, \mathbf{R})$. Using this representation, Eq. (5.2) can be expressed as

$$\langle O(\mathbf{r}, \mathbf{R}) \rangle = \sum_{i,j} \langle \chi_i(\mathbf{R}, t) | O_{ij}(\mathbf{R}) | \chi_j(\mathbf{R}, t) \rangle_{\mathbf{R}}, \tag{5.4}$$

where only the integration over the nuclear coordinates $\mathbf{R}$ remains.

In case the electronic eigenstates $\{\Phi_i(\mathbf{r}, \mathbf{R})\}$, as well as the operator $\hat{O}(\mathbf{r}, \mathbf{R})$, have a weak dependence on the nuclear coordinates $\mathbf{R}$, one can simplify the above expression and obtain [30]

$$\langle O(\mathbf{r}, \mathbf{R}) \rangle \approx \sum_{i,j} O_{ij} \chi_{ij}(t), \tag{5.5}$$

where we have defined the reduced density matrix, representing the overlap of the nuclear wave packets on the chosen electronic states

$$\chi_{ij}(t) = \langle \chi_i(\mathbf{R}, t) | \chi_j(\mathbf{R}, t) \rangle_{\mathbf{R}}. \tag{5.6}$$

The off-diagonal elements of the reduced density matrix represent complex functions which are called electronic coherences. The diagonal elements of the reduced density matrix are real positive numbers, which give the populations of the electronic states [31].

As was pointed out in Ref. [30], the electronic decoherence is caused by the fast spread of the nuclear wave packets along the involved nuclear degrees of freedom. The time scale of this process depends on the individual contributions along the different vibrational modes, as well as on the interplay between them. If a strong decoherence arises even in one vibrational mode, i.e. the overlap of the wave packets evolving on the corresponding electronic states, Eq. (5.6), gets very small, the system will lose coherence in general [30].

5.2.2 Two-level electron-nuclear model

Let us consider the one-dimensional model consisting two electronic states, which describes a charge transfer from the left site $|L\rangle$ to the right site $|R\rangle$ of a system with

two symmetric sites coupled by a harmonic string of frequency $\nu = 1/M$, where M is the reduced mass of the nuclei.

The Hamiltonian of this model has the following form [166]

$$\hat{H} = -\frac{\nabla^2}{2M} + \frac{\nu}{2}R^2 + h(R)(|L\rangle\langle R| + |R\rangle\langle L|), \tag{5.7}$$

where the electronic energy of each of the two equivalent sites is chosen to be the zero of the energy scale, and the coupling between the sites,

$$h(R) = h_0 + h_1 R, \tag{5.8}$$

is taken to be a linear function of the dimensionless distortion $R = \tilde{R} - R_0$ of the string from its equilibrium point R_0.

In the diagonal representation, the Hamiltonian, Eq. (5.7), can be written in the following form

$$\hat{H} = -\frac{\nabla^2}{2M} + V_1(R)|\Phi_1\rangle\langle\Phi_1| + V_2(R)|\Phi_2\rangle\langle\Phi_2|, \tag{5.9}$$

where $|\Phi_1\rangle$, $|\Phi_2\rangle$, and $V_1(R)$, $V_2(R)$ are the two electronic eigenstates and eigenenergies, respectively. One can easily see, that this representation can be obtained by the following manipulation with the electronic states

$$\begin{aligned} |\Phi_1\rangle =& \frac{1}{\sqrt{2}}(|L\rangle + |R\rangle), \\ |\Phi_2\rangle =& \frac{1}{\sqrt{2}}(|L\rangle - |R\rangle). \end{aligned} \tag{5.10}$$

The resulting potential energy surfaces can be expressed as

$$\begin{aligned} V_1(R) &= \frac{\nu}{2}R^2 + h(R), \\ V_2(R) &= \frac{\nu}{2}R^2 - h(R), \end{aligned} \tag{5.11}$$

which are two harmonic potentials with equivalent strength shifted vertically and horizontally from each other.

Without loss of generality, one can assume that each electronic state, $|L\rangle$ and $|R\rangle$, is associated with some electronic orbital, $\varphi_L(r)$ and $\varphi_R(r)$, respectively. Transforming these orbitals to the chosen diagonal representation, we obtain

$$\begin{aligned} \varphi_1(r) =& \frac{1}{\sqrt{2}}(\varphi_L(r) + \varphi_R(r)), \\ \varphi_2(r) =& \frac{1}{\sqrt{2}}(\varphi_L(r) - \varphi_R(r)). \end{aligned} \tag{5.12}$$

It is seen that creating a charge at $t = 0$ in some particular orbital, say $\varphi_L(r)$, we

automatically prepare the electronic state of the system which is a linear combination of the adiabatic electronic states

$$|\Phi(t=0)\rangle = |L\rangle = \frac{1}{\sqrt{2}}(|\Phi_1\rangle + |\Phi_2\rangle), \tag{5.13}$$

triggering in such a way the follow-up charge beatings from one site of a system to the other.

The goal of our consideration is to demonstrate the effects of the nuclear dynamics on the coherent oscillation of the charge. Due to the loss of coherence, it is expected that at some point the charge migration oscillations will be damped and the charge will get stuck. To illustrate this, we will calculate the expectation value of the density operator, given by

$$\hat{\rho}(r) = (\varphi_1^*(r)|\Phi_1\rangle + \varphi_2^*(r)|\Phi_2\rangle)(\varphi_1(r)\langle\Phi_1| + \varphi_2(r)\langle\Phi_2|), \tag{5.14}$$

on the full molecular wavefunction $\Psi(r, R, t)$ obtained by numerically exact solution of the Schrödinger equation with Hamiltonian (5.9).

To be specific, let us fix the numerical values for the parameters of the system as follows: $M = 0.1$ a.u.m., $h_0 = 0.01$, $h_1 = 0.003$, and $R_0 = 4$ a.u. It is worth to mention that the considered model describes the energy of the system during stretching or compressing the string from its equilibrium point. We would like to note that parameters of the model do not have a direct relation to any real molecule. The values are chosen only to demonstrate, as clearly as possible, the interplay between the electron and the nuclear dynamics. In particular, the selected value for the reduced mass of the system leads to the fact that only a few oscillations of the charge take place before the nuclear motion comes into play. This allows, in turn, to visualize clearly the oscillation of the electronic density, as well as the effect of electronic decoherence.

The adiabatic potential energy surfaces, see Eqs. (5.11), corresponding to the above chosen parameters are shown in Fig. 5.1. We see that in the adiabatic picture the energy levels of the system represent two displaced harmonic oscillator potentials. This creates different gradients on the corresponding electronic states at the equilibrium, leading in such a way to a diminishing with time spatial overlap between the nuclear wave packet components and thus to decoherence.

The above presented model does not specify explicitly the molecular orbitals $\varphi_L(r)$ and $\varphi_R(r)$. Indeed, the non-adiabatic dynamics depends only on the form of potential energy surfaces but does not relate directly to the structure of molecular orbitals. The behavior of the created charge density, however, is crucially affected by the particular form of orbitals. In our study we chose left and right molecular orbitals, $\varphi_L(r)$ and $\varphi_R(r)$, respectively, in the form of normalized Gaussian functions with a width parameter $\sigma = 0.7$, centered on the hypothetical nuclei. Left panel of Fig. 5.2 illustrates the localized molecular orbitals, computed at equilibrium nuclear distance

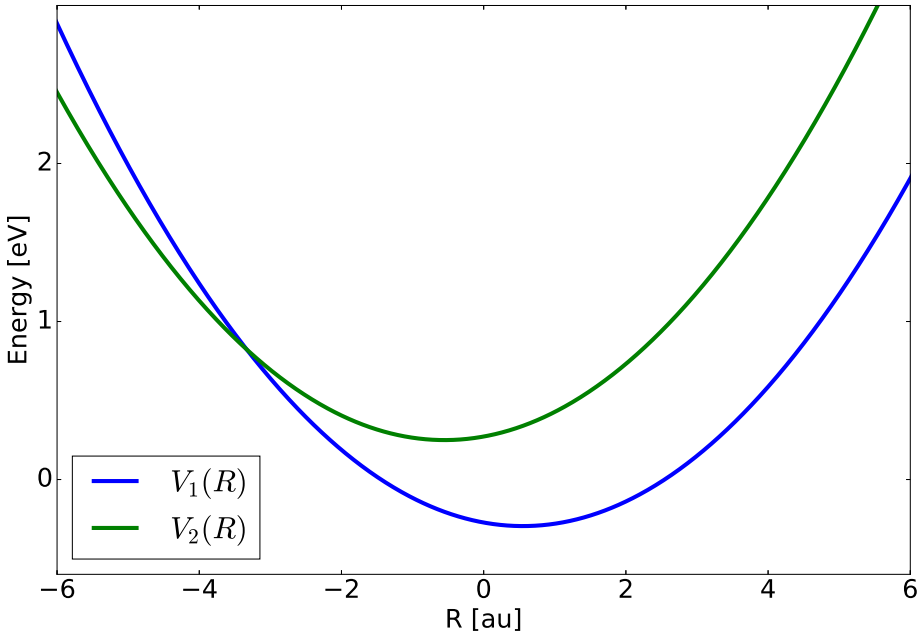

Figure 5.1: Adiabatic potential energy surfaces of the two-level electron-nuclear model. It is clearly seen that two identical electronic potentials are displaced from each other leading in such a way to an opposite nuclear gradients around equilibrium point.

R_0, while in the right panel, the adiabatic representations of the molecular orbitals, $\varphi_1(r)$ and $\varphi_2(r)$, are shown. In both panels, the horizontal axis of this picture, r, is taken along the molecular axis and is centered between the nuclei. One can see that orbital $\varphi_1(r)$ is constructed by the weighted sum of the localized orbitals, while orbital $\varphi_2(r)$ by their difference. It is clear that the positions of molecular orbitals will change according to the nuclear motion, indicating the fact that electrons follow their nuclei.

Let us now examine the evolution of the system supposing that the initial nuclear wave packet is splitted between the electronic states in proportion 1:1 (as suggested by Eq. (5.13)). We assume that the initial nuclear distribution has a Gaussian form with width parameter $\sigma = 0.5$ centered at the equilibrium point. Since the initial wavefunction is constructed from a linear combination of states, both electronically and nuclearly, one can expect that non-trivial electron-nuclear dynamics will be induced. We solved the time-dependent Schrödinger Eq. (2.1) for the presented model numerically. Our calculations show that the nuclear wave packets, $\chi_1(R,t)$ and $\chi_2(R,t)$, which represent the nuclear density on the corresponding electronic state, start to move in opposite directions oscillating back and forth with identical periods of around 30 fs. Knowledge of the time-dependent nuclear wavefunctions allows one to reconstruct the full molecular wavefunction, Eq. (5.1), at any fixed moment of time.

This allows us to calculate the time-dependent electronic density, taking into account the effect of the nuclear dynamics. For pedagogical reasons, however, it is useful to

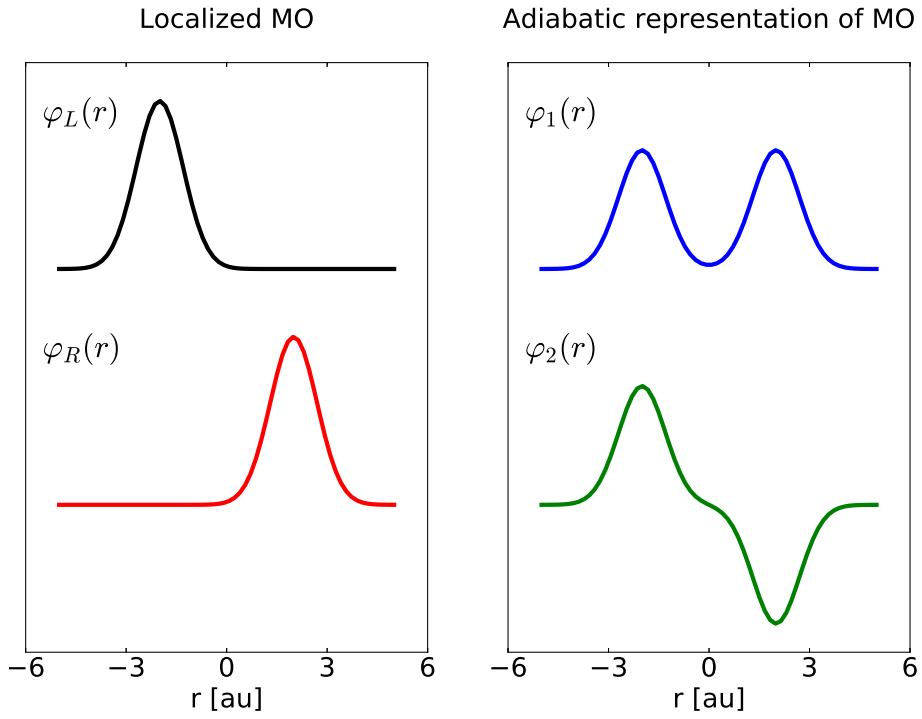

Figure 5.2: Left panel: Localized molecular orbitals of the left, $\varphi_L(r)$, and right, $\varphi_R(r)$, sites of the system. Right panel: Adiabatically transformed molecular orbitals representing the weighted sum, $\varphi_1(r)$, and difference, $\varphi_2(r)$, of the corresponding localized molecular orbitals. The x-axis r represents a molecular axis centered between nuclei.

consider the result of the action of the density operator on the molecular wavefunction before integrating over the nuclear degrees of freedom (see Eq. (5.4)). It allows, in turn, to visualize the electronic density on different positions in the nuclear configurations space. In Fig. 5.3 we show snapshots of the electronic density calculated at three different instants of time. In the left panel, one can see that the initial ($t = 0$) density is localized on the left site of the system. The electronic density then starts to oscillate with a composite frequency being a sum of many contributions stemming from all possible energy differences between the populated eigenstates of the full molecular Hamiltonian, Eq. (5.9), the so-called vibronic states. The middle panel of Fig. 5.3 shows the time instant when the electronic density has almost completely migrated to the opposite site of the system. This is the first moment of time when the electronic density appears on the right site of the system, performing in such a way oscillations with a half-period of about 3.85 fs. The right panel of Fig. 5.3 depicts the situation when the dephasing in the electronic dynamics starts to play a role. It is clearly seen that in the region around the nuclear equilibrium point, the electronic density is localized on the left site of the system, while the electronic density of the stretched and the compressed string (positive and negative deformations on the x-axis, respectively) is distributed almost equally between the left and the right molecular orbitals. The difference in the time scales of the electronic oscillations on the different nuclear configurations comes

from the set of vibronic levels involved in the dynamics. Although the energies of the vibronic states do not depend on R, due to involvement of a manifold of states in the migration process, one can interpret this as a result of the dependence of the electronic energies, $V_i(R)$, on nuclear degrees of freedom.

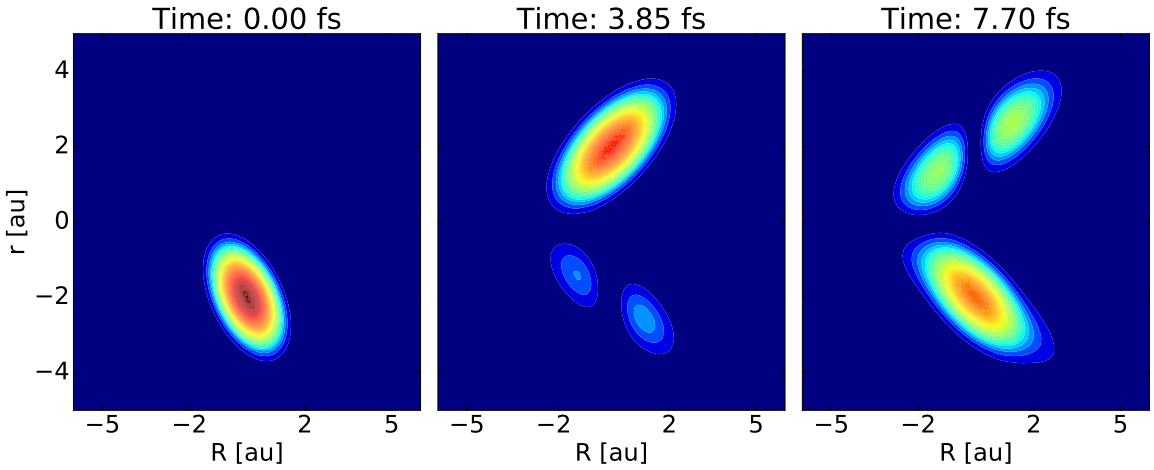

Figure 5.3: Snapshots of the time-dependent electronic density calculated by applying the operator $\hat{\rho}(r)$, see Eq. (5.14), on the full molecular wavefunction $\Psi(r, R, t)$ obtained by the numerical solution of the Schrödinger Eq. (2.1). Left panel: Initial electronic density localized on the left site of the system. Middle panel: Electronic density calculated at $t = 3.85$ fs. It is seen that electronic density has almost completely migrated on the right site of the system. Right panel: Electronic density calculated at $t = 7.70$ fs. The differences in the time scale of the electronic dynamics on the different nuclear points lead to a dephasing of the electronic coherence. For a better visibility, the density is plotted in a logarithmic scale.

Despite the possibility to calculate a nuclear-resolved electronic density of the molecule, the analysis of this quantity can be rather complicated due to contributions from many nuclear degrees of freedom. Indeed, considering the electronic density along a selected vibrational mode does not give a direct information about the electronic dynamics on the other modes. Therefore, integrated quantities, such as the reduced nuclear density matrix, Eq. (5.6), become useful for the interpretation of the electronic decoherence caused by the nuclear dynamics. In Fig. 5.4 time-dependent matrix elements of the reduced nuclear density matrix are presented. On the diagonal, the populations of the electronic states are shown. Their time-independence indicates that the two electronic states are not coupled and thus the system does not exhibit non-adiabatic transitions. The off-diagonal matrix elements represent complex functions that oscillate with frequencies defined by the appropriately averaged differences between the involved vibronic levels. Furthermore, it is clearly seen that the off-diagonal terms $\chi_{12}(t)$ and $\chi_{21}(t)$ are experiencing fluctuations of the magnitude. This is a direct consequence of the fact that starting from a fully coherent state the system starts to decohere due to the influence of the nuclear motion. Since our model consists of two harmonic oscillators with identical frequency, the coherence will completely recover after every oscillation of the nuclear density, i.e. when the nuclear wave packets moving on the

two potential energy surfaces return to a position when they overlap completely.

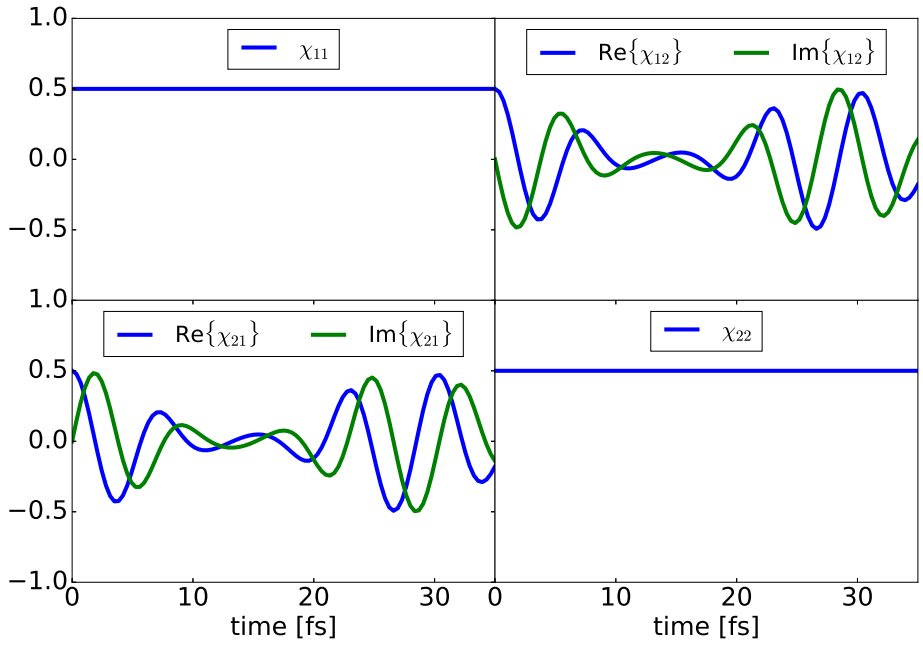

Figure 5.4: Time-dependent matrix elements of the reduced density matrix, Eq. (5.6), calculated for the two-level electron-nuclear model of charge transfer. The diagonal matrix elements represent integrated populations of the electronic states. The off-diagonal complex terms reflect the degree of electronic coherence. It is seen that initially fully coherent states start to loose their coherence reaching a minimum at around 15 fs. Since the considered system is a one-dimensional harmonic oscillator, the electronic coherence recovers when the nuclear densities approach the initially prepared state at around 30 fs.

The integration of the electronic density over the nuclear degrees of freedom allows one to extract information about the electronic dynamics of the system in general. Fig. 5.5 shows the evolution of the integrated electronic density for the described model calculated via Eq. (5.4). We observe that the charge performs one clear oscillation before the nuclear dynamics perturbs the coherence of the electronic states. In the time interval between 10 and 20 fs the charge is smeared between the nuclei. During this time the electronic dynamics is almost completely damped due to the very little overlap between the nuclear wave packets.

Our fully quantum simulation of the electron-nuclear dynamics shows that the electronic decoherence appearing as a result of the nuclear motion is a rather complicated effect, which depends on several parameters of the system. For example, increasing the horizontal displacement between electronic states will lead to a faster decrease of the overlap of the nuclear wave packets and thus to a shortening of the decoherence time. At the same time, the vertical gap between the energy levels affects the time scale of electronic motion, and therefore increasing this gap will lead to the possibility to observe several oscillations of the electronic density before the nuclear dynamics eventually perturbs the picture. The particular form of the potential energy surfaces

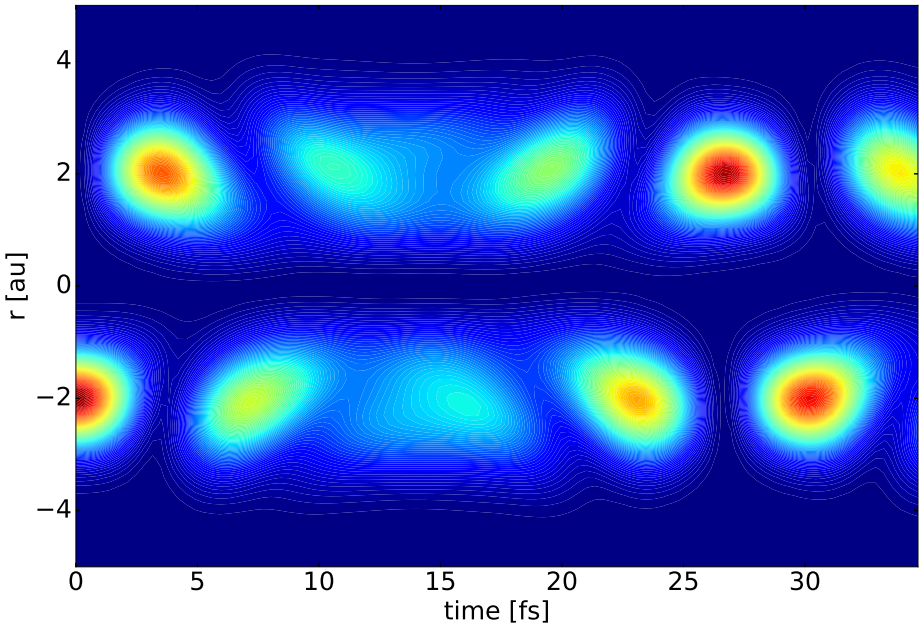

Figure 5.5: Time evolution of the electronic density along the molecular axis of the system after initial localization of the charge in orbital $\varphi_L(r)$. The triggered charge beatings are damaged by the nuclear motion. We see that the charge performs one clear oscillation before the nuclear dynamics perturbs the coherence of the electronic states. Later, the coherence is recovered when the system approaches the initial state.

is important as well, since it determines the vibronic levels of the system, affecting in such a way the distribution of the migration frequencies. In the case of several nuclear degrees of freedom, the interplay between the various factors can be quite entangled, requiring thus an explicit investigation of every particular system prepared under specific initial conditions. The next section is aimed at demonstrating that contrary to the previously reported [30, 31] few femtoseconds decoherence times, complicated molecules, in which the pure electronic coherence survives for longer times, seem to exist.

5.3 Electron-nuclear dynamics in propiolic acid molecule

In this section we will illustrate the influence of the nuclear dynamics on the oscillations of the charge created upon ionization of the propiolic acid molecule. As was shown in subsection 4.3.2 of the present thesis, the removal of a HOMO−1 electron triggers a charge migration in the propiolic acid driven by the hole-mixing mechanism. In the absence of perturbations coming from the movement of the nuclei, the charge

performs long-lived oscillations along the molecular chain with a period of about 6.2 fs. A question of particular interest is, of course, how long the charge oscillations could survive under the decoherence coming from the nuclear dynamics of the molecule.

In order to shed light on this problem, we perform a full-dimensional simulation of the quantum dynamics of the molecule close to the Franck-Condon region. In this case, the potential energy surfaces can be approximated by Taylor polynomials up to second order, a model which is known as the vibronic-coupling Hamiltonian [45, 167]. Within this approximation, the Hamiltonian can be written as

$$\hat{H} = \hat{T}_n + \hat{\nu}_0 + \hat{\mathbf{W}}, \tag{5.15}$$

where $\hat{T}_n$ and $\hat{\nu}_0$ denote the kinetic and the potential energy of the neutral unperturbed reference ground state, respectively. Using a harmonic approximation for the vibrational modes, $\hat{T}_n$ and $\hat{\nu}_0$ can be expressed as

$$\hat{T}_n = -\frac{1}{2}\sum_i \omega_i \frac{\partial^2}{\partial Q_i^2}, \tag{5.16}$$

$$\hat{\nu}_0 = \frac{1}{2}\sum_i \omega_i Q_i^2, \tag{5.17}$$

where atomic units and mass- and frequency-weighted normal-mode coordinates Q_i are used, with ω_i denoting the frequency of mode i. The matrix $\hat{\mathbf{W}}$ contains information about the diabatic cationic states, and the non-adiabatic couplings between them. Using the standard vibronic-coupling theory, Taylor expansion of the matrix elements of $\hat{\mathbf{W}}$ can be written as

$$W_{kk} = E_k + \sum_i \kappa_i^k Q_i + \sum_i \gamma_i^k Q_i^2, \tag{5.18}$$

$$W_{kl} = \sum_i \lambda_i^{kl} Q_i, \tag{5.19}$$

where E_k is the vertical ionization energy of state k, κ_i^k and γ_i^k are the linear and quadratic coupling parameter of state k for normal mode i, respectively, and λ_i^{kl} is the linear coupling parameter between states k and l within the normal mode i.

The propiolic acid belongs to the C_s symmetry point group and thus posses two irreducible representations. The molecule has 15 normal vibration modes (see Table 5.1), 11 totally symmetric modes of a' symmetry and 4 coupling modes of a'' symmetry. The normal modes have been obtained at the TDDFT/B3LYP [158] level of theory with the DZP basis set [160] using the Gaussian package [159].

We included the first four cationic states of the propiolic acid into model. This choice is motivated by the fact that the remaining cationic states are located relatively far in energy from selected ones (see also Fig. 4.3), and thus can be eliminated from consideration by the appropriately prepared ionization laser pulse. The potential

Mode number	Symmetry	Frequency [cm^{-1}]
1	a'	178.0
2	a''	251.6
3	a'	462.2
4	a'	582.4
5	a''	621.5
6	a''	674.2
7	a'	755.0
8	a''	766.5
9	a'	797.1
10	a'	1200.8
11	a'	1463.9
12	a'	1812.0
13	a'	2349.8
14	a'	3668.0
15	a'	3686.2

Table 5.1: Normal modes included in the vibronic-coupling Hamiltonian of the propiolic acid molecule.

energy surfaces of these states have been calculated in the same way as was described in subsection 4.3.2 of the present thesis. Using these surfaces, the parameters of the vibronic-coupling Hamiltonian were obtained through a least-square fit procedure.

The propagation of the nuclear wave packets with the above presented Hamiltonian is performed using MCTDH method. In order to reduce the computation time, different vibrational modes were grouped and treated as multidimensional single particles (see Table 5.2). A primitive basis of harmonic oscillator functions has been used in order to represent each nuclear degree of freedom. The number of DVR functions was chosen such that it ensures that the maximal population of the last grid point is lower than 10^{-4}. The number of single-particle functions is dictated by the maximum population of the highest natural orbital and is chosen to be lower than 10^{-3}. The initial wave packet is constructed by populating the ionized states from the ground neutral state according to the nuclear dependent hole-mixing parameters along the 15 nuclear degrees of freedom, assuming ionization from orbital $15a'$.

In Fig. 5.6 the evolution of the matrix elements of the reduced nuclear density matrix, Eq. (5.6), calculated between the involved electronic levels is shown. In the upper panel, the diagonal elements, corresponding to the adiabatic populations of the electronic states are presented. It is seen that the system is initially prepared in a linear combination of states one and three. The initial weights of the participated states are defined by the corresponding integrated hole-mixing parameters (see also Fig. (4.3)). Later, the non-adiabatic couplings lead to a redistribution of the populations between the involved electronic states. In the lower panel, the time evolution of the coherence between levels one and three is presented. One can see that the fully coherent initial

Normal modes	SPF basis	Primitive basis
(1,2,3)	[8,8,8,8]	(12,10,10)
(4,5,6)	[8,8,8,8]	(10,12,10)
(7,8,9)	[8,8,8,8]	(10,10,10)
(10,11,12,13)	[8,8,8,8]	(10,10,14,12)
(14,15)	[8,8,8,8]	(10,10)

Table 5.2: Combination of vibrational modes into the multidimensional single particles for the propiolic acid molecule. The number of single-particle functions for each state, as well as the number of primitive basis functions along each mode, are also shown.

electronic state starts to lose its coherence on a time scale of about 10 fs. This shows that before the nuclear dynamics comes into play the system has time to perform two to three oscillations of the charge. The time scale of the charge oscillations is found to be slightly faster than predicted by the static-nuclei approximation (about 5.1 fs against 6.2 fs, respectively). This change is caused by the fact that the involved cationic states have slightly different nuclear dependence. It leads, in turn, to the vibronic levels which are shifted further in energy than the pure electronic energies used in calculations with fixed nuclei. Contrary to the above presented model of coupled dynamics in harmonic oscillator potentials, the coherence in the present case is not recovered within the time the propagation was performed. This indicates that at least one vibrational mode participating in the dynamics has lost its coherence due to the different time scale of the nuclear oscillations on the corresponding electronic states.

Using the reconstructed full molecular wavefunction, we computed the expectation value of the hole density operator, Eq. (4.1). The evolution of the resulting $Q(z,t)$ along the molecular axis z is plotted in Fig. 5.7. We see that at the initial moment of time, the charge is localized on the carbon triple bond and, due to the hole mixing of the involved cationic states, starts to migrate to the carboxyl group of the molecule and back. The nuclear dynamics perturbs the electronic oscillations leading to the damping of the charge migration within about 10 fs. It is clearly seen that the charge has time to perform several oscillations before the strong decoherence suspends its ultrafast motion and distributes it between the two sites of the molecule.

In this section, we presented an example of a complex system in which the decoherence coming from the nuclear dynamics is relatively slow. The propiolic acid cation studied here is the very promising molecule for the experimental investigations. The molecule has a rather large dipole moment in the neutral state and thus can be relatively easily aligned by appropriate electromagnetic fields. Due to the particular form of the ionization spectra, as well as due to the symmetry properties of the system, the laser pulse can be applied such that only the desired electronic states get populated, triggering in this way the follow-up charge beatings. As we showed, the created hole will have time to perform several oscillations before the nuclear dynamics dephases

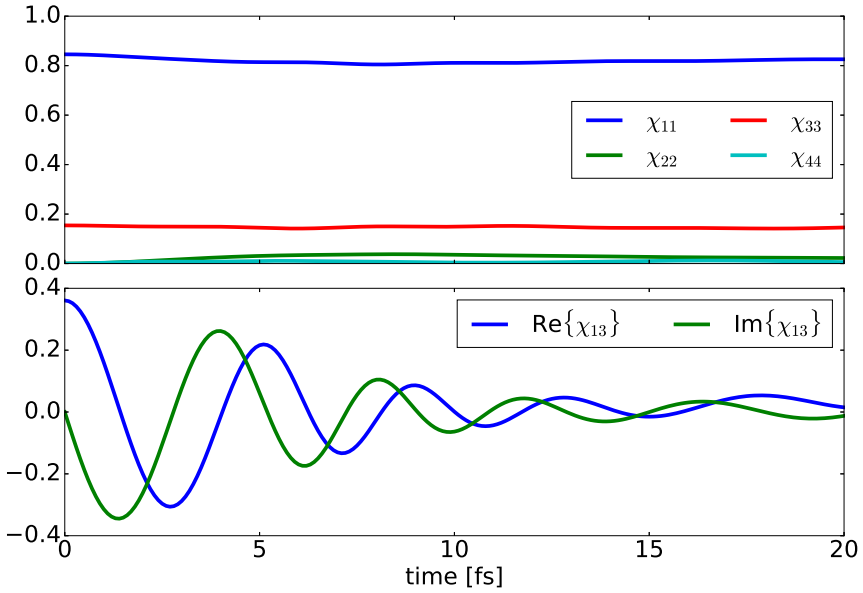

Figure 5.6: Time-dependent matrix elements of the reduced density matrix, Eq. (5.6), calculated for the dynamics in the propiolic acid cation. Upper panel: The diagonal matrix elements, representing the integrated populations of the electronic states. Lower panel: The off-diagonal complex term indicating the coherence between states one and three. The coherence between the remaining states is close to zero.

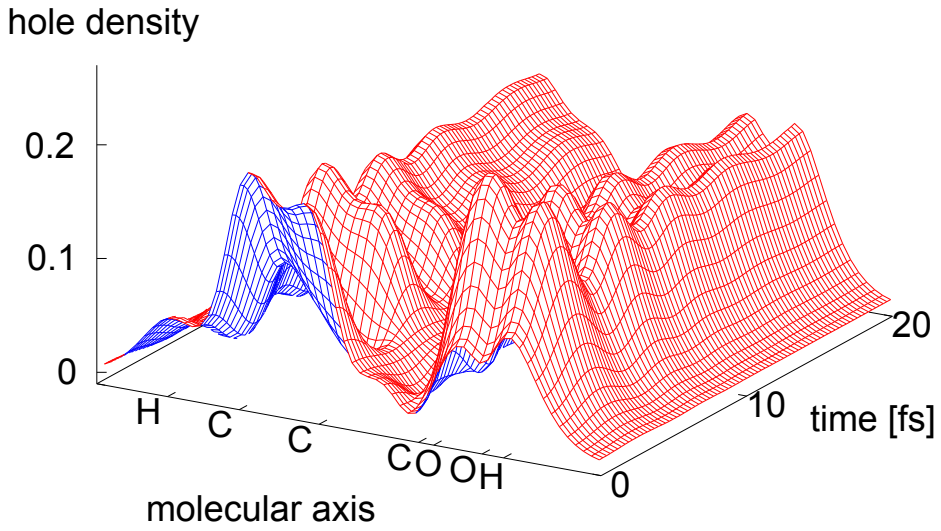

Figure 5.7: Time evolution of the hole density along the molecular axis of the propiolic acid, after the ionization out of molecular orbital $15a'$. The appeared charge migration dynamics is perturbed by the influence of the nuclear motion. We see that after 10 fs the oscillations of the charge are almost completely stopped.

them and finally traps the charge. We argue that the described properties of the system can be very suitable for the experimental observation of the purely electronic dynamics in molecules.

5.4 Control of electron-nuclear dynamics

Quantum control of molecular processes in terms of attochemistry implies manipulation of the electronic dynamics only. In this section we will exemplify on a simple one-dimensional model the concept of attosecond control of a molecular fragmentation. It will be demonstrated that by an appropriate combination of two identical Gaussian laser pulses one is able to manipulate the dynamics of electronic density and in this way to control the molecular reactivity.

Let us consider a model which is similar to the one that was described in subsection 5.2.2 of the present thesis. Our goal is to simulate the process of charge transfer between two molecular orbitals of a system with potential energy surfaces that imply an opposite behavior of the nuclear wave packets, namely, a bound and a dissociating states. The Hamiltonian of such two-level system can be expressed in the form of Eq. (5.9) in which the lower electronic state $V_1(R)$ is bound, while the higher one, $V_2(R)$, is dissociative. Adiabatic potential energy surfaces corresponding to the described situation are shown in the upper panel of Fig. 5.8. This model represents the electronic states of a hypothetical ionized molecule AB^+. We assume that in the dissociation limit the molecule fragments differently – the lower electronic state corresponds to the situation when charge is located on fragment A, while the higher electronic state leads to the localization of the charge on species B.

Molecular orbitals of the AB^+ molecule are constructed from uncorrelated orbitals $\varphi_L(r)$ and $\varphi_R(r)$ in the same way as was discussed in subsection 5.2.2. The difference is that in the present example the corresponding weights of the mixing depend on the nuclear coordinate R

$$\begin{aligned} \varphi_1(r,R) =& a(R)\varphi_L(r) + b(R)\varphi_R(r), \\ \varphi_2(r,R) =& b(R)\varphi_L(r) - a(R)\varphi_R(r), \end{aligned} \tag{5.20}$$

where relation $|a(R)|^2+|b(R)|^2 = 1$ fulfills for any nuclear configuration R. In the region around the nuclear equilibrium point, the correlation between electrons of fragments A and B are strong leading to a strong mixing of orbitals in both cationic states. At the same time, in the dissociation limit, the electrons of the different fragments of the molecule do not interact making the two states pure 1h ones, corresponding to the situation that the hole is either in $\varphi_L(r)$ orbital or in $\varphi_R(r)$. In the lower panel of Fig. 5.8, the orbital mixing parameters $a(R)$ and $b(R)$ used in the present calculations are shown. The uncorrelated orbitals $\varphi_L(r)$ and $\varphi_R(r)$ are chosen the same as described earlier in subsection 5.2.2.

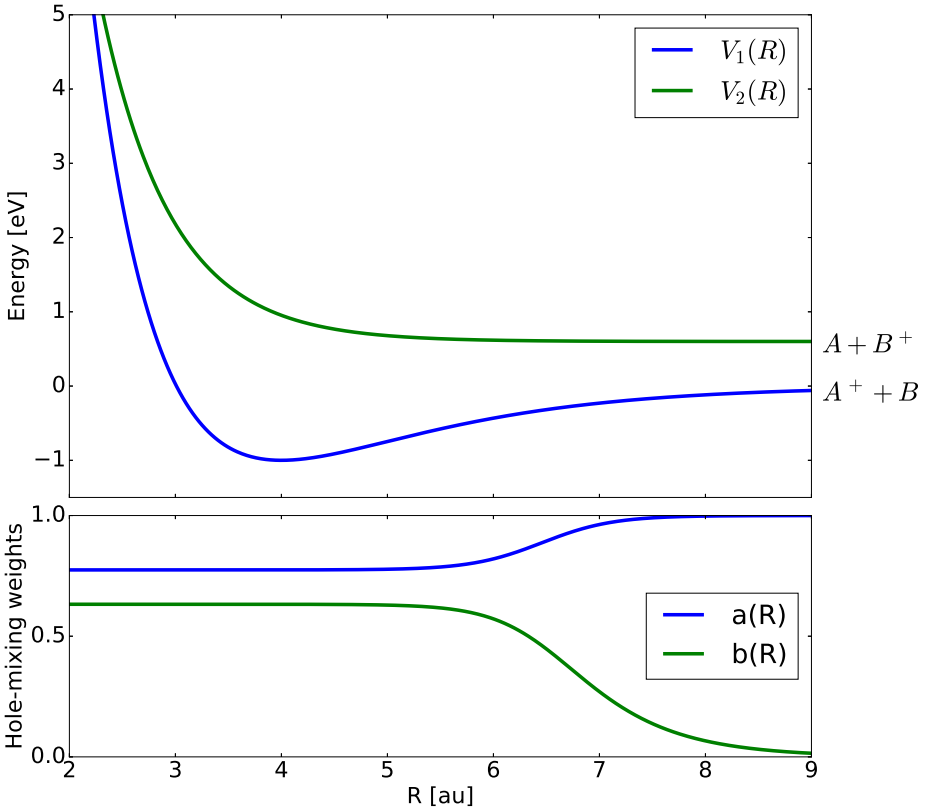

Figure 5.8: Upper panel: Adiabatic potential energy surfaces of the two-level molecular fragmentation model. The lower electronic state $V_1(R)$ is strongly bound while the higher one, $V_2(R)$, is dissociative. On dissociation limit the molecule breaks into fragments – the state $|\Phi_1\rangle$ corresponds to situation when charge is located on A fragment while the state $|\Phi_2\rangle$ leads to localization of the charge on B specie. Lower panel: Nuclear depend hole mixing parameters. It is seen that in the region around nuclear equilibrium point the orbitals are strongly mixed while on dissociation limit the correlation effects become weaker.

We start with the description of the evolution of the system in the absence of the external laser fields. The initial state is expressed as

$$|\Psi(r, R, t = 0)\rangle = a(R)\chi(R)|\Phi_1\rangle + b(R)\chi(R)|\Phi_2\rangle, \tag{5.21}$$

where $\chi(R)$ is the Gaussian wave packet with the following parameters: $\sigma = 0.3$, $R_0 = 3.9$ a.u. It is seen that the wave function is prepared as a linear combination of electronic states inducing in such a way electronic dynamics. The reduced mass of the nuclei is chosen to be 0.5 a.u.m. ensuring that the nuclear motion is fast enough to visualize clearly the physical processes of interest.

What is the expected dynamics of the system? It is clear that such prepared nuclear wave packets will evolve in accordance to the structure of the corresponding potential energy surfaces $V_1(R)$ and $V_2(R)$. The part of the nuclear wave packet $\chi_1(R, t = 0) = a(R)\chi(R)$ promoted to the bound potential will oscillate back and forth with some frequency while the remaining part $\chi_2(R, t = 0) = b(R)\chi(R)$ will roll out on

the $V_2(R)$ potential, i.e. the system will dissociate. In Fig. 5.9 the electronic density of the system, calculated using Eq. (5.4) is presented. It is seen that the charge initially placed on the left site of the system starts to oscillate with a period of about 2.5 fs. Due to the movement of the nuclear wave packet on the dissociative state, the system loses its coherence after about 12 fs resulting in a disappearance of the charge beatings. Yellow dashed lines indicate the averaged positions of the fragments moving on the corresponding electronic state. One can see that the charge partially leaves with fragment B on state $|\Phi_2\rangle$ whereas the remaining part of the charge is distributed between the nuclei of the bound ion AB^+ on state $|\Phi_1\rangle$.

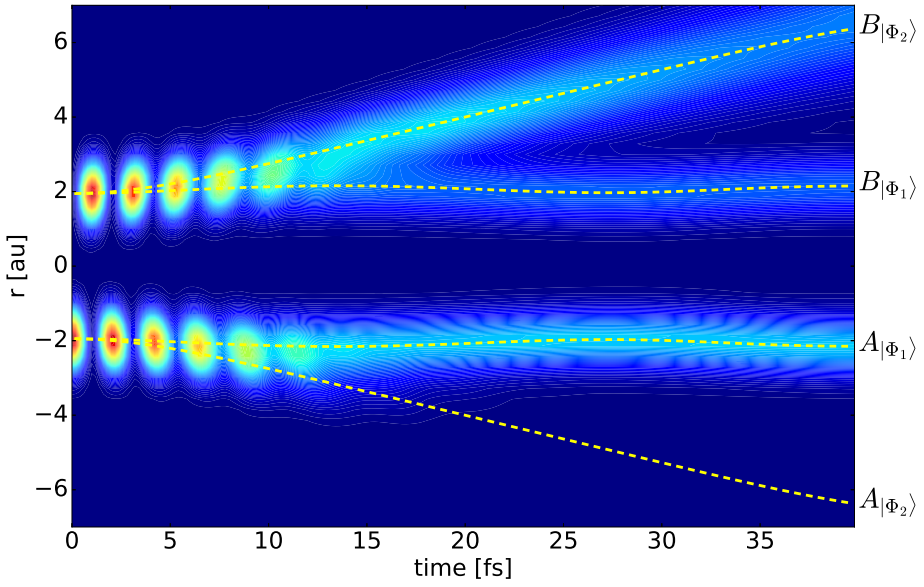

Figure 5.9: Time-dependent electronic density plotted along the molecular axis of the system after the charge is initially localized in orbital $\varphi_L(r)$. It is seen that the charge performs oscillations from one site of the system to the other with a period of about 2.5 fs. Due to movement of the nuclear wave packet on dissociative state, the system loses its coherence at about 12 fs leading to the disappearance of the charge beatings. Yellow dashed lines indicate the averaged positions of the fragments moving on the corresponding electronic state. One can see that the charge partially leaves with fragment B on state $|\Phi_2\rangle$ whereas the remaining part of the charge is distributed between the nuclei of the bound ion AB^+ on state $|\Phi_1\rangle$.

Let us now apply a laser field on the system. The interaction of the system with the field is treated in the frame of the dipole approximation (see subsection 2.4.5 of the present thesis). The transition dipole moment between the electronic states is chosen to be 6 a.u. Our goal is to examine the possibility to achieve control over the molecular fragmentation by the two-pulse technique discussed in subsection 3.4.4 of the present thesis. For this, it will suffice to bring the system in the particular electronic state which thus will automatically lead to the desired follow-up nuclear rearrangement. The optimal sequence of pulses that can carry out such a transition was found by the optimization of the laser pulse frequency, the intensity, the duration, the phase,

the position of the first and the second laser pulses. As one can see, the number of parameters to be optimized is greater then in the static case discussed earlier, indicating the fact that the dynamics of the system now is much more complicated.

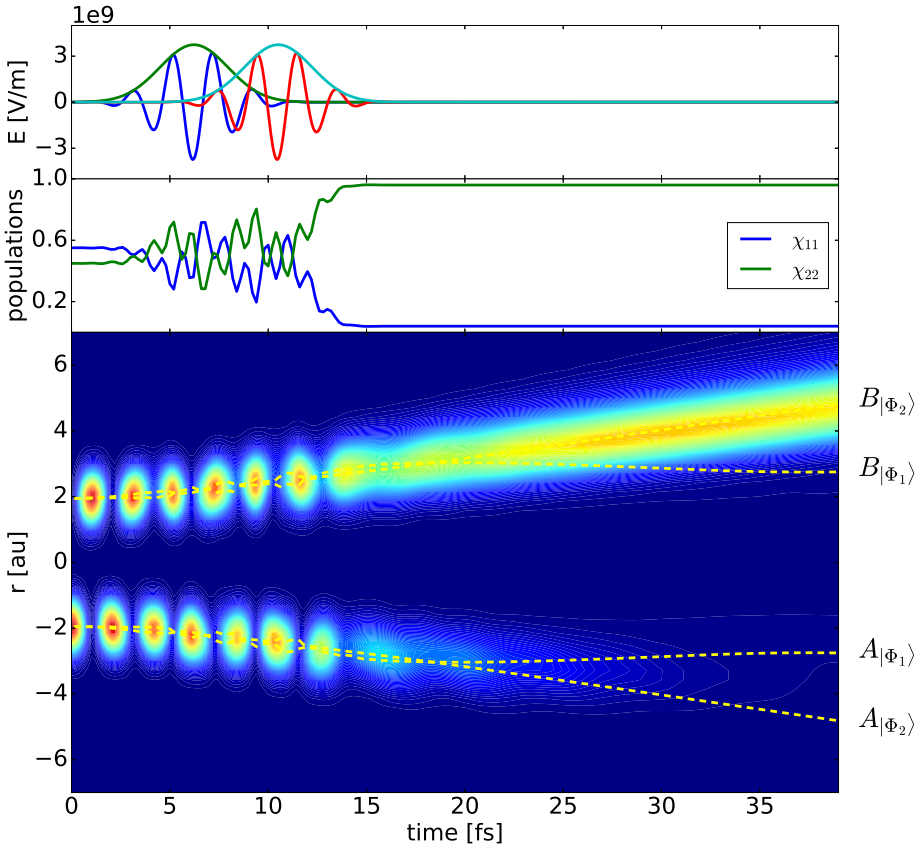

Figure 5.10: Control of the molecular fragmentation by an external laser field. The laser pulse is designed to force the dissociation of the molecule. Upper panel: Two identical Gaussian laser pulses with parameters optimized to achieve the desired quantum control. Middle panel: Evolution of the adiabatic populations of the electronic states. Lower panel: Time-dependent electronic density calculated along the molecular axis. We see that after applying the laser field, the charge is almost completely localized on fragment B leading in such a way to the dissociation of the system.

Let us first analyze the situation when the system is controlled in a way to achieve almost complete dissociation. The obtained laser pulse sequence plotted together with the time evolution of the electronic density is shown in Fig. 5.10. The middle panel of the picture illustrates the evolution of the adiabatic populations of the electronic states. It is clearly seen that starting from a linear combination of states, the specifically designed laser field bring the system to its higher electronic state. At the same time, the charge oscillating back and forth between the left and right moieties of the system almost completely localizes on fragment B. Moreover, one can seen that such kind of control leads to the dissociation of the system with a speed defined by the kinetic energy of the nuclei moving on the higher electronic state. Importantly, the laser pulse affects the system only on the electronic level and the subsequent nuclear dynamics

takes place without any external influence, illustrating thus the concept of the purely electronic control of the chemical reaction.

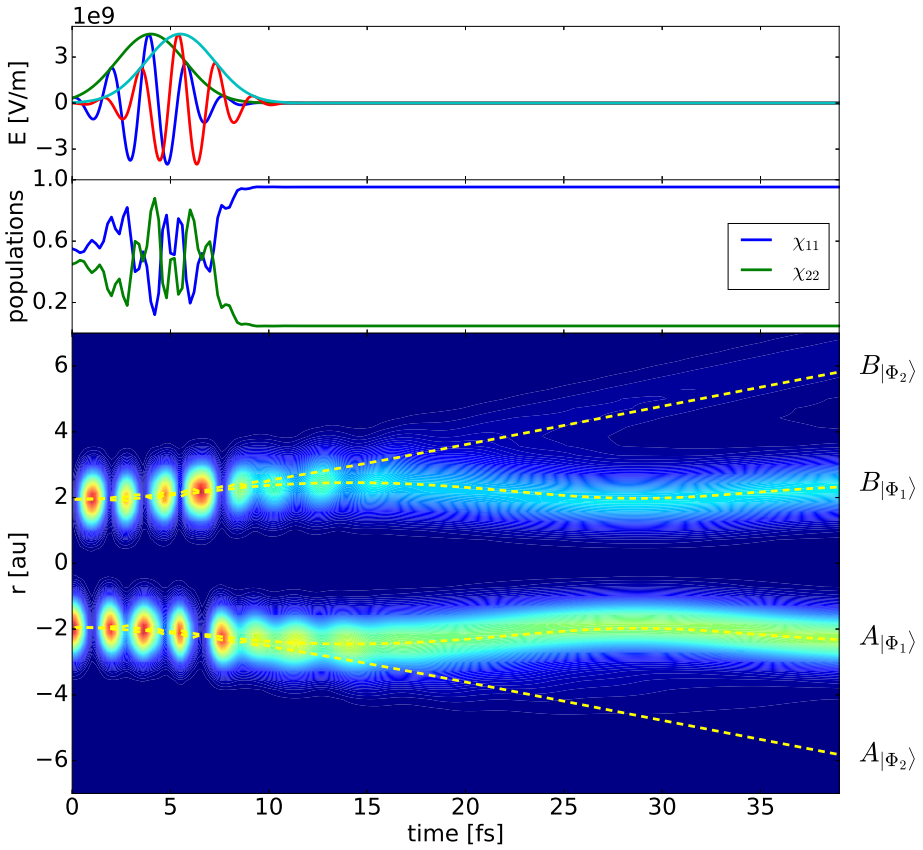

Figure 5.11: Control of the molecular fragmentation by an external laser field. The laser pulse is designed to prevent the dissociation of the molecule. Upper panel: Two identical Gaussian laser pulses with parameters optimized to achieve the desired quantum control. Middle panel: Evolution of the adiabatic populations of the electronic states. Lower panel: Time-dependent electronic density plotted along the molecular axis. We see that after applying the laser field, the charge is redistributed between A and B fragments of the molecule preventing in such a way the dissociation of the system.

An opposite situation is presented in Fig. 5.11. The two identical laser pulses are designed to prevent dissociation of the system. In the middle panel of the picture, the time evolution of the adiabatic populations of the electronic states is presented. It is seen that after applying the external field, the system is driven such that it almost completely lends on its lower electronic state. In the lower panel of Fig. 5.11, the time-dependent electronic density is plotted. The charge initially localized on the left site of the system is finally redistributed along the molecular axis. The molecule remains bound, oscillating with a frequency reflecting the swinging motion of the nuclear wave packet inside the potential well of the lower electronic state.

Concluding this section, we would like to point out that although the parameters of the model were chosen to exemplify the idea of the attosecond molecular control, they

are fully within the ranges of the expected values in real molecules. For example, one can expect that the MePeNNA molecule studied in subsection 4.3.1 of the present thesis will experience the similar behavior. Our preliminary calculations show that the potential energy surfaces corresponding to the two lower cationic states have an opposite nuclear topology. Accordingly, localization of the charge on one of the two sites of the molecule will directly affect its reactivity. The full quantum mechanical simulation of the described situation is rather complicated due to non-trivial nuclear dynamics appearing in this system. However, using the approaches presented in the present chapter, it seems to be realistic to tackle this interesting problem.

5.5 Conclusions

In this chapter we considered several physical effects appearing upon the correlated treatment of the electronic and nuclear motion. It was shown on a model system how the ultrafast electronic charge dynamics is influenced be the slower nuclear motion. We demonstrated that the electronic decoherence caused by nuclear rearrangement leads to a damping of the electronic density oscillations. The presented example allows one to better understand the different factors which affect the electronic decoherence, as well as to see their dependence on the particular form of the involved potential energy surfaces.

Our full-dimensional *ab initio* calculations of the electron-nuclear dynamics performed on the manifold of four cationic states of the propiolic acid molecule have shown that the electronic decoherence time can be rather long, allowing one to observe several oscillations of the charge before nuclear dynamics eventually traps it.

In the last section of the chapter, the model situation which illustrates the attosecond control of a molecular fragmentation is presented. It was shown how one can turn the rearrangement of the nuclei in required direction by controlling the electronic dynamics only. The possibility to achieve good enough control over the complicated electron-nuclear dynamics by using quantum control methods described in previous chapter is provided. We argue that this model may be used to exemplify the paradigm of attochemistry. It was demonstrated that a chemical reaction can be controlled be steering the initial electronic dynamics step which eventually leads to a full control over the molecular reactivity.

This is a rhetorical question to figure out whether the dissociation leads to the localization of the charge in a molecule or the control of the charge position affects the follow-up nuclear dynamics. This two points of view, namely, the one which is based

on the validity of the potential energy surfaces picture and the other one which is more chemically-based, reflect the same physical phenomena appearing upon ionization of a molecule. The control of the charge migration will, under any scenario, offer new ways to manipulate the dynamics of the whole molecule.

6

Conclusions and Outlook

This chapter provides a summary of the results obtained and discusses possible future directions in studying electron-nuclear dynamics in external electromagnetic fields

In this work we investigated the multifaceted interplay between the faster electron and the slower nuclear dynamics appearing upon ionization of a molecular system in the presence of an external electromagnetic field. The possibilities to manipulate quantum molecular dynamics by applying specifically tailored ultrashort laser pulses were inspected and analyzed. Theoretical approaches allowing to obtain a laser field which is able to steer the desired evolution of a quantum system were developed. We proposed a simple analytical expression connecting the evolution of the populations in a two-level quantum system along a predefined path with the explicit form of the applied laser field. In case of more complicated systems, we showed that using direct search algorithms for solving the quantum control problem it is possible to find Gaussian-shaped laser pulses that can drive the evolution of the system in a predefined way. Employing the presented methodologies, we demonstrated by fully *ab initio* calculations on experimentally interesting molecules that the charge migration can be controlled on a few femtosecond time scale. It was shown that simple laser pulses can be used to manipulate the many-body quantum dynamics of the electronic density, either localizing or redistributing it along the molecular chain.

We studied how the correlated treatment of the electronic and nuclear dynamics affects the coherence of the electronic wave packet. Our investigation on a simple model system allowed for a detailed analysis of the factors which influence the charge oscillations, as well as of the conditions under which the ultrafast electronic dynamics can survive for a rather long time. We demonstrated by full-dimensional calculations on the propiolic acid molecule that the electronic decoherence time can be long enough to allow one to observe several oscillations of the charge before nuclear dynamics eventually traps it. Utilizing the strong coupling between the electronic and the nuclear motion, we exemplified the key idea of the attosecond control of a molecular reactivity. It was demonstrated on a simple model of molecular fragmentation that the nuclear rearrangement can be guided by a manipulation of the electronic dynamics only. Using the two-delayed-laser-pulses technique developed in this thesis, we have shown that the specifically tailored ultrashort laser field can either amplify or almost completely prevent the dissociation of the system. We argue that this example clearly illustrates the concept of attochemistry and thus can be used as a starting point to deepen our understanding of the possibilities to control chemical reactions.

The dissociation process presented in this work as an example of a simple chemical reaction is a very natural way for a molecule to dispose of its excess electronic energy. In reality, however, much more interesting transformations can occur. An intriguing situation appears when two or even more molecules participate in a chemical reaction. In this case, it is easy to imagine that there are much more opportunities for the electrons to influence the chemical reactivity. By redistributing electronic density between different functional sites in one of the molecules, it is possible to directly affect reaction pathways between the species in the mixture, and thus to initiate specific rearrangements of the nuclei between the desired reagents. In this way, it becomes possible not only to control the behavior of the particular molecule but rather

to predefine chemical reactions in which it can participate, as well as to preselect a particular outcome of these processes. Therefore, theoretical investigations of the possibilities to manipulate nuclear rearrangement through the control of the electronic motion on a very early stage of the evolution of a quantum system is an important direction for future investigations. We would like to note that the fully *ab initio* simulation of the chemical transformations caused by the correlated electron-nuclear dynamics of moderate sized molecules becomes possible with the help of the approaches developed and presented in this thesis. There is, however, still a lot to be done.

As it was stated in the present thesis, the electronic decoherence coming from the nuclear motion may crucially affect the possibility to observe dynamical changes of the electronic observable properties in time. The physical origin of the decoherence is the dephasing of the electronic oscillations taking place on different nuclear configuration points. In our calculations the initial phase of the involved cationic states is taken to be identical at every nuclear geometry, i.e. we assumed that the initial decoherence of the electronic wave packet is negligible. In reality, however, when the ionization is performed with a realistic laser pulse, the effect of the initial phase must be taken into account. In this respect, it has to be studied how the explicit treatment of the ionization process influences the initial coherence of the electronic subsystem. *Ab initio* simulation of the dynamics of ionization, meanwhile, requires an accurate description of the electron leaving into the continuum. Therefore, the development of theoretical approaches allowing to represent the wavefunction of the electron far away from the molecular region is an important direction for the future studies to go.

Another stumbling block in the theoretical simulations of non-adiabatic molecular dynamics is the proper description of the nuclear rearrangement. While the multi-dimensional quantum dynamics of a molecule on bound electronic states can be relatively easy described within the vibronic-coupling model, the representation of dissociative electronic states is still a big challenge for theory. At the same time, from the experimental point of view the detection of molecular fragments is an important source of information about fundamental processes appearing on a molecular level. It is clear that the accurate theoretical modeling and numerical simulations are essential for the design of new experimental schemes and for the interpretation of the outcomes of the already performed complex measurements. Thus, in our opinion, the field of attochemistry will benefit substantially from the further development of theoretical approaches allowing to deal with quantum nuclear dynamics of weakly bound and dissociative systems.

We hope that our study and suggested directions for possible improvements will stimulate further theoretical and experimental work on the possibilities to control chemical reactions via the manipulation of the electron dynamics.

A

Appendix

In this appendix an alternative fully ab initio method allowing one to describe the correlated motion of electrons and nuclei inside a molecule is presented

Almost every molecular quantum dynamics method available nowadays is based on the picture of electronic states provided by the Born–Oppenheimer approximation. The major outcome of this approach is the representation of the evolution of the system on potential energy surfaces coupled non-adiabatically to each other. In this case, the numerical treatment of the multi-level dynamics is typically limited to cases when only very few electronic states are considered. This restriction is dictated by the fact that one needs to solve the time-dependent Schrödinger equation for every potential energy surface involved into consideration which is numerically rather expensive (for details see section 2.2 of the present thesis).

About ten years ago in his pioneering work [166], Cederbaum showed that the complete time-dependent wavefunction of a system of electrons and nuclei can be factorized into an electronic wavefunction and a nuclear wavefunction. This concept leads to time-dependent Schrödinger equations for each subsystem which could be solved either in a time-dependent Born–Oppenheimer approximation [166] or in a formally exact way [168]. The exact solution, contrary to the Born–Oppenheimer case, accounts for the full correlation between the two subsystems, regardless of the mass and energy of the nuclear one. It allows, in turn, to treat the non-adiabatic nuclear dynamics by solution of only one nuclear Schrödinger equation which nevertheless takes into account the full electronic dynamics, without a reference to the Born–Oppenheimer electronic states.

Despite the bright promise of the exact factorization approach, it stumbled on several computational problems which restricted its current application only to analysis of exactly solvable models [166, 168–173], theoretical extensions of the quantum mechanical concepts [171, 174–181], or implementation within mixed quantum-classical schemes [173, 178, 180, 182–190]. Until now, however, a numerical algorithm which allows one to solve the exact factorization problem directly has not been reported. The main goal of the present study is to put forward several useful mathematical approaches which can allow one to apply the exact factorization formalism to previously inaccessible situations.

To be specific, let us present here the set of coupled exact equations obtained by substitution of the following ansatz for the full molecular wavefunction

$$\Psi(\mathbf{r}, \mathbf{R}, t) = \chi(\mathbf{R}, t)\Phi(\mathbf{r}, \mathbf{R}, t), \tag{A.1}$$

into the time-dependent Schrödinger Eq. (2.1). Here, $\chi(\mathbf{R}, t)$ is the nuclear wavefunction and $\Phi(\mathbf{r}, \mathbf{R}, t)$ is the electronic conditional wavefunction that satisfies the partial normalization condition

$$\langle \Phi(\mathbf{r}, \mathbf{R}, t) | \Phi(\mathbf{r}, \mathbf{R}, t) \rangle_{\mathbf{r}} = 1, \tag{A.2}$$

for any fixed nuclear configuration, $\mathbf{R}$, at any moment of time. We omit the full derivation of the equations and present here only the final result (for details see

Ref. [169])

$$\left(\hat{H}_e(\mathbf{r},\mathbf{R}) + \hat{U}_{en}^{coup}[\Phi,\chi] - \varepsilon(\mathbf{R},t)\right)\Phi(\mathbf{r},\mathbf{R},t) = i\frac{\partial}{\partial t}\Phi(\mathbf{r},\mathbf{R},t), \tag{A.3}$$

$$\left(\sum_\alpha \frac{1}{2M_\alpha}(-i\nabla_\alpha + \mathbf{A}_\alpha(\mathbf{R},t))^2 + \varepsilon(\mathbf{R},t)\right)\chi(\mathbf{R},t) = i\frac{\partial}{\partial t}\chi(\mathbf{R},t), \tag{A.4}$$

where $\hat{H}_e(\mathbf{r},\mathbf{R})$ is the familiar Born–Oppenheimer electronic Hamiltonian (see Eq. (2.3)). The electron-nuclear coupling operator $\hat{U}_{en}^{coup}[\Phi,\chi]$, scalar potential $\varepsilon(\mathbf{R},t)$ and vector coupling $\mathbf{A}_\alpha(\mathbf{R},t)$ terms are

$$\begin{aligned}\hat{U}_{en}^{coup}[\Phi,\chi] = \sum_\alpha \frac{1}{M_\alpha}\Bigg[&\frac{(-i\nabla_\alpha - \mathbf{A}_\alpha(\mathbf{R},t))^2}{2} \\ &+ \left(\frac{-i\nabla_\alpha\chi(\mathbf{R},t)}{\chi(\mathbf{R},t)} + \mathbf{A}_\alpha(\mathbf{R},t)\right)\cdot(-i\nabla_\alpha - \mathbf{A}_\alpha(\mathbf{R},t))\Bigg],\end{aligned} \tag{A.5}$$

$$\varepsilon(\mathbf{R},t) = \langle\Phi(\mathbf{r},\mathbf{R},t)|\hat{H}_e(\mathbf{r},\mathbf{R}) + \hat{U}_{en}^{coup}[\Phi,\chi] - i\frac{\partial}{\partial t}|\Phi(\mathbf{r},\mathbf{R},t)\rangle_{\mathbf{r}}, \tag{A.6}$$

$$\mathbf{A}_\alpha(\mathbf{R},t) = \langle\Phi(\mathbf{r},\mathbf{R},t)| - i\nabla_\alpha|\Phi(\mathbf{r},\mathbf{R},t)\rangle_{\mathbf{r}}. \tag{A.7}$$

As one can see, the representation of the molecular wavefunction in the form of Eq. (A.1) leads to the decomposition of the time-dependent Schrödinger equation in two coupled evolution equations which describe the correlated motion of nuclei and electrons in a molecule. Eq. (A.4) is similar to the standard nuclear equation of motion (see Eq. (2.18)) appearing as a result of the Born–Oppenheimer approximation. The difference is that in the present case, the nuclear wave packet is moving on the time-dependent potential accounting for the non-adiabatic effects. The electronic Eq. (A.3) describes how the electronic wave function follows the nuclear evolution and contains the full dynamical coupling to the nuclear degrees of freedom, encoded in the operator $\hat{U}_{en}^{coup}[\Phi,\chi]$. In the spirit of the Born–Oppenheimer approach, the resulting equations can be interpreted as effectively mixing all involved electronic states and in such a way producing only one equation of motion for the nuclear wave-packet, which nevertheless takes into account the non-adiabatic dynamics on all involved electronic states.

Despite the possibility to derive a formally exact set of coupled equations for the factorized electron-nuclear motion, the real numerical solution of this problem is still very challenging. In particular, the propagation of both equations in time requires to calculate the action of the gradient ∇ and the Laplace ∇^2 operators with respect to the nuclear coordinates on the electronic wavefunction $\Phi(\mathbf{r},\mathbf{R},t)$. In most practically relevant cases, the electronic Hamiltonian $\hat{H}_e(\mathbf{r},\mathbf{R})$, in turn, can be computed only for a very limited number of nuclear configurations due to the enormous numerical complexity of the problem. At the same time, the solution of the electronic Eq. (A.3) implies that the electronic wavefunction will "accumulate" with time properties of the

operator $\hat{H}_e(\mathbf{r},\mathbf{R}) + \hat{U}_{en}^{coup}[\Phi,\chi] - \varepsilon(\mathbf{R},t)$ in an exponential manner. This explicitly follows from the formal solution, Eq. (3.2), of the time-dependent Schrödinger equation. These factors result in fast oscillations of the electronic wavefunction with respect to nuclear degrees of freedom $\mathbf{R}$, leading thereby to inapplicability of the usual grid-based methods for calculation of the derivative operators along a limited number of nuclear configurations.

Although the Born–Oppenheimer approach results in a set of dynamical equations accounting for the evolution of the nuclear wave packets on the manifold of involved electronic states, the idea by itself does not go beyond the assumption that the electronic basis set, obtained as a solution of the time-independent Schrödinger equation with electronic Hamiltonian $\hat{H}_e(\mathbf{r},\mathbf{R})$, will vary slowly during the rearrangement of the nuclei. This concept can be used for treating the exact factorization problem as well. In particular, one can expect that the electronic wavefunction can be expanded in a basis of the stationary electronic states $\{\Phi_k(\mathbf{r},\mathbf{R})\}$ associated with the Born–Oppenheimer electronic Hamiltonian in the following way

$$\Phi(\mathbf{r},\mathbf{R},t) = \sum_k c_k(\mathbf{R},t)\exp\left[i\varphi_k(\mathbf{R},t)\right]\Phi_k(\mathbf{r},\mathbf{R}), \tag{A.8}$$

where the real functions $c_k(\mathbf{R},t)$ and $\varphi_k(\mathbf{R},t)$ represent the weight factor and the phase of the corresponding electronic state $\Phi_k(\mathbf{r},\mathbf{R})$, respectively. Due to the large difference in the time scales of the electronic and the nuclear motion, the introduced functions will vary slowly along the nuclear degrees of freedom, since they reflect the non-adiabatic changes in the populations and phases of the involved electronic states caused by the relatively slow nuclear motion. Even in the case when the non-adiabatic transitions are triggered, for example, by the influence of external laser fields acting directly on the electronic wavefunction, the time step of propagation can be chosen small enough to ensure a smooth change in the functions $c_k(\mathbf{R},t)$ and $\varphi_k(\mathbf{R},t)$.

The introduced ansatz, Eq. (A.8), for representation of the electronic wavefunction allows one to follow the evolution of the weights $c_k(\mathbf{R},t)$ and phases $\varphi_k(\mathbf{R},t)$ of the corresponding electronic states explicitly. It provides, in turn, the opportunity to calculate the action of the gradient and the Laplacian operators in a composite way. Assuming that the electronic basis $\{\Phi_k(\mathbf{r},\mathbf{R})\}$ has a weak dependence on the nuclear degrees of freedom $\mathbf{R}$ (e.g. by choosing an appropriate diabatic representation), one can express the action of the required operators in the following way

$$\nabla\Phi = \sum_k (\nabla c_k + i c_k \nabla\varphi_k)\exp\left[i\varphi_k\right]\Phi_k, \tag{A.9}$$

$$\nabla^2\Phi = \sum_k (\nabla^2 c_k + 2i\nabla c_k\cdot\nabla\varphi_k - c_k(\nabla\varphi_k)^2 + i c_k\nabla^2\varphi_k)\exp\left[i\varphi_k\right]\Phi_k. \tag{A.10}$$

Contrary to the usual methods for calculation of the time-dependent expansion coefficients, we eliminate the rapidly oscillating phases and use the properties of the

derivative of complex functions. In this way, we obtain semi-analytical expressions for the action of the derivative operators, while the required contributions, namely, the gradients ∇c_k, $\nabla \varphi_k$, and the Lapacians $\nabla^2 c_k$, $\nabla^2 \varphi_k$, can be calculated using the usual grid-based approaches.

Using the presented formulas for the action of the derivative operators on the electronic wavefunction, one can easily obtain the explicit form of the non-adiabatic vector and scalar couplings

$$\langle \Phi | \nabla | \Phi \rangle_{\mathbf{r}} = \sum_k (c_k \nabla c_k + i c_k^2 \nabla \varphi_k), \tag{A.11}$$

$$\langle \Phi | \nabla^2 | \Phi \rangle_{\mathbf{r}} = \sum_k (c_k \nabla^2 c_k + 2 i c_k \nabla c_k \nabla \varphi_k - c_k^2 (\nabla \varphi_k)^2 + i c_k^2 \nabla^2 \varphi_k), \tag{A.12}$$

where the orthogonality of the basis states $\langle \Phi_i | \Phi_j \rangle_{\mathbf{r}} = \delta_{ij}$ was used.

The obtained expressions allows one to reconstruct the vector and scalar potentials, $\mathbf{A}_\alpha(\mathbf{R}, t)$ and $\varepsilon(\mathbf{R}, t)$, respectively, as well as all the required terms in the electron-nuclear coupling operator $\hat{U}_{en}^{coup}[\Phi, \chi]$. Using the presented scheme, one can solve the system of Eqs. (A.3) and (A.4) iteratively, treating the weights $c_k(\mathbf{R}, t)$ and the phases $\varphi_k(\mathbf{R}, t)$ separately. Although the presented equations look quite cumbersome, their numerical solution can be performed relatively easy. For example, the more challenging electronic Eq. (A.3) represents in this form just the propagation of the electronic wavefunction on every fixed nuclear point of the grid with the matrix of the operator $\hat{H}_e(\mathbf{r}, \mathbf{R})$, while the remaining part of the full operator can be expressed as additional quantities which modify the corresponding eigenvalues only. The solution of the nuclear Schrödinger Eq. (A.4) can be obtained as well, since it represents a very well studied problem of the propagation of the initial wave packet on a known potential. The only difference is that the potential depends on time and is defined by the solution of the electronic Eq. (A.3). We would like to emphasize additionally that despite using the Born–Oppenheimer electronic states as a basis to expand the electronic wavefunction, Eq. (A.8), the resulting equations which need to be solved are obtained within the exact factorization approach. Contrary to treating the evolution of the nuclear coefficients on every included electronic state, we solve here a set of the electronic Schrödinger equations for every nuclear point on the grid, obtaining in this way the potential which thus drive the evolution of the total nuclear wavefunction.

The scheme presented has, however, some accompanying disadvantages. The weight factors $c_k(\mathbf{R}, t)$ and the phases $\varphi_k(\mathbf{R}, t)$ are continuous functions over the whole nuclear domain $\mathbf{R}$. While the nuclear wavefunctions $\chi_k(\mathbf{R}, t)$ operated within the Born–Oppenheimer approximation are vanishing on the borders of the nuclear interval, the coefficients in the expansion (A.8) are, in general, not. This implies certain difficulties in calculating the action of the derivative operators on the borders of the chosen grid due to the fact that these operators are non-local. Another complexity lies in the rather unusual operations which are need to be performed for the calculation of the gradients and Laplacians of the electronic wavefunction, Eqs. (A.9) and (A.10), as

well as the coupling terms, Eqs. (A.11) and (A.12). Indeed, in order to overcome the non-locality limitations discussed above, one can use global basis representation of the corresponding weights and phases. This leads, however, to the necessity to compute different products between functions represented in some predefined basis set which is not a trivial mathematical task. Despite the discussed limitations, the presented approach provides a tool which allows for the very first time the direct numerical solution of the exact factorization problem.

Let us now illustrate the described methodology on a concrete numerical example. We will exemplify the direct solution of the exact factorization problem on the two-level model described in subsection 5.2.2 of the present thesis. The parameters of the model are chosen to be the same as was used before. Our goal here is to perform numerical propagation of the nuclear wave packet driven by Eqs. (A.3) and (A.4), and compare the obtained results with the exact solution presented earlier. We use direct numerical representation of the required functions on the grid. The gradients and the Laplacians are calculated using the standard finite-difference method.

In Fig. A.1 we show snapshots of the nuclear density moving on the corresponding electronic states together with the weight factors $c_k(R,t)$. Within the exact factorization formalism the nuclear density on a particular state can be obtained by a projection of the total density on the corresponding electronic state in the following way

$$|\chi_k^{\mathrm{exf}}(\mathbf{R},t)|^2 = |\langle\Phi_k(\mathbf{r},\mathbf{R})|\Phi(\mathbf{r},\mathbf{R},t)\rangle_{\mathbf{r}}|^2 = |c_k(\mathbf{R},t)\chi(\mathbf{R},t)|^2, \tag{A.13}$$

where we have introduced superscript in order to distinguish the obtained densities from those which are calculated by the numerical integration of the time-dependent Schrödinger equation for dynamics on the predefined electronic potentials. If for the exact factorization problem we choose the same electronic basis set $\{\Phi_k(\mathbf{r},\mathbf{R})\}$ as the one used for constructing the Born–Oppenheimer nuclear potentials $V_k(\mathbf{R})$, the obtained nuclear densities $|\chi_k^{\mathrm{exf}}(\mathbf{R},t)|^2$ and $|\chi_k(\mathbf{R},t)|^2$, respectively, should be equivalent. In the upper panel of Fig. A.1 the evolution of the nuclear densities calculated by the exact factorization approach (solid lines) plotted together with the reference densities obtained through the Born–Oppenheimer approach (dots) is shown. We see that, as expected, $|\chi_k^{\mathrm{exf}}(\mathbf{R},t)|^2$ coincide with $|\chi_k(\mathbf{R},t)|^2$. We note that within the exact factorization we obtain one nuclear wavefunction $\chi(\mathbf{R},t)$ and $\chi_k^{\mathrm{exf}}(\mathbf{R},t)$ are just its appropriately extracted components (see Eq. (A.13)). In the lower panel of Fig. A.1 the evolution of the weight factors $c_k(R,t)$ is shown. It is clearly seen that the weights of the corresponding electronic states are changing in time according to the redistribution of the electronic wavefunction between the involved electronic states.

As was pointed out in the beginning of this appendix, the form of the electronic Schrödinger Eq. (A.3) implies that the properties of the corresponding Hamilton operator will be accumulated to the solution at every iteration time step. At the same time, the finite-difference method chosen for the calculation of the derivative operators is not very precise on the borders of the nuclear grid. This, in turn, leads to numerical

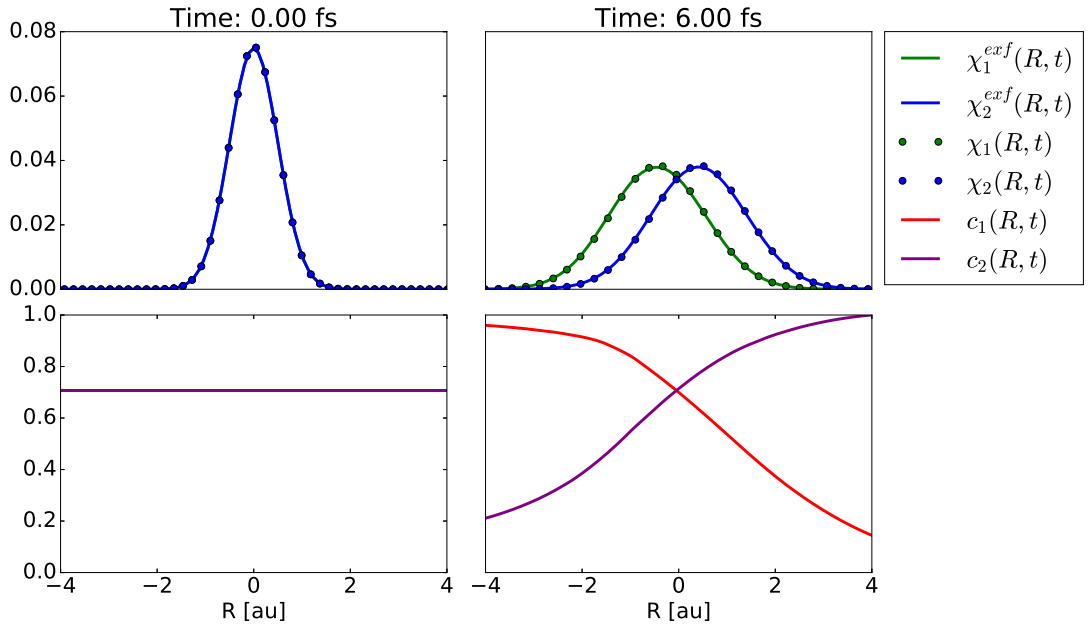

Figure A.1: Upper panel: Time-dependent nuclear densities moving on the corresponding electronic states reconstructed from the total nuclear density via Eq. (A.13). The total nuclear density was calculated by the direct numerical solution of the exact factorization problem, Eqs. (A.3) and (A.4). Dots indicate nuclear densities computed by usual numerical integration of the time-dependent Schrödinger equation for dynamics on the predefined potentials. Lower panel: Evolution of the weights factors $c_k(R,t)$ which indicate distribution of the electronic density between involved electronic states.

deviations appearing on the borders of the grid which grow with time. At some point the accumulated numerical errors become large, preventing the subsequent propagation of the electronic subsystem. It is worth noting that this problem does not appear when one works within the time-dependent Born–Oppenheimer version [166] of the exact factorization approach. In this case, the electronic wavefunction does not accumulate the errors stemming from numerical treatment of the derivative operators since the electronic Hamiltonian in this case is reduced to the usual Born–Oppenheimer form. The calculation of the derivative couplings is very stable in that case, which allows one to propagate the nuclear wave packet for an infinitely long time.

Although the presented approach utilizes the concept of the electronic states initially appearing within the Born–Oppenheimer approach, the resulting equations are based on the exact factorization formalism. From a practical point of view, the introduced representation of the electronic wavefunction allows one to solve the exact factorization Eqs. (A.3) and (A.4) numerically for problems beyond those where the explicit form of the full molecular wavefunction $\Psi(\mathbf{r},\mathbf{R},t)$ can be obtained in advance. A direction for future research in this field is to develop the formalism which will allow to represent the weight factors $c_k(\mathbf{R},t)$ and the phases $\varphi_k(\mathbf{R},t)$ on a predefined nuclear basis set, allowing in this way to reduce the numerical errors and consequently to increase the propagation time.

Bibliography

[1] A. H. Zewail, "Femtochemistry: Atomic-Scale Dynamics of the Chemical Bond Using Ultrafast Lasers (Nobel Lecture)", *Angewandte Chemie International Edition*, vol. 39, no. 15, pp. 2586–2631, Aug. 2000.

[2] A. H. Zewail, "Femtochemistry. Past, present, and future", *Pure and Applied Chemistry*, vol. 72, no. 12, Jan. 2000.

[3] A. H. Zewail, "Femtochemistry: Atomic-Scale Dynamics of the Chemical Bond", *The Journal of Physical Chemistry A*, vol. 104, no. 24, pp. 5660–5694, Jun. 2000.

[4] A. H. Zewail, *Femtochemistry: Ultrafast Dynamics of the Chemical Bond*, ser. World Scientific series in 20th Century Chemistry. Singapore: World Scientific, 1994, vol. I and II.

[5] M. Nisoli, P. Decleva, F. Calegari, A. Palacios, and F. Martín, "Attosecond Electron Dynamics in Molecules", *Chemical Reviews*, vol. 117, no. 16, pp. 10 760–10 825, Aug. 2017.

[6] F. Lépine, M. Y. Ivanov, and M. J. J. Vrakking, "Attosecond molecular dynamics: fact or fiction?", *Nature Photonics*, vol. 8, no. 3, pp. 195–204, Feb. 2014.

[7] F. Krausz and M. Ivanov, "Attosecond physics", *Reviews of Modern Physics*, vol. 81, no. 1, pp. 163–234, Feb. 2009.

[8] F. Calegari, G. Sansone, S. Stagira, C. Vozzi, and M. Nisoli, "Advances in attosecond science", *Journal of Physics B: Atomic, Molecular and Optical Physics*, vol. 49, no. 6, p. 062 001, Mar. 2016.

[9] G. Sansone, E. Benedetti, F. Calegari, C. Vozzi, L. Avaldi, R. Flammini, L. Poletto, P. Villoresi, C. Altucci, R. Velotta, S. Stagira, S. De Silvestri, and M. Nisoli, "Isolated Single-Cycle Attosecond Pulses", *Science*, vol. 314, no. 5798, pp. 443–446, Oct. 2006.

[10] E. Goulielmakis, M. Schultze, M. Hofstetter, V. S. Yakovlev, J. Gagnon, M. Uiberacker, A. L. Aquila, E. M. Gullikson, D. T. Attwood, R. Kienberger, F. Krausz, and U. Kleineberg, "Single-Cycle Nonlinear Optics", *Science*, vol. 320, no. 5883, pp. 1614–1617, Jun. 2008.

[11] M. Drescher, M. Hentschel, R. Kienberger, M. Uiberacker, V. Yakovlev, A. Scrinzi, T. Westerwalbesloh, U. Kleineberg, U. Heinzmann, and F. Krausz, "Time-resolved atomic inner-shell spectroscopy", *Nature*, vol. 419, no. 6909, pp. 803–807, Oct. 2002.

[12] H. Niikura, D. M. Villeneuve, and P. B. Corkum, "Mapping Attosecond Electron Wave Packet Motion", *Physical Review Letters*, vol. 94, no. 8, Mar. 2005.

[13] O. Smirnova, Y. Mairesse, S. Patchkovskii, N. Dudovich, D. Villeneuve, P. Corkum, and M. Y. Ivanov, "High harmonic interferometry of multi-electron dynamics in molecules", *Nature*, vol. 460, no. 7258, pp. 972–977, Aug. 2009.

[14] O. Smirnova, S. Patchkovskii, Y. Mairesse, N. Dudovich, and M. Y. Ivanov, "Strong-field control and spectroscopy of attosecond electron-hole dynamics in molecules", *Proceedings of the National Academy of Sciences*, vol. 106, no. 39, pp. 16 556–16 561, Sep. 2009.

[15] E. Goulielmakis, Z.-H. Loh, A. Wirth, R. Santra, N. Rohringer, V. S. Yakovlev, S. Zherebtsov, T. Pfeifer, A. M. Azzeer, M. F. Kling, S. R. Leone, and F. Krausz, "Real-time observation of valence electron motion", *Nature*, vol. 466, no. 7307, pp. 739–743, Aug. 2010.

[16] S. Eberhard, G. Finazzi, and F.-A. Wollman, "The Dynamics of Photosynthesis", *Annual Review of Genetics*, vol. 42, no. 1, pp. 463–515, Dec. 2008.

[17] A. Bauer, F. Westkämper, S. Grimme, and T. Bach, "Catalytic enantioselective reactions driven by photoinduced electron transfer", *Nature*, vol. 436, no. 7054, pp. 1139–1140, Aug. 2005.

[18] D. Becker, A. Adhikary, and M. D. Sevilla, "The Role of Charge and Spin Migration in DNA Radiation Damage", in *Charge Migration in DNA*, P. Avouris, B. Bhushan, D. Bimberg, K. von Klitzing, H. Sakaki, R. Wiesendanger, and T. Chakraborty, Eds., Berlin: Springer, 2007, pp. 139–175.

[19] F. Calegari, A. Trabattoni, A. Palacios, D. Ayuso, M. C. Castrovilli, J. B. Greenwood, P. Decleva, F. Martín, and M. Nisoli, "Charge migration induced by attosecond pulses in bio-relevant molecules", *Journal of Physics B: Atomic, Molecular and Optical Physics*, vol. 49, no. 14, p. 142 001, Jul. 2016.

[20] J. Jortner and M. A. Ratner, Eds., *Molecular Electronics*, ser. A "chemistry for the 21st century" monograph. Oxford: Blackwell Science, 1997.

[21] V. May and O. Kühn, *Charge and Energy Transfer Dynamics in Molecular Systems*. Weinheim: Wiley-VCH, Dec. 2003.

[22] L. Cederbaum and J. Zobeley, "Ultrafast charge migration by electron correlation", *Chemical Physics Letters*, vol. 307, no. 3-4, pp. 205–210, Jul. 1999.

[23] A. I. Kuleff and L. S. Cederbaum, "Ultrafast correlation-driven electron dynamics", *Journal of Physics B: Atomic, Molecular and Optical Physics*, vol. 47, no. 12, p. 124 002, Jun. 2014.

[24] A. I. Kuleff and L. S. Cederbaum, "Charge migration in different conformers of glycine: The role of nuclear geometry", *Chemical Physics*, vol. 338, no. 2-3, pp. 320–328, Sep. 2007.

[25] S. Lünnemann, A. I. Kuleff, and L. S. Cederbaum, "Charge migration following ionization in systems with chromophore-donor and amine-acceptor sites", *The Journal of Chemical Physics*, vol. 129, no. 10, p. 104 305, Sep. 2008.

[26] A. I. Kuleff, S. Lünnemann, and L. S. Cederbaum, "Electron-correlation-driven charge migration in oligopeptides", *Chemical Physics*, vol. 414, pp. 100–105, Mar. 2013.

[27] S. Lünnemann, A. I. Kuleff, and L. S. Cederbaum, "Ultrafast charge migration in 2-phenylethyl-N,N-dimethylamine", *Chemical Physics Letters*, vol. 450, no. 4-6, pp. 232–235, Jan. 2008.

[28] D. Mendive-Tapia, M. Vacher, M. J. Bearpark, and M. A. Robb, "Coupled electron-nuclear dynamics: Charge migration and charge transfer initiated near a conical intersection", *The Journal of Chemical Physics*, vol. 139, no. 4, p. 044 110, Jul. 2013.

[29] M. Vacher, M. J. Bearpark, and M. A. Robb, "Communication: Oscillating charge migration between lone pairs persists without significant interaction with nuclear motion in the glycine and Gly-Gly-NH-CH_3 radical cations", *The Journal of Chemical Physics*, vol. 140, no. 20, p. 201 102, May 2014.

[30] C. Arnold, O. Vendrell, and R. Santra, "Electronic decoherence following photoionization: Full quantum-dynamical treatment of the influence of nuclear motion", *Physical Review A*, vol. 95, no. 3, Mar. 2017.

[31] M. Vacher, M. J. Bearpark, M. A. Robb, and J. P. Malhado, "Electron Dynamics upon Ionization of Polyatomic Molecules: Coupling to Quantum Nuclear Motion and Decoherence", *Physical Review Letters*, vol. 118, no. 8, Feb. 2017.

[32] F. Remacle, R. Levine, and M. Ratner, "Charge directed reactivity: a simple electronic model, exhibiting site selectivity, for the dissociation of ions", *Chemical Physics Letters*, vol. 285, no. 1-2, pp. 25–33, Mar. 1998.

[33] R. Weinkauf, P. Aicher, G. Wesley, J. Grotemeyer, and E. W. Schlag, "Femtosecond versus Nanosecond Multiphoton Ionization and Dissociation of Large Molecules", *The Journal of Physical Chemistry*, vol. 98, no. 34, pp. 8381–8391, Aug. 1994.

[34] R. Weinkauf, E. W. Schlag, T. J. Martinez, and R. D. Levine, "Nonstationary Electronic States and Site-Selective Reactivity", *The Journal of Physical Chemistry A*, vol. 101, no. 42, pp. 7702–7710, Oct. 1997.

[35] E. Schlag, S.-Y. Sheu, D.-Y. Yang, H. Selzle, and S. Lin, "Distal Charge Transport in Peptides", *Angewandte Chemie International Edition*, vol. 46, no. 18, pp. 3196–3210, Apr. 2007.

[36] L. Lehr, T. Horneff, R. Weinkauf, and E. W. Schlag, "Femtosecond Dynamics after Ionization: 2-Phenylethyl-N, N-dimethylamine as a Model System for Nonresonant Downhill Charge Transfer in Peptides", *The Journal of Physical Chemistry A*, vol. 109, no. 36, pp. 8074–8080, Sep. 2005.

[37] W. Cheng, N. Kuthirummal, J. L. Gosselin, T. I. Sølling, R. Weinkauf, and P. M. Weber, "Control of Local Ionization and Charge Transfer in the Bifunctional Molecule 2-Phenylethyl-N, N-dimethylamine Using Rydberg Fingerprint Spectroscopy", *The Journal of Physical Chemistry A*, vol. 109, no. 9, pp. 1920–1925, Mar. 2005.

[38] F. Calegari, D. Ayuso, A. Trabattoni, L. Belshaw, S. De Camillis, S. Anumula, F. Frassetto, L. Poletto, A. Palacios, P. Decleva, J. B. Greenwood, F. Martin, and M. Nisoli, "Ultrafast electron dynamics in phenylalanine initiated by attosecond pulses", *Science*, vol. 346, no. 6207, pp. 336–339, Oct. 2014.

[39] L. Belshaw, F. Calegari, M. J. Duffy, A. Trabattoni, L. Poletto, M. Nisoli, and J. B. Greenwood, "Observation of Ultrafast Charge Migration in an Amino Acid", *The Journal of Physical Chemistry Letters*, vol. 3, no. 24, pp. 3751–3754, Dec. 2012.

[40] P. M. Kraus, B. Mignolet, D. Baykusheva, A. Rupenyan, L. Horny, E. F. Penka, G. Grassi, O. I. Tolstikhin, J. Schneider, F. Jensen, L. B. Madsen, A. D. Bandrauk, F. Remacle, and H. J. Wörner, "Measurement and laser control of attosecond charge migration in ionized iodoacetylene", *Science*, vol. 350, no. 6262, pp. 790–795, Nov. 2015.

[41] M. Born and R. Oppenheimer, "Zur Quantentheorie der Molekeln", *Annalen der Physik*, vol. 389, no. 20, pp. 457–484, 1927.

[42] M. Born and K. Huang, *Dynamical Theory of Crystal Lattices*, ser. Oxford classic texts in the physical sciences. Oxford: Oxford University Press, 1954.

[43] C. J. Ballhausen and A. E. Hansen, "Electronic Spectra", *Annual Review of Physical Chemistry*, vol. 23, no. 1, pp. 15–38, Oct. 1972.

[44] W. Domcke, D. Yarkony, and H. Köppel, Eds., *Conical Intersections: Electronic Structure, Dynamics & Spectroscopy*. Singapore: World Scientific Publishing, 2004.

[45] H. Köppel, W. Domcke, and L. S. Cederbaum, "Multimode Molecular Dynamics Beyond the Born-Oppenheimer Approximation", in *Advances in Chemical Physics*, I. Prigogine and S. A. Rice, Eds., vol. 57, Hoboken: John Wiley & Sons, Inc., Jan. 1984, pp. 59–246.

[46] E. B. Wilson, J. C. Decius, and P. C. Cross, *Molecular Vibrations: The Theory of Infrared and Raman Vibrational Spectra*. New York: Dover Publications, 1980.

[47] J. P. Malhado, M. J. Bearpark, and J. T. Hynes, "Non-adiabatic dynamics close to conical intersections and the surface hopping perspective", *Frontiers in Chemistry*, vol. 2, Nov. 2014.

[48] M. Baer, *Beyond Born-Oppenheimer: Conical Intersections and Electronic Non-Adiabatic Coupling Terms*. Hoboken: Wiley, 2006.

[49] F. T. Smith, "Diabatic and Adiabatic Representations for Atomic Collision Problems", *Physical Review*, vol. 179, no. 1, pp. 111–123, Mar. 1969.

[50] T. Pacher, L. S. Cederbaum, and H. Köppel, "Adiabatic and Quasidiabatic States in a Gauge Theoretical Framework", in *Advances in Chemical Physics*, I. Prigogine and S. A. Rice, Eds., vol. 84, Hoboken: John Wiley & Sons, Inc., Jan. 1993, pp. 293–391.

[51] C. A. Mead and D. G. Truhlar, "Conditions for the definition of a strictly diabatic electronic basis for molecular systems", *The Journal of Chemical Physics*, vol. 77, no. 12, pp. 6090–6098, Dec. 1982.

[52] A. I. Kuleff, J. Breidbach, and L. S. Cederbaum, "Multielectron wave-packet propagation: General theory and application", *The Journal of Chemical Physics*, vol. 123, no. 4, p. 044 111, Jul. 2005.

[53] C. Lanczos, "An iteration method for the solution of the eigenvalue problem of linear differential and integral operators", *Journal of Research of the National Bureau of Standards*, vol. 45, no. 4, p. 255, Oct. 1950.

[54] C. Leforestier, R. H. Bisseling, C. Cerjan, M. D. Feit, R. Friesner, A. Guldberg, A. Hammerich, G. Jolicard, W. Karrlein, H.-D. Meyer, N. Lipkin, O. Roncero, and R. Kosloff, "A comparison of different propagation schemes for the time dependent Schrödinger equation", *Journal of Computational Physics*, vol. 94, no. 1, pp. 59–80, May 1991.

[55] T. Helgaker, P. Jørgensen, and J. Olsen, *Molecular Electronic-Structure Theory*. New York: Wiley, 2000.

[56] J. Schirmer, L. S. Cederbaum, and O. Walter, "New approach to the one-particle Green's function for finite Fermi systems", *Physical Review A*, vol. 28, no. 3, pp. 1237–1259, Sep. 1983.

[57] J. Schirmer, A. B. Trofimov, and G. Stelter, "A non-Dyson third-order approximation scheme for the electron propagator", *The Journal of Chemical Physics*, vol. 109, no. 12, pp. 4734–4744, Sep. 1998.

[58] I. Mayer, *Simple Theorems, Proofs, and Derivations in Quantum Chemistry*, ser. Mathematical and Computational Chemistry. Boston: Springer US, 2003.

[59] A. Szabo and N. S. Ostlund, *Modern Quantum Chemistry: Introduction to Advanced Electronic Structure Theory*. Mineola: Dover Publications, 1996.

[60] R. K. Nesbet, *Variational Principles and Methods in Theoretical Physics and Chemistry*. New York: Cambridge University Press, 2002.

[61] C. C. J. Roothaan, "New Developments in Molecular Orbital Theory", *Reviews of Modern Physics*, vol. 23, no. 2, pp. 69–89, Apr. 1951.

[62] T. Koopmans, "Über die Zuordnung von Wellenfunktionen und Eigenwerten zu den Einzelnen Elektronen Eines Atoms", *Physica*, vol. 1, no. 1-6, pp. 104–113, Jan. 1934.

[63] A. L. Fetter and J. D. Walecka, *Quantum Theory of Many-Particle Systems*. Mineola: Dover Publications, 2003.

[64] L. S. Cederbaum and W. Domcke, "Theoretical Aspects of Ionization Potentials and Photoelectron Spectroscopy: A Green's Function Approach", in *Advances in Chemical Physics*, I. Prigogine and S. A. Rice, Eds., vol. 36, Hoboken: John Wiley & Sons, Inc., Jan. 1977, pp. 205–344.

[65] A. A. Abrikosov, L. P. Gor'kov, and I. E. Dzyaloshinskii, *Methods of quantum field theory in statistical physics*, Rev. English ed. New York: Dover Publications, 1975.

[66] J. Schirmer, "Beyond the random-phase approximation: A new approximation scheme for the polarization propagator", *Physical Review A*, vol. 26, no. 5, pp. 2395–2416, Nov. 1982.

[67] J. Schirmer, "Closed-form intermediate representations of many-body propagators and resolvent matrices", *Physical Review A*, vol. 43, no. 9, pp. 4647–4659, May 1991.

[68] F. Mertins and J. Schirmer, "Algebraic propagator approaches and intermediate-state representations. I. The biorthogonal and unitary coupled-cluster methods", *Physical Review A*, vol. 53, no. 4, pp. 2140–2152, Apr. 1996.

[69] W. von Niessen, J. Schirmer, and L. Cederbaum, "Computational methods for the one-particle green's function", *Computer Physics Reports*, vol. 1, no. 2, pp. 57–125, Apr. 1984.

[70] A. B. Trofimov and J. Schirmer, "Molecular ionization energies and ground- and ionic-state properties using a non-Dyson electron propagator approach", *The Journal of Chemical Physics*, vol. 123, no. 14, p. 144 115, Oct. 2005.

[71] J. Schirmer and A. B. Trofimov, "Intermediate state representation approach to physical properties of electronically excited molecules", *The Journal of Chemical Physics*, vol. 120, no. 24, pp. 11 449–11 464, Jun. 2004.

[72] M. Schneider, D. Y. Soshnikov, D. M. P. Holland, I. Powis, E. Antonsson, M. Patanen, C. Nicolas, C. Miron, M. Wormit, A. Dreuw, and A. B. Trofimov, "A fresh look at the photoelectron spectrum of bromobenzene: A third-order non-Dyson electron propagator study", *The Journal of Chemical Physics*, vol. 143, no. 14, p. 144 103, Oct. 2015.

[73] D. J. Griffiths, *Introduction to Electrodynamics*. Upper Saddle River: Prentice Hall, 2007.

[74] F. Catoni, D. Boccaletti, R. Cannata, V. Catoni, E. Nichelatti, and P. Zampetti, *The Mathematics of Minkowski Space-Time*, ser. Frontiers in Mathematics. Basel: Birkhäuser Verlag, 2008.

[75] L. N. Hand and J. D. Finch, *Analytical Mechanics*. Cambridge: Cambridge University Press, 1998.

[76] S. T. Ali and M. Engliš, "Quantization methods: A guide for physicists and analysts", *Reviews in Mathematical Physics*, vol. 17, no. 04, pp. 391–490, May 2005.

[77] L. D. Landau and E. M. Lifshitz, *The Classical Theory of Fields*, 3rd ed., ser. Course of theoretical physics. Oxford: Pergamon Press, 1971, vol. 2.

[78] T. W. B. Kibble and F. H. Berkshire, *Classical Mechanics*, 5th ed. London: Imperial College Press, 2004.

[79] R. P. Feynman, R. B. Leighton, and M. Sands, *The Feynman Lectures on Physics. Vol. 2: Mainly Electromagnetism and Matter*, New Millenium ed. New York: Basic Books, 2010.

[80] J. D. Jackson, *Classical Electrodynamics*, 3rd ed. New York: Wiley, 1999.

[81] J. D. Jackson, "From Lorenz to Coulomb and other explicit gauge transformations", *American Journal of Physics*, vol. 70, no. 9, pp. 917–928, Sep. 2002.

[82] A. D. Bandrauk, F. Fillion-Gourdeau, and E. Lorin, "Atoms and molecules in intense laser fields: gauge invariance of theory and models", *Journal of Physics B: Atomic, Molecular and Optical Physics*, vol. 46, no. 15, p. 153 001, Aug. 2013.

[83] C. Cohen-Tannoudji, B. Diu, and F. Laloë, *Quantum mechanics*. New York: Wiley, 1977.

[84] M. Schwartz, "Electric Dipole Approximation and the Canonical Formalism in Electrodynamics", *Physical Review*, vol. 123, no. 5, pp. 1903–1908, Sep. 1961.

[85] F. Krausz, "The birth of attosecond physics and its coming of age", *Physica Scripta*, vol. 91, no. 6, p. 063 011, Jun. 2016.

[86] E. Goulielmakis, V. S. Yakovlev, A. L. Cavalieri, M. Uiberacker, V. Pervak, A. Apolonski, R. Kienberger, U. Kleineberg, and F. Krausz, "Attosecond Control and Measurement: Lightwave Electronics", *Science*, vol. 317, no. 5839, pp. 769–775, Aug. 2007.

[87] A. Wirth, M. T. Hassan, I. Grguras, J. Gagnon, A. Moulet, T. T. Luu, S. Pabst, R. Santra, Z. A. Alahmed, A. M. Azzeer, V. S. Yakovlev, V. Pervak, F. Krausz, and E. Goulielmakis, "Synthesized Light Transients", *Science*, vol. 334, no. 6053, pp. 195–200, Oct. 2011.

[88] M. T. Hassan, A. Wirth, I. Grguraš, A. Moulet, T. T. Luu, J. Gagnon, V. Pervak, and E. Goulielmakis, "Invited Article: Attosecond photonics: Synthesis and control of light transients", *Review of Scientific Instruments*, vol. 83, no. 11, p. 111 301, Nov. 2012.

[89] N. V. Golubev and A. I. Kuleff, "Control of populations of two-level systems by a single resonant laser pulse", *Physical Review A*, vol. 90, no. 3, Sep. 2014.

[90] W. S. Warren, H. Rabitz, and M. Dahleh, "Coherent Control of Quantum Dynamics: The Dream Is Alive", *Science*, vol. 259, no. 5101, pp. 1581–1589, Mar. 1993.

[91] A. Monmayrant, S. Weber, and B. Chatel, "A newcomer's guide to ultrashort pulse shaping and characterization", *Journal of Physics B: Atomic, Molecular and Optical Physics*, vol. 43, no. 10, p. 103 001, May 2010.

[92] D. Dong and I. Petersen, "Quantum control theory and applications: a survey", *IET Control Theory & Applications*, vol. 4, no. 12, pp. 2651–2671, Dec. 2010.

[93] C. Brif, R. Chakrabarti, and H. Rabitz, "Control of quantum phenomena: past, present and future", *New Journal of Physics*, vol. 12, no. 7, p. 075 008, Jul. 2010.

[94] J. Cao, C. J. Bardeen, and K. R. Wilson, "Molecular π pulses: Population inversion with positively chirped short pulses", *The Journal of Chemical Physics*, vol. 113, no. 5, pp. 1898–1909, Aug. 2000.

[95] N. V. Vitanov, T. Halfmann, B. W. Shore, and K. Bergmann, "Laser-Induced Population Transfer by Adiabatic Passage Techniques", *Annual Review of Physical Chemistry*, vol. 52, no. 1, pp. 763–809, Oct. 2001.

[96] K. Bergmann, H. Theuer, and B. W. Shore, "Coherent population transfer among quantum states of atoms and molecules", *Reviews of Modern Physics*, vol. 70, no. 3, pp. 1003–1025, Jul. 1998.

[97] N. V. Vitanov, A. A. Rangelov, B. W. Shore, and K. Bergmann, "Stimulated Raman adiabatic passage in physics, chemistry, and beyond", *Reviews of Modern Physics*, vol. 89, no. 1, Mar. 2017.

[98] P. Král, I. Thanopulos, and M. Shapiro, "Colloquium: Coherently controlled adiabatic passage", *Reviews of Modern Physics*, vol. 79, no. 1, pp. 53–77, Jan. 2007.

[99] P. Brumer and M. Shapiro, "Control of unimolecular reactions using coherent light", *Chemical Physics Letters*, vol. 126, no. 6, pp. 541–546, May 1986.

[100] D. J. Tannor, R. Kosloff, and S. A. Rice, "Coherent pulse sequence induced control of selectivity of reactions: Exact quantum mechanical calculations", *The Journal of Chemical Physics*, vol. 85, no. 10, pp. 5805–5820, Nov. 1986.

[101] R. Kosloff, S. Rice, P. Gaspard, S. Tersigni, and D. Tannor, "Wavepacket dancing: Achieving chemical selectivity by shaping light pulses", *Chemical Physics*, vol. 139, no. 1, pp. 201–220, Dec. 1989.

[102] E. Barnes and S. Das Sarma, "Analytically Solvable Driven Time-Dependent Two-Level Quantum Systems", *Physical Review Letters*, vol. 109, no. 6, Aug. 2012.

[103] A. Garon, S. J. Glaser, and D. Sugny, "Time-optimal control of SU(2) quantum operations", *Physical Review A*, vol. 88, no. 4, Oct. 2013.

[104] C. Lan, T.-J. Tarn, Q.-S. Chi, and J. W. Clark, "Analytic controllability of time-dependent quantum control systems", *Journal of Mathematical Physics*, vol. 46, no. 5, p. 052 102, May 2005.

[105] L. M. K. Vandersypen and I. L. Chuang, "NMR techniques for quantum control and computation", *Reviews of Modern Physics*, vol. 76, no. 4, pp. 1037–1069, Jan. 2005.

[106] Y. Nakamura, Y. A. Pashkin, and J. S. Tsai, "Rabi Oscillations in a Josephson-Junction Charge Two-Level System", *Physical Review Letters*, vol. 87, no. 24, Nov. 2001.

[107] A. Greilich, S. E. Economou, S. Spatzek, D. R. Yakovlev, D. Reuter, A. D. Wieck, T. L. Reinecke, and M. Bayer, "Ultrafast optical rotations of electron spins in quantum dots", *Nature Physics*, vol. 5, no. 4, pp. 262–266, Apr. 2009.

[108] D. P. Bertsekas, *Constrained Optimization and Lagrange Multiplier Methods*, ser. Optimization and neural computation series. Belmont: Athena Scientific, 1996.

[109] E. Polak, *Optimization: Algorithms and Consistent Approximations*, ser. Applied mathematical sciences 124. New York: Springer-Verlag, 1997.

[110] J. C. Spall, *Introduction to Stochastic Search and Optimization: Estimation, Simulation, and Control*, ser. Wiley-Interscience series in discrete mathematics and optimization. Hoboken: Wiley-Interscience, 2003.

[111] A. P. Peirce, M. A. Dahleh, and H. Rabitz, "Optimal control of quantum-mechanical systems: Existence, numerical approximation, and applications", *Physical Review A*, vol. 37, no. 12, pp. 4950–4964, Jun. 1988.

[112] W. Zhu, J. Botina, and H. Rabitz, "Rapidly convergent iteration methods for quantum optimal control of population", *The Journal of Chemical Physics*, vol. 108, no. 5, pp. 1953–1963, Feb. 1998.

[113] J. Werschnik and E. K. U. Gross, "Tailoring laser pulses with spectral and fluence constraints using optimal control theory", *Journal of Optics B: Quantum and Semiclassical Optics*, vol. 7, no. 10, S300–S312, Oct. 2005.

[114] J. Werschnik and E. K. U. Gross, "Quantum optimal control theory", *Journal of Physics B: Atomic, Molecular and Optical Physics*, vol. 40, no. 18, R175–R211, Sep. 2007.

[115] C. Audet and J. E. Dennis, "Mesh Adaptive Direct Search Algorithms for Constrained Optimization", *SIAM Journal on Optimization*, vol. 17, no. 1, pp. 188–217, Jan. 2006.

[116] M. Abramson, C. Audet, G. Couture, J. J. Dennis, S. Le Digabel, and C. Tribes, *NOMAD. A blackbox optimization software*, Mar. 2017.

[117] J. Breidbach and L. S. Cederbaum, "Migration of holes: Formalism, mechanisms, and illustrative applications", *The Journal of Chemical Physics*, vol. 118, no. 9, pp. 3983–3996, Mar. 2003.

[118] H. Hennig, J. Breidbach, and L. S. Cederbaum, "Charge transfer driven by electron correlation: A non-Dyson propagator approach", *The Journal of Chemical Physics*, vol. 122, no. 13, p. 134 104, Apr. 2005.

[119] H. Hennig, J. Breidbach, and L. S. Cederbaum, "Electron Correlation as the Driving Force for Charge Transfer: Charge Migration Following Ionization in *N*-Methyl Acetamide", *The Journal of Physical Chemistry A*, vol. 109, no. 3, pp. 409–414, Jan. 2005.

[120] J. Breidbach and L. S. Cederbaum, "Migration of holes: Numerical algorithms and implementation", *The Journal of Chemical Physics*, vol. 126, no. 3, p. 034 101, Jan. 2007.

[121] A. I. Kuleff and A. Dreuw, "Theoretical description of charge migration with a single Slater-determinant and beyond", *The Journal of Chemical Physics*, vol. 130, no. 3, p. 034 102, Jan. 2009.

[122] S. Lünnemann, A. I. Kuleff, and L. S. Cederbaum, "Ultrafast electron dynamics following outer-valence ionization: The impact of low-lying relaxation satellite states", *The Journal of Chemical Physics*, vol. 130, no. 15, p. 154 305, Apr. 2009.

[123] A. I. Kuleff, S. Lünnemann, and L. S. Cederbaum, "Ultrafast Charge Migration Following Valence Ionization of 4-Methylphenol: Jumping over the Aromatic Ring", *The Journal of Physical Chemistry A*, vol. 114, no. 33, pp. 8676–8679, Aug. 2010.

[124] A. I. Kuleff, S. Lünnemann, and L. S. Cederbaum, "Ultrafast reorganization of the hole charge created upon outer-valence ionization of porphyrins", *Chemical Physics*, vol. 399, pp. 245–251, May 2012.

[125] T. Kuś, B. Mignolet, R. D. Levine, and F. Remacle, "Pump and Probe of Ultrafast Charge Reorganization in Small Peptides: A Computational Study through Sudden Ionizations", *The Journal of Physical Chemistry A*, vol. 117, no. 40, pp. 10 513–10 525, Oct. 2013.

[126] B. Mignolet, R. D. Levine, and F. Remacle, "Charge migration in the bifunctional PENNA cation induced and probed by ultrafast ionization: a dynamical study", *Journal of Physics B: Atomic, Molecular and Optical Physics*, vol. 47, no. 12, p. 124 011, Jun. 2014.

[127] M. Vacher, D. Mendive-Tapia, M. J. Bearpark, and M. A. Robb, "The second-order Ehrenfest method", *Theoretical Chemistry Accounts*, vol. 133, no. 7, Jul. 2014.

[128] V. Despré, A. Marciniak, V. Loriot, M. C. E. Galbraith, A. Rouzée, M. J. J. Vrakking, F. Lépine, and A. I. Kuleff, "Attosecond Hole Migration in Benzene Molecules Surviving Nuclear Motion", *The Journal of Physical Chemistry Letters*, vol. 6, no. 3, pp. 426–431, Feb. 2015.

[129] Z. Li, O. Vendrell, and R. Santra, "Ultrafast Charge Transfer of a Valence Double Hole in Glycine Driven Exclusively by Nuclear Motion", *Physical Review Letters*, vol. 115, no. 14, Oct. 2015.

[130] M. Vacher, L. Steinberg, A. J. Jenkins, M. J. Bearpark, and M. A. Robb, "Electron dynamics following photoionization: Decoherence due to the nuclear-wave-packet width", *Physical Review A*, vol. 92, no. 4, Oct. 2015.

[131] G. Hermann, C. Liu, J. Manz, B. Paulus, J. F. Pérez-Torres, V. Pohl, and J. C. Tremblay, "Multidirectional Angular Electronic Flux during Adiabatic Attosecond Charge Migration in Excited Benzene", *The Journal of Physical Chemistry A*, vol. 120, no. 27, pp. 5360–5369, Jul. 2016.

[132] A. J. Jenkins, M. Vacher, M. J. Bearpark, and M. A. Robb, "Nuclear spatial delocalization silences electron density oscillations in 2-phenyl-ethyl-amine (PEA) and 2-phenylethyl-N,N-dimethylamine (PENNA) cations", *The Journal of Chemical Physics*, vol. 144, no. 10, p. 104 110, Mar. 2016.

[133] A. J. Jenkins, M. Vacher, R. M. Twidale, M. J. Bearpark, and M. A. Robb, "Charge migration in polycyclic norbornadiene cations: Winning the race against decoherence", *The Journal of Chemical Physics*, vol. 145, no. 16, p. 164 103, Oct. 2016.

[134] M. Lara-Astiaso, D. Ayuso, I. Tavernelli, P. Decleva, A. Palacios, and F. Martín, "Decoherence, control and attosecond probing of XUV-induced charge migration in biomolecules. A theoretical outlook", *Faraday Discuss.*, vol. 194, pp. 41–59, 2016.

[135] M. Vacher, F. E. A. Albertani, A. J. Jenkins, I. Polyak, M. J. Bearpark, and M. A. Robb, "Electron and nuclear dynamics following ionisation of modified bismethylene-adamantane", *Faraday Discuss.*, vol. 194, pp. 95–115, 2016.

[136] D. Ayuso, A. Palacios, P. Decleva, and F. Martín, "Ultrafast charge dynamics in glycine induced by attosecond pulses", *Phys. Chem. Chem. Phys.*, vol. 19, no. 30, pp. 19 767–19 776, 2017.

[137] S. Bag, S. Chandra, and A. Bhattacharya, "Molecular Attochemistry in Non-polar Liquid Environment: Ultrafast Charge Migration Dynamics through Gold-Thiolate and Gold-Selenolate Linkages", *Phys. Chem. Chem. Phys.*, 2017.

[138] M. Hollstein, R. Santra, and D. Pfannkuche, "Correlation-driven charge migration following double ionization and attosecond transient absorption spectroscopy", *Physical Review A*, vol. 95, no. 5, May 2017.

[139] M. Lara-Astiaso, A. Palacios, P. Decleva, I. Tavernelli, and F. Martín, "Role of electron-nuclear coupled dynamics on charge migration induced by attosecond pulses in glycine", *Chemical Physics Letters*, May 2017.

[140] V. Schwanen and F. Remacle, "Photoinduced Ultrafast Charge Transfer and Charge Migration in Small Gold Clusters Passivated by a Chromophoric Ligand", *Nano Letters*, Aug. 2017.

[141] K. Spinlove, M. Vacher, M. Bearpark, M. Robb, and G. Worth, "Using quantum dynamics simulations to follow the competition between charge migration and charge transfer in polyatomic molecules", *Chemical Physics*, vol. 482, pp. 52–63, Jan. 2017.

[142] H. Timmers, Z. Li, N. Shivaram, R. Santra, O. Vendrell, and A. Sandhu, "Coherent Electron Hole Dynamics Near a Conical Intersection", *Physical Review Letters*, vol. 113, no. 11, Sep. 2014.

[143] B. D. Bruner, Z. Mašín, M. Negro, F. Morales, D. Brambila, M. Devetta, D. Faccialà, A. G. Harvey, M. Ivanov, Y. Mairesse, S. Patchkovskii, V. Serbinenko, H. Soifer, S. Stagira, C. Vozzi, N. Dudovich, and O. Smirnova, "Multidimensional high harmonic spectroscopy of polyatomic molecules: detecting sub-cycle laser-driven hole dynamics upon ionization in strong mid-IR laser fields", *Faraday Discuss.*, vol. 194, pp. 369–405, 2016.

[144] I. Barth, J. Manz, Y. Shigeta, and K. Yagi, "Unidirectional Electronic Ring Current Driven by a Few Cycle Circularly Polarized Laser Pulse: Quantum Model Simulations for Mg-Porphyrin", *Journal of the American Chemical Society*, vol. 128, no. 21, pp. 7043–7049, May 2006.

[145] I. Barth and J. Manz, "Periodic Electron Circulation Induced by Circularly Polarized Laser Pulses: Quantum Model Simulations for Mg Porphyrin", *Angewandte Chemie International Edition*, vol. 45, no. 18, pp. 2962–2965, Apr. 2006.

[146] N. V. Golubev and A. I. Kuleff, "Control of charge migration in molecules by ultrashort laser pulses", *Physical Review A*, vol. 91, no. 5, May 2015.

[147] N. V. Golubev, V. Despré, and A. I. Kuleff, "Quantum control with smoothly varying pulses: general theory and application to charge migration", *Journal of Modern Optics*, vol. 64, no. 10-11, pp. 1031–1041, Jun. 2017.

[148] M. Ruberti, V. Averbukh, and P. Decleva, "B-spline algebraic diagrammatic construction: Application to photoionization cross-sections and high-order harmonic generation", *The Journal of Chemical Physics*, vol. 141, no. 16, p. 164 126, Oct. 2014.

[149] J. Breidbach and L. S. Cederbaum, "Universal Attosecond Response to the Removal of an Electron", *Physical Review Letters*, vol. 94, no. 3, Jan. 2005.

[150] L. S. Cederbaum, W. Domcke, J. Schirmer, and W. V. Niessen, "Correlation Effects in the Ionization of Molecules: Breakdown of the Molecular Orbital Picture", in *Advances in Chemical Physics*, I. Prigogine and S. A. Rice, Eds., vol. 65, Hoboken: John Wiley & Sons, Inc., Jan. 1986, pp. 115–159.

[151] A. I. Kuleff and L. S. Cederbaum, "Radiation Generated by the Ultrafast Migration of a Positive Charge Following the Ionization of a Molecular System", *Physical Review Letters*, vol. 106, no. 5, Jan. 2011.

[152] J. Cao, C. J. Bardeen, and K. R. Wilson, "Molecular "π Pulse" for Total Inversion of Electronic State Population", *Physical Review Letters*, vol. 80, no. 7, pp. 1406–1409, Feb. 1998.

[153] T. H. Dunning, "Gaussian Basis Functions for Use in Molecular Calculations. I. Contraction of (9s5p) Atomic Basis Sets for the First-Row Atoms", *The Journal of Chemical Physics*, vol. 53, no. 7, pp. 2823–2833, Oct. 1970.

[154] A. M. Weiner, "Femtosecond pulse shaping using spatial light modulators", *Review of Scientific Instruments*, vol. 71, no. 5, pp. 1929–1960, May 2000.

[155] T. Witte, D. Zeidler, D. Proch, K. L. Kompa, and M. Motzkus, "Programmable amplitude- and phase-modulated femtosecond laser pulses in the mid-infrared", *Optics Letters*, vol. 27, no. 2, p. 131, Jan. 2002.

[156] H. J. Wörner, *Private communication*, 2016.

[157] P. Hohenberg and W. Kohn, "Inhomogeneous Electron Gas", *Physical Review*, vol. 136, no. 3B, B864–B871, Nov. 1964.

[158] P. J. Stephens, F. J. Devlin, C. F. Chabalowski, and M. J. Frisch, "Ab Initio Calculation of Vibrational Absorption and Circular Dichroism Spectra Using Density Functional Force Fields", *The Journal of Physical Chemistry*, vol. 98, no. 45, pp. 11 623–11 627, Nov. 1994.

[159] M. J. Frisch, G. W. Trucks, H. B. Schlegel, G. E. Scuseria, M. A. Robb, J. R. Cheeseman, G. Scalmani, V. Barone, B. Mennucci, G. A. Petersson, H. Nakatsuji, M. Caricato, X. Li, H. P. Hratchian, A. F. Izmaylov, J. Bloino, G. Zheng, J. L. Sonnenberg, M. Hada, M. Ehara, K. Toyota, R. Fukuda, J. Hasegawa, M. Ishida, T. Nakajima, Y. Honda, O. Kitao, H. Nakai, T. Vreven, J. A. Montgomery Jr., J. E. Peralta, F. Ogliaro, M. Bearpark, J. J. Heyd, E. Brothers, K. N. Kudin, V. N. Staroverov, R. Kobayashi, J. Normand, K. Raghavachari, A. Rendell, J. C. Burant, S. S. Iyengar, J. Tomasi, M. Cossi, N. Rega, J. M. Millam, M. Klene, J. E. Knox, J. B. Cross, V. Bakken, C. Adamo, J. Jaramillo, R. Gomperts, R. E. Stratmann, O. Yazyev, A. J. Austin, R. Cammi, C. Pomelli, J. W. Ochterski, R. L. Martin, K. Morokuma, V. G. Zakrzewski, G. A. Voth, P. Salvador, J. J. Dannenberg, S. Dapprich, A. D. Daniels, Ö. Farkas, J. B. Foresman, J. V. Ortiz, J. Cioslowski, and D. J. Fox, *Gaussian 09 Revision E.01*, Gaussian Inc., Wallingford CT, 2009.

[160] A. Canal Neto, E. Muniz, R. Centoducatte, and F. Jorge, "Gaussian basis sets for correlated wave functions. Hydrogen, helium, first- and second-row atoms", *Journal of Molecular Structure: THEOCHEM*, vol. 718, no. 1-3, pp. 219–224, Mar. 2005.

[161] W. Von Niessen, G. Bieri, J. Schirmer, and L. Cederbaum, "Hole-mixing effects in the ionization of some unsaturated oxo-compounds", *Chemical Physics*, vol. 65, no. 2, pp. 157–176, Mar. 1982.

[162] H.-D. Meyer, F. Gatti, and G. Worth, Eds., *Multidimensional Quantum Dynamics: MCTDH Theory and Applications*. Weinheim: Wiley-VCH, 2009.

[163] M. Vacher, J. Meisner, D. Mendive-Tapia, M. J. Bearpark, and M. A. Robb, "Electronic Control of Initial Nuclear Dynamics Adjacent to a Conical Intersection", *The Journal of Physical Chemistry A*, vol. 119, no. 21, pp. 5165–5172, May 2015.

[164] M. Vacher, D. Mendive-Tapia, M. J. Bearpark, and M. A. Robb, "Electron dynamics upon ionization: Control of the timescale through chemical substitution and effect of nuclear motion", *The Journal of Chemical Physics*, vol. 142, no. 9, p. 094 105, Mar. 2015.

[165] M. Beck, A. Jäckle, G. Worth, and H.-D. Meyer, "The multiconfiguration time-dependent Hartree (MCTDH) method: a highly efficient algorithm for propagating wavepackets", *Physics Reports*, vol. 324, no. 1, pp. 1–105, Jan. 2000.

[166] L. S. Cederbaum, "Born–Oppenheimer approximation and beyond for time-dependent electronic processes", *The Journal of Chemical Physics*, vol. 128, no. 12, p. 124 101, Mar. 2008.

[167] G. A. Worth and L. S. Cederbaum, "Beyond Born-Oppenheimer: Molecular Dynamics Through a Conical Intersection", *Annual Review of Physical Chemistry*, vol. 55, no. 1, pp. 127–158, Jun. 2004.

[168] A. Abedi, N. T. Maitra, and E. K. U. Gross, "Exact Factorization of the Time-Dependent Electron-Nuclear Wave Function", *Physical Review Letters*, vol. 105, no. 12, Sep. 2010.

[169] A. Abedi, N. T. Maitra, and E. K. U. Gross, "Correlated electron-nuclear dynamics: Exact factorization of the molecular wavefunction", *The Journal of Chemical Physics*, vol. 137, no. 22, 22A530, Dec. 2012.

[170] E. Khosravi, A. Abedi, and N. T. Maitra, "Exact Potential Driving the Electron Dynamics in Enhanced Ionization of $H_2{}^+$", *Physical Review Letters*, vol. 115, no. 26, Dec. 2015.

[171] F. G. Eich and F. Agostini, "The adiabatic limit of the exact factorization of the electron-nuclear wave function", *The Journal of Chemical Physics*, vol. 145, no. 5, p. 054 110, Aug. 2016.

[172] B. F. E. Curchod and F. Agostini, "On the Dynamics through a Conical Intersection", *The Journal of Physical Chemistry Letters*, vol. 8, no. 4, pp. 831–837, Feb. 2017.

[173] E. Khosravi, A. Abedi, A. Rubio, and N. T. Maitra, "Electronic non-adiabatic dynamics in enhanced ionization of isotopologues of hydrogen molecular ions from the exact factorization perspective", *Phys. Chem. Chem. Phys.*, vol. 19, no. 12, pp. 8269–8281, 2017.

[174] G. Albareda, H. Appel, I. Franco, A. Abedi, and A. Rubio, "Correlated Electron-Nuclear Dynamics with Conditional Wave Functions", *Physical Review Letters*, vol. 113, no. 8, Aug. 2014.

[175] S. K. Min, A. Abedi, K. S. Kim, and E. K. U. Gross, "Is the Molecular Berry Phase an Artifact of the Born-Oppenheimer Approximation?", *Physical Review Letters*, vol. 113, no. 26, Dec. 2014.

[176] Y. Suzuki, A. Abedi, N. T. Maitra, K. Yamashita, and E. K. U. Gross, "Electronic Schrödinger equation with nonclassical nuclei", *Physical Review A*, vol. 89, no. 4, Apr. 2014.

[177] G. Albareda, A. Abedi, I. Tavernelli, and A. Rubio, "Universal steps in quantum dynamics with time-dependent potential-energy surfaces: Beyond the Born-Oppenheimer picture", *Physical Review A*, vol. 94, no. 6, Dec. 2016.

[178] B. F. E. Curchod, F. Agostini, and E. K. U. Gross, "An exact factorization perspective on quantum interferences in nonadiabatic dynamics", *The Journal of Chemical Physics*, vol. 145, no. 3, p. 034 103, Jul. 2016.

[179] R. Requist, F. Tandetzky, and E. K. U. Gross, "Molecular geometric phase from the exact electron-nuclear factorization", *Physical Review A*, vol. 93, no. 4, Apr. 2016.

[180] A. Schild, F. Agostini, and E. K. U. Gross, "Electronic Flux Density beyond the Born–Oppenheimer Approximation", *The Journal of Physical Chemistry A*, vol. 120, no. 19, pp. 3316–3325, May 2016.

[181] A. Scherrer, F. Agostini, D. Sebastiani, E. K. U. Gross, and R. Vuilleumier, "On the Mass of Atoms in Molecules: Beyond the Born-Oppenheimer Approximation", *Physical Review X*, vol. 7, no. 3, Aug. 2017.

[182] A. Abedi, F. Agostini, and E. K. U. Gross, "Mixed quantum-classical dynamics from the exact decomposition of electron-nuclear motion", *Europhysics Letters*, vol. 106, no. 3, p. 33 001, May 2014.

[183] F. Agostini, A. Abedi, and E. K. U. Gross, "Classical nuclear motion coupled to electronic non-adiabatic transitions", *The Journal of Chemical Physics*, vol. 141, no. 21, p. 214 101, Dec. 2014.

[184] F. Agostini, A. Abedi, Y. Suzuki, S. K. Min, N. T. Maitra, and E. K. U. Gross, "The exact forces on classical nuclei in non-adiabatic charge transfer", *The Journal of Chemical Physics*, vol. 142, no. 8, p. 084 303, Feb. 2015.

[185] F. Agostini, S. K. Min, and E. K. U. Gross, "Semiclassical analysis of the electron-nuclear coupling in electronic non-adiabatic processes", *Annalen der Physik*, vol. 527, no. 9-10, pp. 546–555, Oct. 2015.

[186] S. K. Min, F. Agostini, and E. K. U. Gross, "Coupled-Trajectory Quantum-Classical Approach to Electronic Decoherence in Nonadiabatic Processes", *Physical Review Letters*, vol. 115, no. 7, Aug. 2015.

[187] Y. Suzuki, A. Abedi, N. T. Maitra, and E. K. U. Gross, "Laser-induced electron localization in $H_2{}^+$: mixed quantum-classical dynamics based on the exact time-dependent potential energy surface", *Phys. Chem. Chem. Phys.*, vol. 17, no. 43, pp. 29 271–29 280, 2015.

[188] F. Agostini, S. K. Min, A. Abedi, and E. K. U. Gross, "Quantum-Classical Nonadiabatic Dynamics: Coupled- vs Independent-Trajectory Methods", *Journal of Chemical Theory and Computation*, vol. 12, no. 5, pp. 2127–2143, May 2016.

[189] Y. Suzuki and K. Watanabe, "Bohmian mechanics in the exact factorization of electron-nuclear wave functions", *Physical Review A*, vol. 94, no. 3, Sep. 2016.

[190] S. K. Min, F. Agostini, I. Tavernelli, and E. K. U. Gross, "Ab Initio Nonadiabatic Dynamics with Coupled Trajectories: A Rigorous Approach to Quantum (De)Coherence", *The Journal of Physical Chemistry Letters*, vol. 8, no. 13, pp. 3048–3055, Jul. 2017.

Eidesstattliche Versicherung

Eidesstattliche Versicherung gemäß §8 der Promotionsordnung der Naturwissenschaftlichen-Mathematischen Gesamtfakultät der Universität Heidelberg

1. Bei der eingereichten Dissertation zu dem Thema "Electron-nuclear dynamics and its control by external electromagnetic fields" handelt es sich um meine eigenständig erbrachte Leistung.

2. Ich habe nur die angegebenen Quellen und Hilfsmittel benutzt und mich keiner unzulässigen Hilfe Dritter bedient. Insbesondere habe ich wörtlich oder sinngemäß aus anderen Werken übernommene Inhalte als solche kenntlich gemacht.

3. Die Arbeit oder Teile davon habe ich bislang nicht an einer Hochschule des In- oder Auslands als Bestandteil einer Prüfungs- oder Qualifikationsleistung vorgelegt.

4. Die Richtigkeit der vorstehenden Erklärungen bestätige ich.

5. Die Bedeutung der eidesstattlichen Versicherung und die strafrechtlichen Folgen einer unrichtigen oder unvollständigen eidesstattlichen Versicherung sind mir bekannt.

Ich versichere an Eides statt, dass ich nach bestem Wissen die reine Wahrheit erklärt und nichts verschwiegen habe.

Heidelberg, den

_____

Unterschrift